

JIMMA UNIVERSITY

JIMMA INSTITUTE OF TECHNOLOGY

FACULTY OF MECHANICAL ENGINEERING

**Thesis Title: Numerical Modelling of Fatigue Crack Growth of
Welded Joint at Elevated Temperature**

**A Thesis Submitted to Faculty of Mechanical Engineering, Jimma Institute of Technology
In partial Fulfillment of the Requirements for the Degree of Masters of Science in
Mechanical Design**

By

YAHYA AHMED

January 2021



JIMMA UNIVERSITY

JIMMA INSTITUTE TECHNOLOGY

FACULTY OF MECHANICAL ENGINEERING

**Thesis Title: Numerical Modelling of Fatigue Crack Growth
of Welded Joint at Elevated Temperature**

Prepared By: Yahiya Ahmed

Main Supervisor: Dr.-Ing. Messay Alemu

Co-Supervisor: Yohanis Dabesa (MSc)

Declaration

I hereby declare that the work, which is presented in this thesis entitled "**Numerical Modeling of Fatigue Crack Growth of Welded Joint at Elevated Temperature**" is my original work. Has not been presented for a degree in any other university, and that all sources of material used for this thesis have been duly acknowledged.

Yahiya Ahmed

Signature

Date

This thesis has been submitted for examination with our approval.


Dr.-Ing. Messay Alemu

Main Supervisor

Signature

Date

Yohanis Dabesa (MSc)



Co-Supervisor

Signature

Date

Approval

Name: Yahiya Ahmed
Degree Masters of Science
Title: Numerical Modeling of Fatigue Crack Growth of Welded Joint at Elevated Temperature

Examining Committee:

Main Supervisor

Dr.-Ing. Messay Alemu _____

Co-Supervisor

Mr Yohanis Dabesa  _____

Chair:

Mr. _____

External Examiner

Dr. _____

Internal Examiner

Date of Approval _____

ABSTRACT

Welding is the extensively utilized permanent joining method plays a significant role in the production and joining of massive components; pressure vessels, ship, bridge, etc. Fatigue failure of welded joints working at elevated temperatures has been a severe problem facing in the world. The leakage due to fracture in these equipment's results in disasters to human life and economy. Even though research has been reported on the fracture and fatigue of welded joint, it only focusses on the residual stresses effects and the influence of the weld toe geometry in failure criteria. The purpose of this study is to model fatigue crack growth behaviour of welded joints at elevated temperature. In this study, both analytical and finite element (FE) approaches have been used to model Welding induced residual stress, to analysis thermomechanical stress and to model thermomechanical fatigue of welded joints. In the modelling of Welding induced residual stress, the heat input during welding results in the formation of residual stress. The critical stress during the analysis of thermomechanical stress which is perpendicular to longitudinal crack growth direction is hoop (circumferential) stress. The Welding induced residual stress and high-temperature effects on crack growth rate with the initial crack length are determined using the equation proposed by Forman. The elevated temperature was found to play a significant role in fatigue crack growth of welded joint works at elevated temperature with the addition of Welding induced residual stress, and thermomechanical produced stresses. Finally, the analytical and FE results were compared with the experimental result; the analytical and FE results are in good agreement with the experimental result. In this study, it was possible to model the behaviour of fatigue crack growth of welded joint at elevated temperature for low cycle fatigue.

Keywords: *Welded joint, Residual stress, thermomechanical stress, thermomechanical fatigue, crack growth*

ACKNOWLEDGEMENT

All praise and humble gratitude be to Almighty ALLAH, who gave me the courage and power to complete such a momentous work successfully. Next, my deep gratitude goes to my principal supervisor Dr-Ignr Messay Alemu for his initiation and supervision of this thesis and for providing me with the necessary guidance, continuous supervision, cooperation and motivation in this study. I believe that effort embodies in this thesis attained from only due to the vibrant and skilful guidance of Dr-Ignr Messay Alemu. Then, I wish to express heartfelt thanks to my associate supervisor, Mr Yohanis Dabesa, for his professional supervision provided during my study. He played a massive role in the completion of this thesis.

Finally, and most importantly, I would like to express my warmest appreciation to my family, for their encouragement, patience, and endless support during my study. I bestow my genuine thanks to others who supported me during this study for their ever-remarkable kind support and assistance.



CONTENTS

ABSTRACT	I
ACKNOWLEDGEMENT	II
CONTENTS	III
LIST OF FIGURES	VI
LIST OF TABLES	VIII
ABBREVIATIONS	IX
LIST OF SYMBOLS	X
1 INTRODUCTION	1
1.1 Background.....	1
1.2 Motivation for the Research.....	2
1.3 Problem Statements.....	4
1.4 Objectives.....	4
1.4.1 General Objective.....	4
1.4.2 Specific Objectives.....	4
1.5 Scope and Limitations.....	5
1.6 Research Methodology.....	5
1.7 Structure of the Thesis.....	7
2 LITERATURE SURVEY	8
2.1 General overview of welded joint.....	8
2.2 Major factors contribute to fatigue failure of welded joint.....	9
2.2.1 Welding induced residual stress.....	10
2.2.2 Thermomechanical stress of welded joint.....	13
2.3 Fatigue crack initiation and propagation of welded joint.....	13
2.4 Mode-I fatigue crack orientation of welded joint.....	15
2.5 Thermomechanical fatigue life prediction approaches.....	17
2.6 Research gap.....	19

3	MODELLING OF WELDING INDUCED RESIDUAL STRESS	20
3.1	Induced Residual Stress of welded joint Overview	20
3.2	Heat source and thermal analysis of Welding.....	21
3.2.1	Heat source model	22
3.2.2	The thermal boundary conditions	25
3.3	Mechanical Analysis	26
3.4	Distribution of Welding induced residual stress	29
3.5	Finite element modelling of Welding induced residual stress	31
3.6	Result and discussion	32
3.6.1	Temperature distribution through the welded joint	32
3.6.2	Welding induced residual stress results and observation	34
3.6.3	Comparisons and validation of results.....	36
4	THERMOMECHANICAL STRESS ANALYSIS OF REACTOR PRESSURE VESSEL	38
4.1	Introduction to a pressure vessel.	38
4.2	Benchmarking pressure vessel analysis	40
4.3	Thermomechanical stress analysis in the analytical approach	41
4.3.1	Mechanical stress analysis.....	42
4.3.2	Thermal stress analysis.....	44
4.4	Finite element methods	51
4.5	Result and discussion	52
4.5.1	Results	52
5	THERMOMECHANICAL FATIGUE MODELLING	56
5.1	Overview of Thermomechanical fatigue.....	56
5.2	Fatigue crack growth modelling.....	58
5.2.1	Modes of loading	58
5.2.2	Stress intensity factor of mechanical load	59
5.2.3	Residual stress intensity factor	61
5.3	Finite element modelling.....	69
5.4	Result and discussion	70
5.4.1	Longitudinal crack along the weld line	70
5.4.2	Circumferential crack growth in the welded joint of the vessel.....	71
5.4.3	XFEM Results	72

6	CONCLUSIONS AND SUGGESTED FUTURE WORK	74
6.1	Conclusions	74
6.2	Recommendation.....	77
	REFERENCES	78
	APPENDIX.....	82



LIST OF FIGURES

Figure 1.1 Pressure vessel welded joint failure.....	2
Figure 1.2 Cracked welded joint shell of the pressure vessel	3
Figure 1.3 Flowchart for the FEM computational and Analytical method.....	6
Figure 2.1 Schematic representation of a metallographic section of welded joint	9
Figure 2.2 Schematic representation of three bar analogy.....	10
Figure 2.3 Schematic representation of the formation of welding induced residual stress.....	11
Figure 2.4 Schematic representation of two stages of fatigue crack growth.	14
Figure 2.5 Low and High cycle fatigue S-N diagram	16
Figure 2.6 Total strain amplitude ($\Delta\varepsilon / 2$), versus number of cycles to fatigue failure (2Nf).....	16
Figure 3.1 Welded Joint Configuration.....	19
Figure 3.2 Double-ellipsoidal volumetric heat source model.....	24
Figure 3.3 Welding heat source model for pass one parameters.....	24
Figure 3.4 Temperature-dependent thermal physical properties of 2.25-Cr-Mo low alloy steel.....	26
Figure 3.5 Temperature-dependent mechanical properties of 2.25-Cr-1Mo low alloy steel.....	29
Figure 3.6 Distribution Longitudinal residual stress profile	30
Figure 3.7 Mesh of welded cross-section.....	29
Figure 3.8 Nodal temperature distribution throughout the welded cross-section	32
Figure 3.9 Graph of temperature distribution throughout the welded cross-section.....	33
Figure 3.10 Mises stress distribution in the welded cross-section.....	34
Figure 3.11 Graph of longitudinal residual stress distribution throughout the welded cross-section.....	35
Figure 3.12 Comparison of analytical results with experimental results	36
Figure 3.13 Comparison of simulation results with experimental results.....	37
Figure 4.1 Schematic representation of horizontal cylindrical pressure vessel.	40
Figure 4.2 Cross-section of the shell of vessel.....	42
Figure 4.3 Hoop stress at the diametrical cross-section.....	42
Figure 4.4 Hoop stress due to internal operating pressure through the radius of the pressure vessel.....	43
Figure 4.5 Radial stress, at the diametrical cross-section	43
Figure 4.6 Radial stress due to internal operating pressure through the radius of the pressure vessel.....	44
Figure 4.7 Schematic representation of the wall of pressure vessel subjected to thermal load	44
Figure 4.8 Temperature variation with the radius of the pressure vessel.....	46
Figure 4.9 Thermal hoop stress of the pressure vessel at different temperature ranges	49
Figure 4.10 Thermal radial stress of the pressure vessel at different temperature.....	50
Figure 4.11 Mesh of the cross-section of the cylindrical pressure vessel.....	51
Figure 4.12 Hoop stress distribution through the radius of the pressure vessel.....	52

Figure 4.13 Radial stress distribution through the radius of the pressure vessel	53
Figure 4.14 Variation of hoop stress with cylindrical pressure vessel radius	54
Figure 4.15 Variation of radial stresses with the cylindrical pressure vessel radius.....	55
Figure 5.1 Fatigue cycle of the reactor pressure vessel	57
Figure 5.2 Three modes of loading that can be applied to a crack.....	58
Figure 5.3 a) Circumferential crack and b) longitudinal crack configuration of welded joint.....	59
Figure 5.4 Schematic illustration of the principle of superposition	61
Figure 5.5 Residual stress variation at different crack aspect ratio.....	63
Figure 5.6 Crack growth rate versus stress intensity factor log-log scale	65
Figure 5.7 Fatigue crack growth due to thermal cyclic load rate versus stress intensity factor.....	66
Figure 5.8 Crack length versus the number of cycles	68
Figure 5.9 Strain-based evaluation of the crack growth versus the number of cycle	68
Figure 5.10 Mesh of the cross-section of the cylindrical pressure vessel	69
Figure 5.11 Longitudinal Von-Mises stress distribution in the welded joint.....	70
Figure 5.12 Longitudinal Von-Mises stress distribution in the welded joint at the crack tip	71
Figure 5.13 Circumferential Von-Mises stress distribution in the welded joint	71
Figure 5.14 Circumferential Von-Mises stress distribution in the welded joint at the crack tip.....	72
Figure 5.15 STATUSXFEM result of welded joint a) circumferential and b) longitudinal crack type.....	72
Figure 5.16 PSILSM result of the welded joint a) circumferential and b) longitudinal crack type	73
Figure 5.17 PHILSM result of welded joint a) longitudinal and b) circumferential crack type	73



LIST OF TABLES

Table 3. 1 Chemical Composition of 2.25-Cr-1Mo low alloy ferritic steel.....	22
Table 3. 2 Parameters of heat source	23
Table 3.3 Welding parameters of each pass.....	23
Table 3.4 Welding condition for each pass.....	24
Table 3.5 Summary of values parameters of thermal boundary conditions.....	25
Table 4.16 Dimension of the vertical cylindrical pressure vessel.....	40
Table 5.17 Load cases of the reactor pressure vessel	57



ABBREVIATIONS

<i>ASME</i>	American Society of mechanical engineering
<i>ASTM</i>	American society of testing material
<i>BM</i>	Base metal
<i>CAE</i>	Computer-aided engineering
<i>CT</i>	Compact tension
<i>CTOD</i>	Crack tip opening displacement
<i>FCG</i>	Fatigue crack growth
<i>FE</i>	Finite element
<i>HAZ</i>	Heat affected zone
<i>HCF</i>	High cycle fatigue
<i>LCF</i>	Low cycle fatigue
<i>LEFM</i>	Linear elastic fracture mechanics
<i>RPV</i>	Reactor pressure vessel
<i>RT</i>	Room temperature
<i>SENB</i>	Single-edge notch bend
<i>SIF</i>	Stress intensity factor
<i>TMF</i>	Thermomechanical fatigue
<i>TRIP</i>	Transformation induced plasticity
<i>WFM</i>	Weight function method
<i>WM</i>	Weld metal
<i>X – FEM</i>	Extended finite element



LIST OF SYMBOLS

<i>Symbol</i>	<i>Description</i>
da / dN	Crack growth rate
$\Delta \varepsilon_{mech} / 2$	Plastic strain
$N_f^{oxidation}$	Fatigue life due to oxidation
$N_f^{fatigue}$	Fatigue life
Δk_{th}	Crack growth threshold
$q_{tot,loss}$	Total heat loss due to the thermal boundary condition
$\sigma(x)$	Stress over the crack site in un-cracked site body
$C(T)$	Paris constant temperature-dependent
α	Thermal expansion coefficient
$m(x, a)$	Weight function
$2N_f$	Number cycles to failure
N_f^{creep}	Fatigue life due to creep
σ_{θ}^T	Total hoop
$CTOD$	Crack tip opening displacement
$T(r)$	Radial function of the temperature
D_{total}	Total damage
Δk	Stress intensity factor range

σ_{θ}^m	Mechanical load produced hoop stress
σ_r^T	Total radial stress
k_{res}	Residual stress intensity factor
σ_r^m	Mechanical load produced radial stress
t	Thickness shell
C	Paris constant
ΔK	Stress intensity factor (SIF) range
$\gamma_{ij,a}$	Shear strain
a	Ratio of external radius to internal radius
K_c	Fracture toughness
σ_{θ}^{th}	Thermal load produced hoop stress
$\frac{dT}{dr}$	Temperature gradient
α	Stefon-Boltzman constant
$\mathcal{E}_{i,a}$	Normal strain
a_f	Length of the front ellipsoidal
D_i	Internal diameter
q_r	Heat loss due to radiation
q_c	Heat loss due to convection
a	Crack length
σ_r^{th}	Thermal load produced radial stress
RT	Room temperature

a/c	Crack aspect ratio
v	Welding speed.
I	Welding current
R	Stress ratio
ε	Emissivity
σ	Divergence of the stress field
T_o	Ambient temperature
ΔT	Temperature difference
u	Welding voltage
T_s	Surface Temperature weldment
a_r	Length of the rear ellipsoidal
h_c	Heat transfer coefficient
Q	Heat input or the energy
b	Extent of the double ellipsoidal
B	Body force per unit volume.
k	Thermal conductivity coefficient
R	Stress ratio
c	Major diameter of ellipsoidal
η	Arc efficiency
C	Walker crack growth constant
E	Young modulus
ν	Poissons ratio

CHAPTER

1

INTRODUCTION

In this chapter, a brief introduction of fatigue crack growth of welded joint at elevated temperature, especially in the case of pressure vessel problem is presented first. The statement of the problem, motivation for the research, objectives, scope, limitations and methodology of the study is explained afterwards. The thesis outline is provided at the end of this chapter.

1.1 Background

Welding engineering is a method of joining metals in which heat and pressure are applied to the contact area between the two components; a filler metal may be added into the joint depending on welding processes. It plays a significant role in the production and joining of huge components; pressure vessel, ship, bridge (Kita-shinagawa-ku, 2015). Welded joint subjected to different types of load, the nature of loading on welded joints is cyclic. Cyclic loading condition leads to fatigue, in which the defect of the weld can grow to critical size finally to fracture of joint. Welded joints can exhibit particularly poor fatigue properties. The fatigue crack begins from the pre-existing crack-like porosity defect, and flaw, which is an inherent feature of a weld toe or root, may occur randomly in the welded joint welding (Velu, 2018a). Failure of welded joint components operates at elevated temperature; pressure vessels, gas turbine, chemical processing equipment has been facing many power plant industries. And making the components out of service and cause enormous injury, economic losses and a series of disasters. These problems are due to fracture in the equipment's, which is mainly caused by fatigue failure. Studying fatigue failure of the welded components started about 200 years ago. However, the main cause of failures of welded power plant components in different industries and the reactor pressure vessel is still fatigue.

At the elevated temperatures, fatigue behaviour and life predictions are extremely more complicated than at room temperature. The thermally-activated fatigue crack growth rate (FCGR) correlates with mechanical properties' degradation as increasing temperature (Lee et al., 2017). Fatigue failure can occur without any obvious warning. Therefore, analyzing the fatigue failure of the welded joint subjected to elevated temperature becomes necessary.

In 2003, the catastrophic failures of the pressure vessel happened in Norway, which killed eight labour and loss of the high amount of chemicals (Baru, 2016). The cause of the accident was identified, as un-careful design, operating and inspection conditions of welded joint of pressure vessel due to poor manufacturing methods using post-weld non-destructive testing was said. Disastrous accidents happened, such as the SS Sultana in 1865 and the Grover shoe factory explosion in 1904 (Atreya and Engineering, 2017) shown Figure 1.1.



Figure 1.1 Pressure vessel welded joint failure (Atreya and Engineering, 2017)

1.2 Motivation for the Research

From the background discussions, it is apparent that Welding is the extensively utilized permanent joining method plays a significant role in the production and joining of a huge component; pressure vessel, ship, bridge, etc. On the other hand, Welding has several defects on the structural integrity and in-service performance of the weldments. These defects are due to imperfection during Welding like; Welding induced residual stress and weld solidification cracks are reported to have degrading on the mechanical strength and possibly cause catastrophic failures

A number of catastrophic failures of power plant components, especially pressure vessel that operates under high temperature and pressure are reported in the recent past. An example of such failures is shown in Figure 1.1. The figure shows that pressure vessel fabricated with shielded metal arc welding and longitudinal cracked during operation. Detailed failure analysis has shown that the failure is due to defects during Welding in addition to the harsh working environment.

The complex working environment, in addition to welding defect problems in these types of structures, needs attention and focus on ensuring the structural integrity of the structures for improved product quality and reliability. It is expected that the effects of elevated temperatures on fatigue crack growth behaviour of welded joint, effects of Welding induced residual stress on fatigue crack growth of welded joint and crack growth rate of cylindrical reactor pressure vessel welded shell at different temperature ranges can be the major contributions from this thesis.

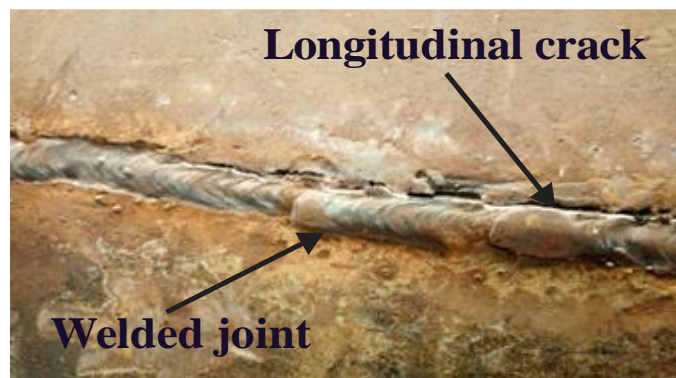


Figure 1. 2 Cracked welded joint shell of the pressure vessel (Hibret Industrial Engineering December 2019)

1.3 Problem Statements

Fatigue failure of welded joints working at elevated temperatures has been a serious problem facing in the world. It causes failure of pressure vessels, gas turbines, and chemical processing equipment's. The leakage due to fracture in these equipment's results in disasters to human life and economy.

Several researchers have proposed different methods to combat the challenges. However, the problem is still facing the world. Some have been proposed residual stress and welding toe geometry effects in failure criteria, which depends on stress concentration approach, but these only cannot justify the failure of many welded components works at elevated temperatures, which are subjected to thermomechanical stress and thermomechanical fatigue cycle. At the elevated temperatures, fatigue behaviour and life predictions are extremely more complicated than at room temperature.

Pressure vessel's welded joint consists of defect due to manufacturing process. The existing defects with the addition of harsh operating environment and conditions, (i.e. high temperature and high-pressure working environment) can affect the rate fatigue life of the pressure vessel.

Therefore, the objective of this study is to address the behaviour of fatigue crack growth of welded joint at the elevated temperature of the reactor pressure vessel at different temperature ranges. Analytical modelling and finite element (FE) modelling will model the more accurate the crack growth behaviour of reactor pressure vessel under elevated temperature and low cyclic fatigue.

1.4 Objectives

1.4.1 General Objective

Investigation of crack growth behaviour of reactor pressure vessel welded joint at elevated temperature using analytical and numerical approaches.

1.4.2 Specific Objectives

- Modelling of Welding induced residual stress
- Analysis of thermomechanical stress of reactor pressure vessel welded joint
- Modelling of thermomechanical fatigue of reactor pressure vessel welded joint

1.5 Scope of the Study

This study focuses on modelling fatigue crack growth of reactor pressure vessel welded joint at elevated temperatures. This can be achieved by using both analytical and FE approaches for modelling the fatigue behaviour of welded joint. For analytical approaches, modelling of Welding induced residual stress, analysis of thermomechanical stress and identifying critical stress. And different fatigue crack rate from previous experimental studies are used. For numerical approaches, different computational tools are used. ABAQUS 6.12 welding interface package is used to simulate welded joint and determine the distribution of Welding induced residual stress. Also, XFEM in ABAQUS 6.12 is used to simulate crack growth behaviour from the welded region of the vessel to other parts. Finally, the analytical and FE results are compared with experimental results.

1.6 Research Methodology

To address the above-mentioned objectives, analytical and numerical methods will be used since the fatigue crack growth of reactor pressure vessel welded joint is largely influenced by thermomechanical stress and thermomechanical fatigue in addition to Welding induced residual stress. Thermomechanical stress analysis technique will be used to analyze the effect of thermomechanical stress and determining critical stress on welded joint and thermomechanical fatigue analysis is used to characterize fatigue crack growth behaviour of welded joint of a reactor pressure vessel under thermal and mechanical loads.

Analytical study crack growth rate Forman law equation of fatigue is studied to determine the fatigue crack growth rate and to predict the fatigue life of reactor pressure vessel welded joint. The commercial computer-aided engineering (CAE) tool ABAQUS 6.12 is employed for both thermomechanical stress analysis and study of fatigue crack growth behaviour.

The flow chart, which consists of steps in conducting the FE and analytical analysis, is shown in Figure 1.2; finally, the analytical and FE results will be compared with experimental results.

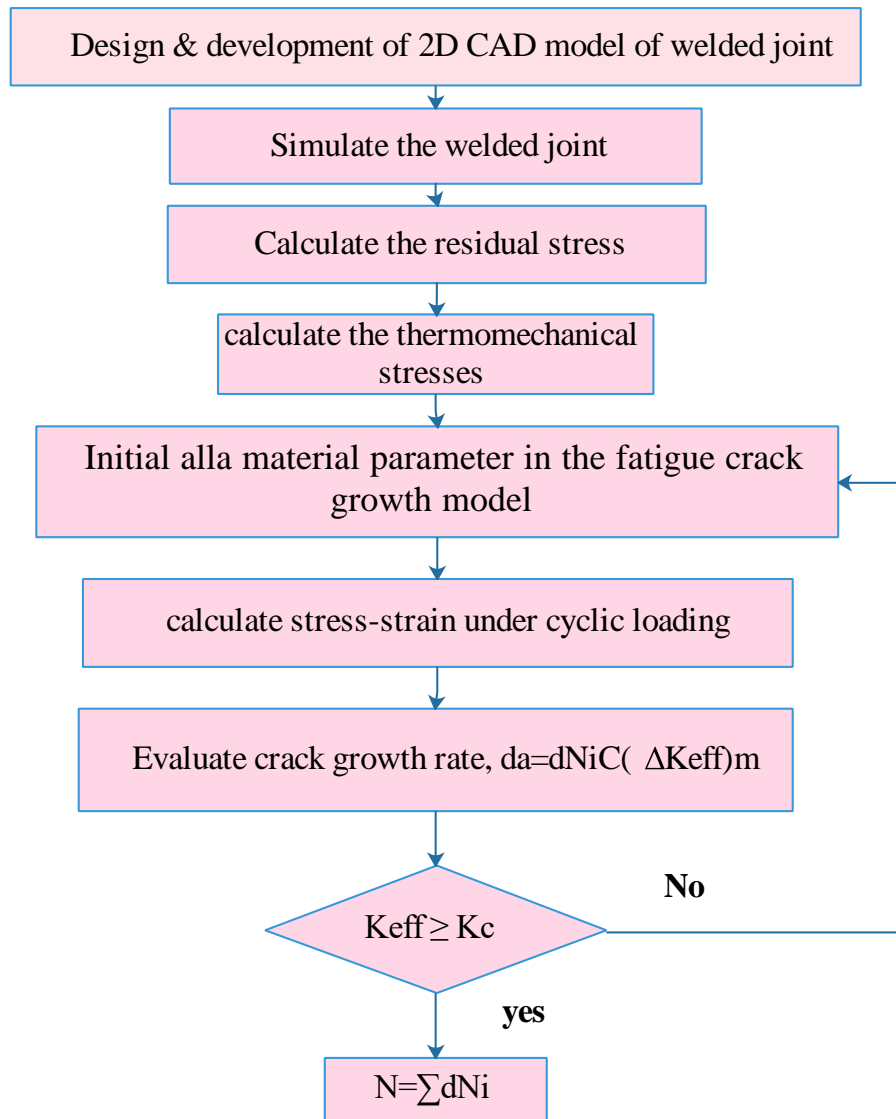


Figure 1. 3 Flowchart for the FEM computational and Analytical method

1.7 Structure of the Thesis

After this introduction section, the thesis is divided into six chapters. The contents of each chapter are briefly outlined as follows.

Chapter 2 contains a review of relevant literature on Welding induced residual stress, effects of residual stress and thermomechanical stress on fatigue crack growth welded joint in case of the pressure vessel. And different types of thermomechanical fatigue life prediction approach are reviewed.

The modelling of Welding induced residual stress is described in chapter 3, which includes modelling of the double ellipsoidal heat source of Welding based on Goldak's parameters, residual stress distribution, the profile and magnitude of Welding induced residual stress in the welded joint by using analytical and FEM. Simulating welded joint using ABAQUS 6.12 welding interface, the output results are validated with the experimental result. Chapter 3 concludes by considering the amount of heat input during the Welding and the reaming heat input after Welding and model the Welding induced residual stress.

Chapter 4 provides thermomechanical stress analysis, the uncoupled thermomechanical stress model is considered in analytical approach which provides a separately mathematical equation of the hoop (circumferential), radial stresses responses for both thermal and mechanical load. And identification of critical stress in addition to Welding induced residual stress are discussed in this chapter. Simulating pressure vessel cross-section under internal operating temperature and pressure using ABAQUS 6.12, the output results are compared with analytical results. Chapter 4 concludes by considering the amount of thermomechanical produced hoop and radial stresses then identifying critical stress, which acts perpendicular to the longitudinal crack growth direction

The thermomechanical fatigue crack modelling technique is discussed in chapter 5. Fatigue crack growth rate equation proposed by Forman is used to predict the number of cycles to crack growth, the effect ranges of temperature on fatigue crack growth rate is analyzed, and the fatigue life prediction results are presented. Chapter 6 includes this study conclusion and feature recommendation for the continuation of this research

CHAPTER

2

LITERATURE SURVEY

In this chapter, the overview of up to date theoretical, numerical and experimental investigation in fatigue crack growth of welded joint is presented. The major factors contributing to fatigue crack growth of welded joint; Welding induced residual stress and thermomechanical stress are discussed. And different types of thermomechanical fatigue life prediction approach are considered. An overview of welded joints, fatigue crack initiation and propagation of welded joints, as well as fatigue crack growth orientation, i.e. that normal and interface crack types to the weld, are presented.

2.1 General overview of welded joint

Welding engineering is a method of joining metals in which heat and pressure are applied to the area of contact between the two components; a filler metal may be added into the joint depending on welding processes. Today welding is being widely used as a joining process in many mechanical industries structural applications such as buildings, bridges, pressure vessels, and ships (Kitashinagawa-ku, 2015). The most commonly used process in due to many advantages compared to another manufacturing processes, thus welded structures are superior in many respects to riveted structures, castings, and forgings due to high joint efficiency, weight saving, reduction time and cost. It is for this reason that Welding is widely used in the fabrication of buildings, bridges, ships, oil-drilling rigs, pipelines, nuclear reactors components, and pressure vessels. The quality requirements of the joints in these fabrications depend on their fitness-for-purpose and differ significantly from one application to the next. Pressure vessels require welds, which can withstand the stresses and high temperatures and pressures experienced in operations, Welds in food processing plants must withstand corrosions by working liquids.

There are now over 75 different types of welding process among fusion welding such as; arc Electron beam welding and laser welding, are commonly used to manufacture those power plant components (Arai T, 2013). In many manufacturing of pressure vessels, conventional shielded metal arc welding (SMAW) types used in a wide range due to low cost, flexibility and portability (John Wiley & Sons, 2016). In material science, a typical weld joint is classified into three basic zones, namely, the base metal (BM), the weld metal (WM) and the heat affected zone (HAZ) based on the material characteristic and the metallographic structure shown in Figure 2.1

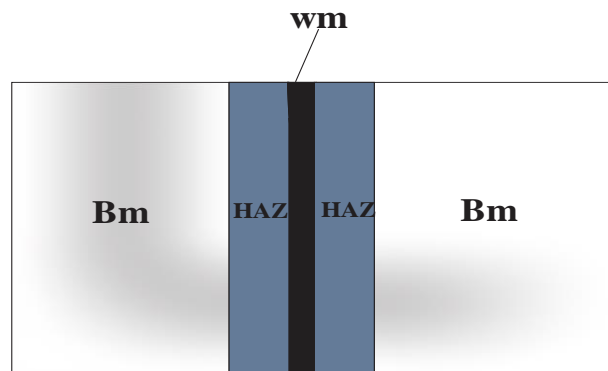


Figure 2.1 Schematic representation of a metallographic section of welded joint

The welded joint consists of different types of defects during Welding that leads the structure to fatigue failure. i.e. consists of stress concentration caused by the discontinuous portion of the weld bead, high tensile residual stress caused by non-uniform thermal expansion and contraction imposed during welding and weld toe opening due to welding error (Fueki et al., 2015).

2.2 Major factors contribute to fatigue failure of welded joint

There are different factors, which contribute in fatigue life of welded joints. These factors can be divided into two. i.e. intrinsic which includes; geometrical discontinuity, weld defect, Welding induced residual stress, thermomechanical property and the elastic-plastic behaviour of welded joints. And extrinsic factors include; stress ratio, loading modes and operating environment (Kang and Luo, 2020). Due to all these factors, it is expected, the initiation and propagation of a crack in a welded joint. The different fatigue failure models of the welded joint are reviewed in terms of both intrinsic and extrinsic factors.

2.2.1 Welding induced residual stress

Residual stresses in welded components result from heterogeneous plastic deformations during the welding thermal cycle. The thermal field result from the welding process in combination with temperature-dependent material properties causes local expansion and contraction that is constrained by less temperature affected material volumes. Locally hindered shrinkage causes tensile residual stresses during cooling and hindered expansion from phase transformation results in local compressive residual stresses. (Phillips, 2016) uses "Three- bar analogy" to simply express the fundamental mechanism that contributes to the formation of residual stress, which is shown in Figure 2.2, "The three-bar analogy" state that where two outer bars of equal length are rigidly connected with a split bar between them. Suppose the gap in the split bar is forcibly closed. In that case, tensile stress will be created in the split bar, and compressive stresses will be created in the outer bars and state that permanent deformation or strain can be expressed as distortion and permanent stress is be expressed as residual stress.

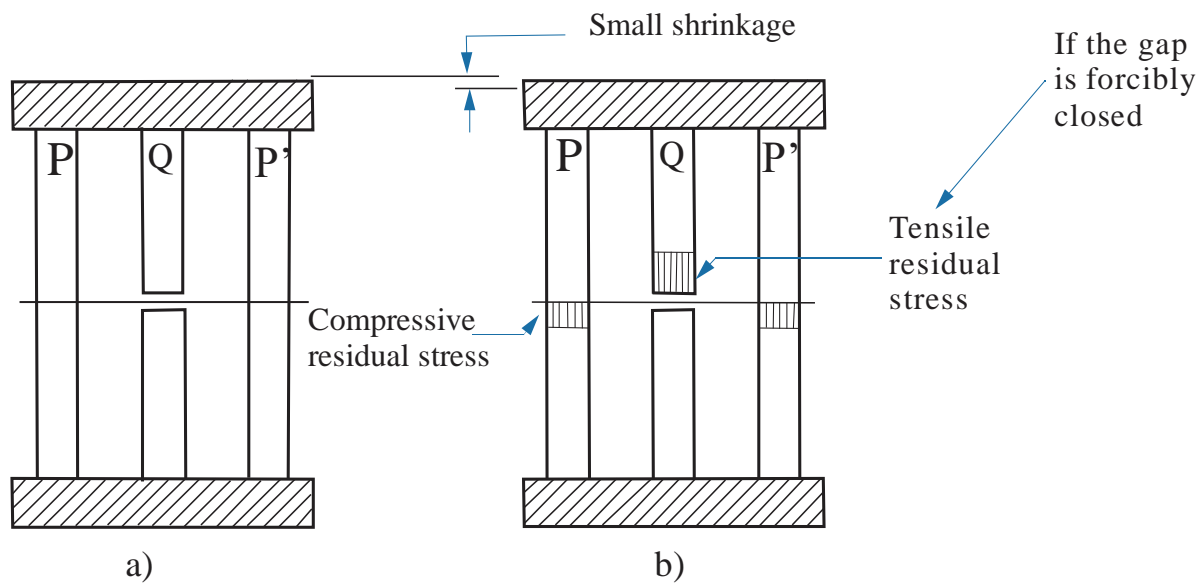


Figure 2.2 Schematic representation of three bar analogy (Phillips, 2016)

Many researchers explain the mechanism of formation of Welding induced residual stress among (Hornsey and Relieving, 2006) explains that Welding induced residual stress results from thermal strains during heating and cooling cycles of the W.M. and its adjacent HAZ. Also, it lists the main cause for the formation of residual stress is the shrinkage restraint by the HAZ and BM, and phase transformation during cooling.

In general, Welding induced residual stress formation can be summarized using schematic representation, as shown in Figure 2.3, the expansion and contraction forces due to non-uniform heat flow act on the WM and its adjacent BM. As WM solidifies and fuse with the BM it is in its maximum expanded state there will be the formation volume expansion causes local thickening in the weld area but doesn't cause a significant amount of plastic strains in the cooler HAZ and BM. The plastic strains stored over the welded joint by thermal cycle are primarily compressive and remains in the welded joint. By the time, that the WM reaches room temperature and the weld will contain a locked-in tensile stress type that is residual stress and sometimes reaches yield magnitude of BM, as far from the weld is usually in compressive with smaller magnitude.

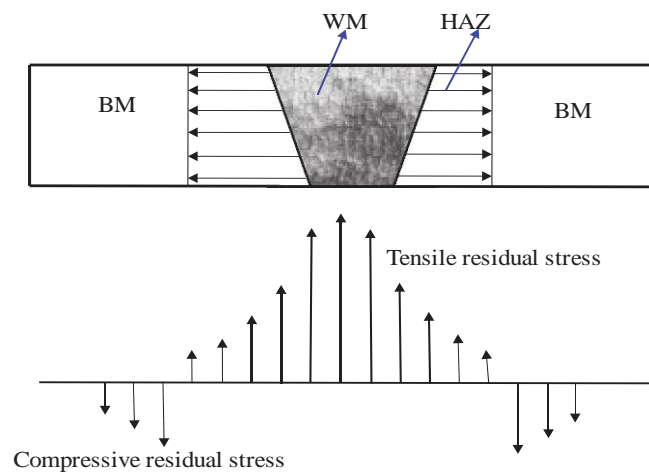


Figure 2.3 Schematic representation of the formation of Welding induced residual stress

2.2.1 Classification of Welding induced residual stress

Residual stress is classified based on their effective scale, as macroscopic and microscopic scale stresses. Macroscopic size stresses occurred at a large scale and distributed homogenously over several grains, also known as body stresses. Whilst the microscopic size scale may vary within single grains. On the other hand, residual stress classified based on the distribution as longitudinal and transversal residual stress. Longitudinal residual stress high in the weld metal and equalized by compressive residual stress near the base metal. Transverse residual stress strongly depends on the restraint of the weld and weld length (Hensel et al., 2018)

2.2.2 Effects of welding induced residual stress on the fatigue of welded joint

Welding induced residual stress can affect the fatigue and creep lifetime by reducing the fatigue and creep lifetime of the weldments. Many researchers have evaluated the uniaxial fatigue behaviour of welded structures, taking into account the effect of weld-induced residual stresses on fatigue life of the welded structure. (Klassen et al., 2017) studied experimental and numerical investigation on the influence of residual stresses on fatigue strength of welded assembly joints. Residual stresses have been measured using X-ray diffraction. The results showed that residual stress redistribution took place during the first load cycle. (Hong, 2016) investigated the relationship between the residual stress level and the applied load ratio on fatigue behaviour of welded joint. They conclude that the effective load ratio combined with applied loading and residual stress becomes a function of crack length, the combination effects between applied load ratio and the residual stress distribution play an important role in weld fatigue behaviour. (Chernyatin et al., 2018) studied the effect of welding residual stress on the fatigue surface crack front. Concluded that, Welding induced residual stress increases the effect of the circular surface crack on the stress intensity factor of the semielliptical crack. In addition, over the service life of the welded components residual stress demonstrates a complex evolution.

Residual stress relaxation occurred when the summation of residual stress and applied stresses reaches the yield state of the material due to subsequent mechanical loading (Benedetti et al., 2020). Welding induced residual stress can change crack tip profile of welded joint (Chernyatin et al., 2018) studied fatigue crack propagation of welded joints in the presence of residual stress, they demonstrate that the presence of Welding induced residual stress changes the semicircular internal surface of cracks of welded joint trends to semielliptical configuration.

2.2.3 Thermomechanical stress of welded joint

(Chaudhry, 2014), perform the detail thermomechanical stress analysis for reactor pressure vessel, by considering non-steady-state using numerical model and the temperature distribution inside surface of the vessel is considered according to various transient, viz., startup, shutdown and emergency condition of RPV. Resulting in the stress distribution across the wall thickness comes with the conclusion the most stressed location in RPV inside wall of vessel interface and the governing transient is emergency shutdown. In same manner (Loadings et al., 2019), presented thermomechanical stress analysis of functionally graded material of thick-walled pressure vessel using analytical and numerical methods the results of the proposed analytical equation and FE model proved that the inhomogeneity constant provides a significant effect on the mechanical and thermal stresses. (G.A. Moraitis, n.d.) developed the key-hole shape and size based on the thermomechanical response of pressure vessel during laser beam welding using the numerical method and concluded that the developed key-hole model is quite generic, efficient and can be successfully applied to the simulation of other joint types.

2.3 Fatigue crack initiation and propagation of welded joint

Welded joint subjected to different types of load, the nature of loading on welded joints is cyclic. Cyclic loading condition leads to fatigue, in which the defect of the weld can grow to critical size finally to fracture of joint. Welded joints can exhibit particularly poor fatigue properties, the fatigue crack begins from the pre-existing crack-like porosity defect, and flaw which is an inherent feature of a weld toe or root may occur randomly in the welded joint during Welding (Velu, 2018a).

Residual stress in the welded joints is another important characteristic. It is well known that in welded structures tensile residual stress may be same as the yield strength of the structure, so the stress range applied, regardless of the load ratio applied controls the fatigue strength of the welded joint. On the other hand, the microstructure mismatch in the mechanical property of different welded components will lead to the initiation and propagation of the fatigue crack (Velu, 2018b).

Many power plant components: For example, steam turbine rotors, pressure vessels are joined by Welding. During operations, these welded joints are exposed to high temperature and corrosive environments. Besides, the metallurgical defects like pores, voids, inclusions and cracks, stress concentration and tensile residual stresses are inevitably introduced in the weld metal (WM) and the heat affected zone (HAZ) during the welding process, which deteriorates both mechanical and fatigue properties of weld joints (Tang et al., 2018a).

The BM, HAZ, and WM of a welded joint constituent have different microstructural and mechanical properties, and there can also be a presence of thermally produced residual stresses in these locations (Shen et al., 2016a). Welded joints are regions where the initiation and propagation of fatigue crack have been observed, mainly at stress concentration points like inclusions and weld defects (Beltrão et al., 2011). In these points, there is stress concentration which is the major factor for fatigue cracks originate were subjected to cyclic loading (Dong and Guedes Soares, 2019)

The initial fatigue crack growth from nuclei to macroscopic cracks occurs in two stages as shown in Figure 2.3, In the initial crack in stage I, the crack grows along with slip systems and thus along with the crystallographic directions of the respective grain. In the subsequent stage II, crack propagation normally occurs in the direction of the maximum principal stress (Beckmann et al., 2018).

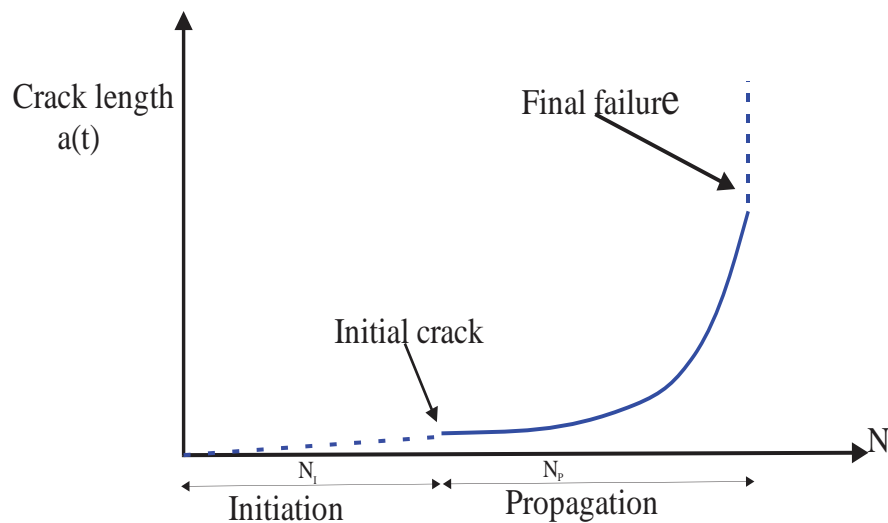


Figure 2.4 Schematic representation of two stages of fatigue crack growth (Beckmann et al., 2017).

Numerous researchers have analyzed the fatigue behaviours of various metals and alloys in recent decades, but few of them have focused on investigating the fatigue of welded joints. (Tang et al., 2018b) studied the fatigue crack growth behaviour of the BM, WM and HAZ section of welded joints. The authors found that the initial mixed-mode cracks shifted to mode I crack propagation in the BM, HAZ and WM. The WM had the highest FCG rate, followed by the HAZ, with the lowest FCG rate for the BM. The FE simulation showed that in the WM and the HAZ, high tensile residual stress values of 275MPa was found which could be accounted for FCG rates in WM and HAZ. (Shen et al., 2016b) perform two types of tests, i.e. single-edge notch bend (SENB) and compact tension (CT) was conducted to evaluate the fatigue crack growth threshold (Δk_{th}) WM, HAZ, and BM of a steam turbine rotors welded joint at different stress ratio ($R = 0.1, 0.5$ and 0.7). Their results show that (k_{th}) is not completely a single material constant but decrease with increasing of stress ratio for single-edge notch bend test type and the initiation of fatigue crack propagation criteria is found to be approximately same for the base metal, HAZ, and WM of the welded joint. They conclude that a good welding technique was adopted that did not degrade the fatigue properties of the welded joint.

2.4 Mode-I fatigue crack orientation of welded joint

Two types of cracks configuration are found in literature, normal cracks and interface cracks. Normal cracks are oriented perpendicular to the weld, while the interface cracks, parallel to the weld. When considering longitudinal-welded joint reactor pressure vessel, the two types of cracks, i.e. normal and interface crack can be expressed in terms of circumferential crack and longitudinal crack respectively

2.4.1 Normal fatigue crack growth to the weld

In mode I, normal crack growth of welded joint commonly found that the crack tip stress field was reduced or amplified according to the direction of the crack transition (Velu, 2018b). Elastic stress field ahead of mode I crack tip in linear elastic regime in cracked homogenous bodies without interfaces is conventionally and leads for initiation and propagation of the crack. Normal fatigue crack of welded joint offer greater resistance against fracture and fatigue than base metals and normal fatigue crack occur when the weldment is highly restrained.

2.4.2 Interface fatigue crack growth to the weld

Interface crack, which is parallel to the welding direction and lies in different zones. Crack in HAZ deviated towards B.M., while cracks in WM and BM grew along a straight path perpendicular to loading axis, without deflection. The HAZ exhibits the highest elastic-plastic fracture toughness, and the W.M. has the lowest (Moghadam and Farhangdoost, 2016). Interface crack is more commonly found than normal crack. Interface crack mostly found at the centre or the side of the weld bead. The interface crack (longitudinal crack) type of welded joint for reactor pressure vessel will be studied in this thesis

Types of fatigue cycle

Commonly there are two forms of fatigues found in literature, which are high cycle fatigue (HCF) and low cycle fatigue (LCF)

1. **High cycle fatigue:** - a type of fatigue when stresses are below the yield strength of the material, and the cycle to failure are generally greater than 10^4 which is called stress-controlled fatigue. High cycle fatigue usually associated with low-stress levels and low-stress amplitude and high-frequency elastic strains.
2. **Low cycle fatigue:** - a type of fatigue when stresses are above the yield strength of the material and cycle to fail typically less than 10^3 but not more than 10^5 and which is called strain-controlled fatigue. Occurs when only there is cyclic plastic strains are generated. Low cycle fatigue requires a material to undergo loading condition when each cycle produces elastic and plastic strain. In low cycle fatigue, the strain range during fatigue life exceeds elastic range and which causes inelastic deformation, so that the structure exhibit a short number of cycles to failure. Figure 2.5 illustrates the difference between high and low cyclic fatigues when observed on the S-N diagram.

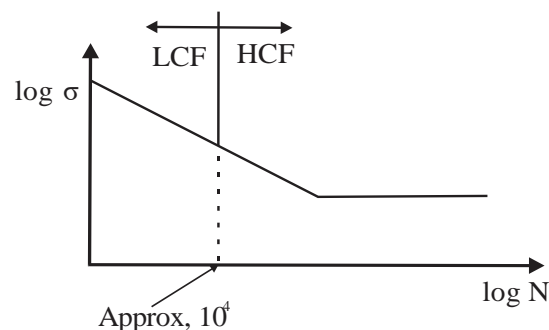


Figure 2.5 Low and High cycle fatigue S-N diagram (Miller, 2014)

2.5 Thermomechanical fatigue life prediction approaches

There are different approaches has been developed to predict the life of engineering components and structures under complex loading condition. It is necessary to accurately predict the fatigue life of components shows fatigue damage or sudden failure could occur. Longitudinal welded reactor pressure vessel subjected to thermomechanical fatigue type crack propagation due to fatigue cycle. And stress is the primary life-limiting factors for reactor pressure vessel, which service under elevated temperature and pressures, especially in power generation components. There are several models proposed by researchers to predict thermomechanical fatigue life by using different approaches; the damage model is based on either energy or strain partitioning,

Strain Based Approaches

I. The Basquin-Mason-Coffin model

This model is based on strain amplitude, states the Manson-Coffin relationship for plastic strain, and it provides only an approximation of the fatigue life of a material due to that the method is based on several compounded assumptions. (Stephen and Brookes, 2009) observed that when the logarithm of plastic strain ($\Delta\varepsilon_{mech}/2$) amplitude was plotted against the logarithm number of cycles to failure ($2N_f$), the result was linear as shown in Figure 2.6,

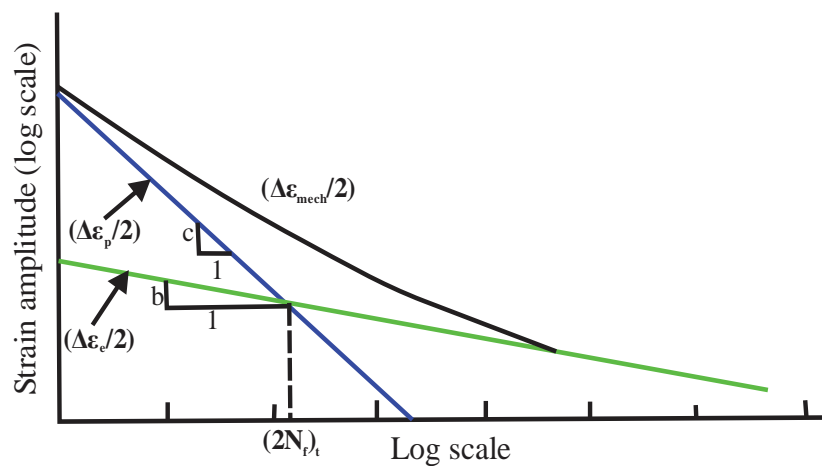


Figure 2.6 Total strain amplitude ($\Delta\varepsilon/2$), versus number of cycles to fatigue failure ($2N_f$)
(Stephen and Brookes, 2009)

II. Von Mises damage model

The von Mises damage model is considered to be a strain-based approach which is used to determine the equivalent strain amplitude, which is driven from normal ($\varepsilon_{i,a}$) and shear ($\gamma_{ij,a}$) strain amplitude in each direction, along with Poisson's ratio (ν)

III. ASME damage model

The ASME damage model was introduced by the ASME boiler and pressure vessel code in 1998. The method is based on the von Mises model, and the equivalent strain amplitude is based on three-dimensional strain ranges. The strain range is the difference between two equivalent points on the hysteresis at two different times, and each point represents a loaded and unloaded condition. The equivalent amplitude strain can be determined to the Basquin-Manson-Coffin curves to predict fatigue life.

On the other hand, there is a different mechanism in the analysis of thermomechanical fatigue (TMF). The convenient damages from three primary sources, i.e. fatigue, environment and creep in the reference (Socie and Socie, 2007) state that; the total damage (fatigue life) is the summation of the three damage processes. This cumulative damage approach is well suited for structures experiencing a variety of mechanical loadings with thermal cycling.

Generally, fatigue crack growth models are derived from fitting mathematical equations to relevant experimental data. The test data and the FCG models are often presented as power function equations, which relate the crack growth rate and crack growth rate (da/dN) to the stress intensity factor (SIF) range (ΔK). One of the first expressions for the constant amplitude fatigue crack growth (FCG) is Paris law (Chen et al., 2018). The stress intensity factor (SIF) may be one of the key factors in the fracture mechanics based fatigue strength assessment of welded joints, which depends on the global geometry of welded joints, weld profile type of load, crack size and crack form.

2.6 Research gap

The literature review indicates research gaps in the area of fatigue crack growth of welded joint at elevated temperature. Although, extensive research has been reported on the fatigue of crack growth of welded joints with the effects of Welding induced residual stress or weld toe geometry only. Thus, there exists a research gap with regard to studies on the crack growth behaviour of welded joints at elevated temperature in the presence of residual stress and thermomechanical stress. Following points needs effective modelling and predict the occurrence of fatigue crack growth of the welded joint.

- I. Analysis of the effect of elevated temperature on fatigue crack growth behaviour of welded joint
- II. Fatigue crack growth rate of welded joint in the presence of residual stress and thermomechanical stress
- III. Fatigue crack growth behaviour of welded joint under mixed modes (*I, II and III*) of loading conditions.

CHAPTER

3

MODELLING OF WELDING INDUCED RESIDUAL STRESS

In this chapter, the formation of Welding induced residual stress of welded joint is discussed under two modelling approaches; namely 1), Analytical modelling approach and 2), Numerical-modeling approach. In the analytical approach, the representation of heat source and thermal analysis, the double ellipsoidal model defined by Goldak's parameters is discussed. Mechanical and thermal aspects of residual stress analysis are performed. Finally, the residual stress distribution of its welded cross-section is analyzed.

3.1 Induced Residual Stress of welded joint Overview

Residual stress is built-up stress in the absence of external forces or thermal gradient within structure or material. Residual stress can be seen as a form of potential energy, and the stress relief acts as means of releasing this potential energy, whether by thermal, peening, vibratory, long term storage (ageing) or even by unintentional "bumpy" as stated in reference (Hornsey and Relieving, 2006). For several factors, residual stress in metal structures occurs during the manufacturing process such as Welding, cold working, rolling, bending, forging, casting and other machining operations.

During the welding thermal cycle residual stress on welded components results from heterogeneous plastic deformation, the expansion and contraction forces act on the weld metal and its adjacent base metal in a welded joint. As the weld metal solidifies and fuses with the base metal, it is in its maximum expanded state. However, at this point, the weld metal and its adjacent base metal are at high temperatures and have little strength or rigidity. The volume expansion causes local thickening in the weld area but is incapable of causing a significant amount of plastic strains in the cooler joint neighbourhoods. On cooling, it attempts to contract to the volume that it would normally occupy at the lower temperature, but it is restrained from doing so by the adjacent cooler base metal (Hensel et al., 2017).

The mechanism of generation of induced welding residual stresses has been studied and proposed by many scholars. Many of them considered the transformation of micro-phases in steel, so-called Transformation induced plasticity (TRIP) (Chang and Teng, 2004). Generally, residual stress in welded components results from heterogeneous plastic deformations during the welding thermal cycle. Welding residual stresses are the effects of the fluctuating inhomogeneous temperature distributions arising in the course of the different welding processes in and around the weld bead (Howes et al., 2002). The magnitude of Welding induced residual stress depends on the amount of heat input during the welding process, and the high heat input results in a large amount of formation of residual stress.

3.2 Heat source and thermal analysis of Welding

The heat supplied by a welding arc produces complex and non-uniform heat transfer in the weldment can result in the change in the microstructure of the weld zone and heat-affected zone. Transient thermal stress and metal movement and finally in the creation of residual stress in the welded components. To analyze these situations, I have to consider the heat source and thermal analysis during Welding.

Residual stress, especially the maximum tensile residual stress and deformation are developed in and around the weld region due to the large temperature gradient generated among the weld zones, i.e. HAZ, WM & BM. The exaggerated welding residual stress in the weld zone and its vicinity seriously affect ultimate strength, fatigue strength and structural stability and reduce manufacturing accuracy. The temperature distribution is strongly influenced by the size and shape of heat source, which can be represented as double ellipsoid defined by Goldak's parameters (Pu et al., 2017). The benchmark problem is a reactor pressure vessel with a longitudinal welded joint shell is selected with specified dimensions and design data; the weld configuration is a single V groove type as shown in Figure 3.1

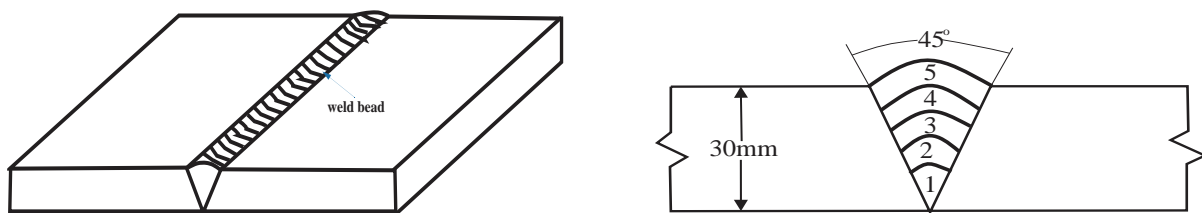


Figure 3.1 welded Joint Configuration

2.25-Cr-1Mo (ASTM A387 grade 22) low alloy ferritic steel is where chosen in this research because 2.25Cr-1Mo steel is an important structural material in nuclear power plants. Due to high resistance to both creep and corrosion at high temperatures between ($450^{\circ}C$ and $650^{\circ}C$) as well as low thermal expansion coefficient (Ren et al., 2019a). Table 3.1 presents chemical compositions by the mass fraction of 2.25Cr-1Mo low ferritic steel/ ASTM A387 Grade 22

Table 3. 1 Chemical Composition of 2.25Cr-1Mo low alloy ferritic steel (Homayounfar, 2009)

Material 2.25-Cr 1Mo grade 55 low alloy carbon steel/ ASTM A387 Grade 22								
Composition	C	Si	Mn	P	S	Cr	Mo	Cu
Mass fraction (%)	0.15	0.5	0.5	0.035	0.03	2.3	1.0	0.3

3.2.1 Heat source model

The heat source model is considered a significant aspect of the welding thermal analysis. To improve the simulation of welding process efficiency "double ellipsoidal volumetric heat source" by Goldak's parameter is used, which is shown in Figure 3.2. The size and shape of the double ellipsoidal heat source model are described by Goldak's parameters, which depend on the welding parameters, which includes the input energy and its travel speed. The thermal gradient and temperature distribution can be obtained by adjusting these parameters.

In the double-ellipsoidal volumetric heat source model, there are two separately heat input regions which can be expressed by the original coordinate system. One region is in the front of the arc centre ($x > 0$) stated by Equation (3.1), the other region is behind of the arc ($x \leq 0$) stated by Equation (3.2). The front half of the source is the quadrant of one ellipsoidal source, and the rear half is the quadrant of another ellipsoid.

The front heat source /heat flux: -

$$q_f(x, y, z) = \frac{6\sqrt{2}f_f Q}{\pi a_f b c \sqrt{\pi}} \cdot \exp\left(-\frac{3x^2}{a_f^2} - \frac{3y^2}{b^2} - \frac{3z^2}{c^2}\right) \quad (x > 0) \quad (3.1)$$

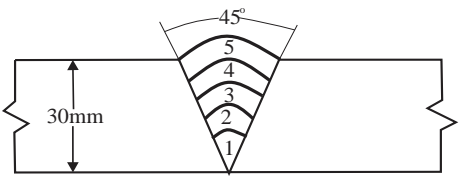
The rear heat source /heat flux: -

$$q_r(x, y, z) = \frac{6\sqrt{2}f_r Q}{\pi a_r b c \sqrt{\pi}} \cdot \exp\left(-\frac{3x^2}{a_r^2} - \frac{3y^2}{b^2} - \frac{3z^2}{c^2}\right) \quad (x \leq 0) \quad (3.2)$$

Where x , y and z are the original coordinate of a double ellipsoid model. a_f Shows the length of the front ellipsoidal, a_r is the length of the rear ellipsoidal, b is the extent of the double ellipsoidal heat source model, c is the double ellipsoidal heat source model. f_f and f_r are parameters which give the fraction of the heat deposited in front and rear respectively.

$$\text{In this research } \begin{cases} f_f = \frac{2 \times a_r}{2} = 1.33 \\ f_r = \frac{2 \times a_f}{a_f + a_r} = 0.66 \end{cases}, f_f + f_r = 2 \quad (3.3)$$

Table 3. 2 Parameters of the heat source (Fu et al., 2015)

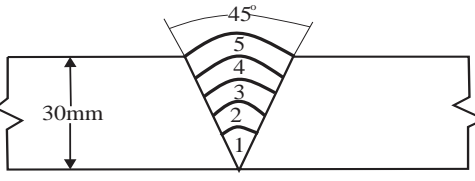
	Weld pass number	Parameters			
		a_f (mm)	a_r (mm)	b (mm)	c (mm)
	1	5	8	4.8	3
	2	8	16	6.3	4
	3	10	20	6.3	4
	4	5	10	13	2.5
	5	5	10	17	3.3

In Equations (3.1 and 3.2) Q is heat input or the energy of the welding heat source and which is given by Equation (3.4)

$$Q = \frac{\eta l u}{v} \quad (3.4)$$

Where η is the arc efficiency set as 0.8 (Chen et al., 2019), l is the welding current, u is welding voltage, v is the welding speed

Table 3.3 Welding parameters of each pass

	Weld pass number	Welding Parameters		
		Current I (A)	Voltage u (v)	Speed v (mm/s)
	1	120	25	15
	2	120	25	4.2
	3	120	25	3.5
	4	120	25	3.1
	5	120	25	2.86

The welding process was performed by a CRK-500 welding machine based on the ASME standard, which provides guidelines for the construction of boilers, pressure vessels, and nuclear components, including requirements for the materials, design, fabrication, examination, inspection, and stamping (Chen et al., 2019)

Table 3.4 Welding condition for each pass

Weld pass number	Welding Parameters			
	Current I (A)	Voltage u (v)	Speed v (mm/s)	Net heat input Q (kJ/mm)
1	120	25	1.5	1.6
2	120	25	4.2	0.57
3	120	25	3.5	0.68
4	120	25	3.1	0.77
5	120	25	2.86	0.83

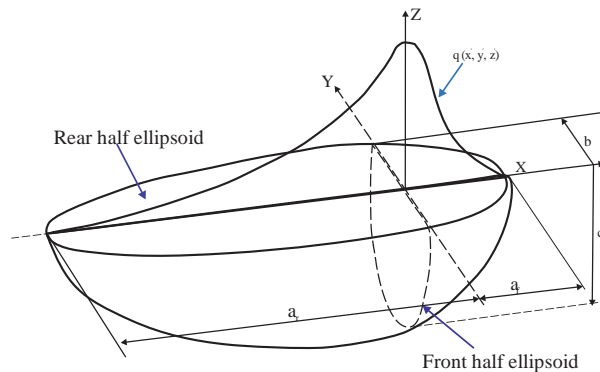


Figure 3.2 Double-ellipsoidal volumetric heat source model (Pu et al., 2017)

A MATLAB program is developed to compute the above-explained Equation (3.1 and 3.2), for pass one values to show welding heat source profile based on Goldak's parameters as shown in Figure 3.3

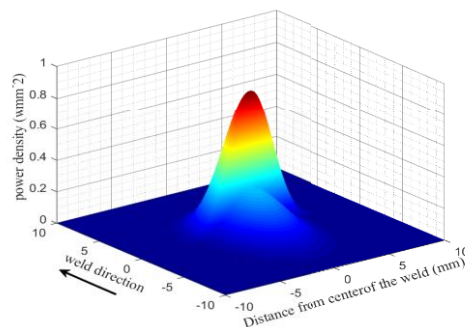


Figure 3.3 Welding heat source model for pass 1 parameters

3.2.2 The thermal boundary conditions

The heat source has a uniform density, and its volume is equal to that of the full weld passes, during multi-pass Welding, there is the interchange of heat between the weldment and its surroundings through convection and radiation so that considering thermal boundary condition is important.

The heat loss due to convection (q_c) is described by Equation (3.5)

$$q_c = -h_c (T_s - T_o) \quad (3.5)$$

The heat loss due to radiation (q_r) is described by Equation (3.6)

$$q_r = -\varepsilon\alpha \left\{ (T_s)^4 - (T_o)^4 \right\} \quad (3.6)$$

Where h_c heat transfer coefficient ($h_c = 270 \text{ J/k}$), T_s is the current external temperature of the weldment (surface Temperature), T_o Ambient temperature ε is emissivity and α is the "Stefon-Boltzman" constant

The total heat loss due to thermal boundary condition is the summation of loss due to radiation and convection which is given by Equation (3.7)

$$q_{tot,loss} = (q_r + q_c) \text{ J.mm}^{-2} \cdot \text{s}^{-1} \quad (3.7)$$

Table 3.5 Summary of values parameters of thermal boundary conditions

Parameters	Value	Heat loss due to convection (q_c)	Heat loss due to radiation (q_r)
h_c	$2.5 \times 10^{-5} \text{ J.mm}^2$	0.0371 J.mm ² .s ⁻¹	0.45 J.mm ⁻² .s ⁻¹
T_s	1510^0 C		
T_o	25^0 C		
ε	0.8		
α	$5.67 \times 10^{-14} \text{ J.mm}^{-2} \cdot \text{s}^{-1} \cdot \text{k}^{-4}$		
Total heat loss			0.4871 J.mm⁻².s⁻¹

In the thermal analysis, the heat input results in a change of temperature-dependent thermo-physical properties of the material which is shown in Figure 3.4

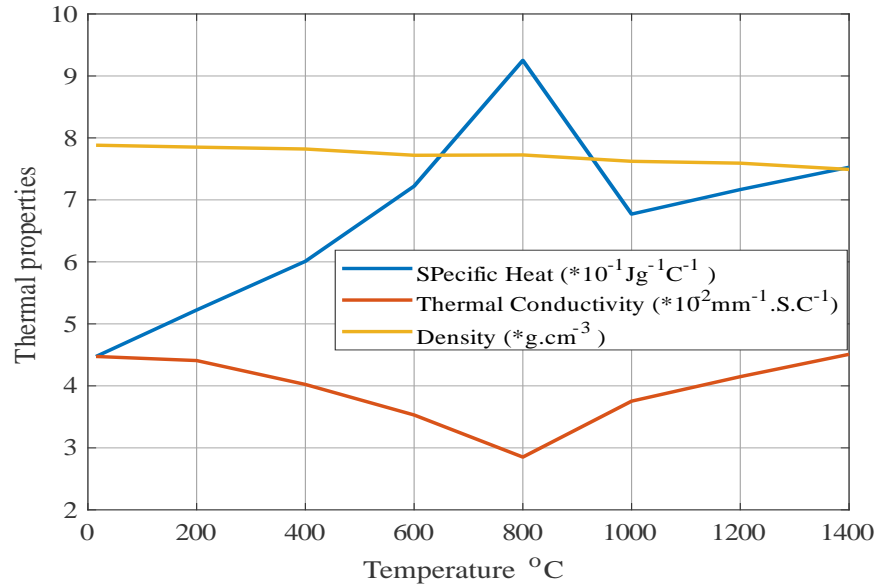


Figure 3.4 Temperature-dependent thermal physical properties of 2.25-Cr 1Mo low alloy steel (Chang and Teng, 2004)

3.3 Mechanical Analysis

For 2.25Cr-1Mo low ferritic steel, because the carbon equivalent is relatively small, it can be inferred that the solid-state phase transformation will have an insignificant influence on the welding residual stress and deformation. Relatively large heat input was used to perform the Welding. The phase fraction of martensite is very limited in the weld metal and heat affected zone (HAZ) stated in reference (Ren et al., 2019a). Based on the two-above reason in this research phase transformation is neglected. During the entire thermal cycle, the time with high temperature is very low creep behaviour is ignored. The total strain due to heat input results in the formation of mechanical and thermal strains will be derived as follow

The equation of equilibrium of finite element in mechanics is given by Equation (3.8)

$$\sigma_{ij,j} + B_i = 0 \quad (3.8)$$

Where σ is the divergence of the stress field and B is body force per unit volume

Therefore, the total strain of this study is stated in Equation (3.9)

$$\varepsilon = \varepsilon_{el} + \varepsilon_{pl} + \varepsilon_{th} + \varepsilon_{\Delta v} \quad (3.9)$$

Where ε_{el} elastic strain, ε_{pl} plastic strain, ε_{th} thermal strain and $\varepsilon_{\Delta v}$ strain due to volumetric change

From Equation (3.9) the elastic strain is given by Equation (3.10)

$$\varepsilon_{el} = \varepsilon - \varepsilon_{pl} - \varepsilon_{th} - \varepsilon_{\Delta v} \quad (3.10)$$

The generalized Hooke's law (constitutive equation) from Equations (3.8 and 3.10) is given by Equation (3.11)

$$\sigma - C_{ij,i} (\varepsilon - \varepsilon_{pl} - \varepsilon_{th} - \varepsilon_{\Delta v}) + B_i = 0 \quad (3.11)$$

From Hooke's law

$$\sigma = C \varepsilon_{el} \quad (3.12)$$

Where σ is induced residual stress due to mechanical deformation caused by non-uniform temperature distribution C , is elastic matrix and given by Equation (3.13)

$$C = \frac{E}{1-\nu^2} \begin{pmatrix} 1 & \nu & 0 \\ \nu & 1 & 0 \\ 0 & 0 & \frac{1-\nu}{2} \end{pmatrix} \quad (3.13)$$

Plane stress analysis is condition is used due to larger plastic zones are more significant for thin sheet material of ductile alloys as stated in reference (Description, 2008), So that the developed residual stress from Equations (3.12 and 3.13) is given by Equation (3.14)

$$\begin{Bmatrix} \sigma_{xx} \\ \sigma_{yy} \\ \sigma_{xy} \end{Bmatrix} = \frac{E}{1-\nu^2} \begin{pmatrix} 1 & \nu & 0 \\ \nu & 1 & 0 \\ 0 & 0 & \frac{1-\nu}{2} \end{pmatrix} \begin{Bmatrix} \varepsilon_{xx} \\ \varepsilon_{yy} \\ \gamma_{xy} \end{Bmatrix} \quad (3.14)$$

Elastic strain due to residual stress given by Equation (3.15)

$$\begin{Bmatrix} \varepsilon_{xx} \\ \varepsilon_{yy} \\ \gamma_{xy} \end{Bmatrix} = \frac{1}{E} \begin{pmatrix} 1 & -\nu & 0 \\ -\nu & 1 & \nu \\ 0 & 0 & 2(1+\nu) \end{pmatrix} \begin{Bmatrix} \sigma_{xx} \\ \sigma_{yy} \\ \sigma_{xy} \end{Bmatrix} \quad (3.15)$$

From Equations (3.8, 3.10 and 3.14) the stress equilibrium is stated by Equation (3.16)

$$C_{ij,i} (\nabla u - \varepsilon_{pl} - \alpha(\Delta T) - \varepsilon_{\Delta v}) + B_i = 0 \quad (3.16)$$

Inserting Equation (3.17) into Equation (3.19) and rearranging gives as stated in Equation (3.17)

$$\frac{E}{1-\nu^2} \begin{pmatrix} 1 & \nu & 0 \\ \nu & 1 & 0 \\ 0 & 0 & \frac{1-\nu}{2} \end{pmatrix} \left[\underbrace{\begin{Bmatrix} \theta_x \\ \theta_y \\ \theta_x + \theta_y \end{Bmatrix}}_A - \underbrace{\begin{Bmatrix} \varepsilon_{xx} \\ \varepsilon_{yy} \\ \gamma_{xy} \end{Bmatrix}}_B - \underbrace{\alpha \begin{Bmatrix} \Delta T \\ \Delta T \\ 0 \end{Bmatrix}}_C + \underbrace{\begin{Bmatrix} \varepsilon_{\Delta v} \\ \varepsilon_{\Delta v} \\ 0 \end{Bmatrix}}_D \right] + \begin{Bmatrix} B_x \\ B_y \\ 0 \end{Bmatrix} = 0 \quad (3.17)$$

Where

A is strain due to small deformation, B is a plastic strain, C is thermal strain and D is strain due to volumetric change

The heat input during welding results in the change of mechanical properties temperature dependent, which is shown in Figure 3.5

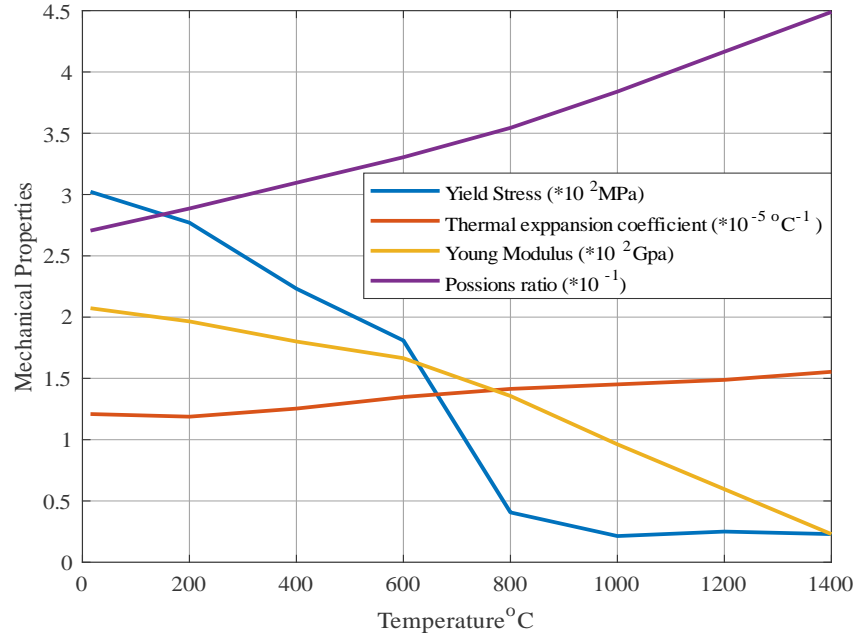


Figure 3.5 Temperature-dependent mechanical properties of 2.25-Cr 1Mo low alloy steel(*Chang and Teng, 2004*)

3.4 Distribution of Welding induced residual stress

There are two different types of distribution of induced residual stress of butt welded joint according to (Gadallah et al., 2018a), i.e. Longitudinal and transversal residual stress. Longitudinal tensile residual stresses are usually high in the weld itself and equalized by compressive residual stress beside the weld. While the transverse residual stress strongly dependent on the restraint, i.e. the plate thickness, temperature gradient during the welding process. If the transient is sufficient transverse residual stresses are generated in the transverse direction of the weld. In this thesis only longitudinal type residual stress is considered, To show the distribution of longitudinal residual stress analytically the equation proposed by Masubuchi and Martin (Arthur et al., 1980) was used. The distribution is characterized by two parameters, the maximum stress in the weld region (σ_o) which obtained from Equation (3.14) and the width of the tension zone of residual stress (c)

$$\sigma(x) = \sigma_o \cdot e^{-\frac{1}{2}\left(\frac{x}{c}\right)^2} \left(1 - \left(\frac{x}{c}\right)^2\right) \quad (3.18)$$

Where σ_o , is the maximum stress at the weld region c , is the width of the tension zone of residual stress, x is the distance along the x-direction. The selected parameters values, $\sigma_o = (300MPa)$, is calculated using Equation (3.16) $c = 10mm$ and $x = 100mm$ based on reference (Schnubel and Huber, 2012). The MATLAB program is developed for Equation (3.18) to show the profile longitudinal residual stress distribution, which is as shown in Figure 3.6, it shows that longitudinal residual stress high tensile at the centre of the weld compressive near the weld and it becomes zero.

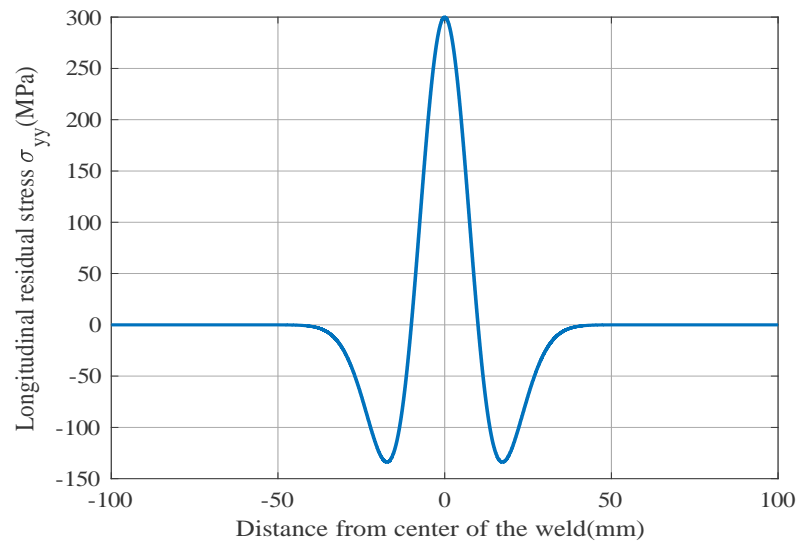


Fig 3.6 Distribution Longitudinal residual stress profile

3.5 Finite element modelling of Welding induced residual stress

2D shell-type finite element model of single "V" groove angle 45° of butt- longitudinal welded joint with width 100 mm and height of 30 mm is modelled. To predict temperature distribution and Welding induced residual stress using the ABAQUS 6.12 welding interface software as shown in Figure 3.7. The elements type in the thermal analysis are DC2D8 (An 8-node quadratic heat transfer quadrilateral), and in mechanical stress, analysis is CPS8 (An 8-node biquadratic plane stress quadrilateral). The total number of nodes is 1398, and the total number of elements is 4237. The total number of weld passes is five passes in the cross-section it is assumed that the BM, WM, have the same material properties.

The finite element model is split up along the X-Y plane to define paths interest to determine profiles of temperature distribution and Welding induced residual stress magnitude and its distribution. Firstly, the welding temperature field is computed according to the given welding conditions; the nodal temperature distribution is used as a thermal load in the subsequent analysis of mechanical analysis. The applied boundary condition are thermal and mechanical boundary conditions. A 2D model with fine mesh near the weld metal and coarse mesh for other parts of the cross-section, the moving heat source is employed to simulate the welding process.

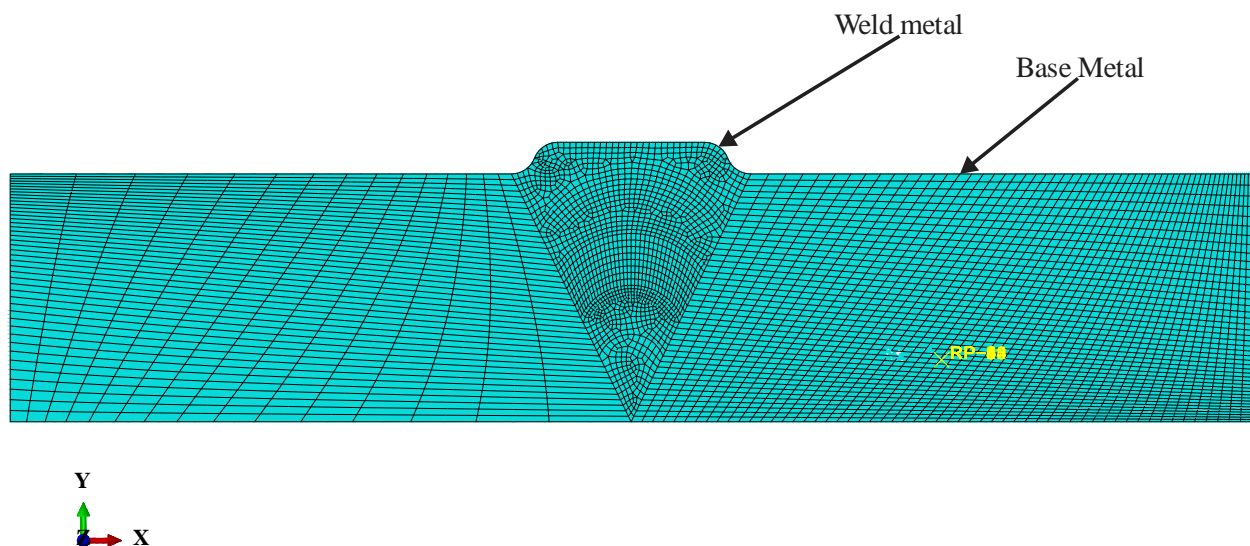


Figure 3.7 Mesh of welded cross section

3.6 Result and discussion

3.6.1 Temperature distribution through the welded joint

The distribution of temperature in the welded cross section is shown in Figure 3.8, and the figure illustrates that significant temperature variation occurs as the heat source moves. The initial temperature of the welded cross-section is same as ambient temperature, which is 25°C , the temperature of weld metal is set to be at the melting temperature of 1500°C , the temperature of HAZ is shown as a series of counters between 600°C and 1200°C . Therefore, there is a gradual change in the temperature distribution in a welded cross-section due to moving heat source. The temperature near the weld bead and HAZ changes rapidly with the distance from the heat source. The beads arrangement and meshes are symmetric in FE model, where the peak temperature profile is asymmetric in the welding cross-section due to different heat input and welding speed.

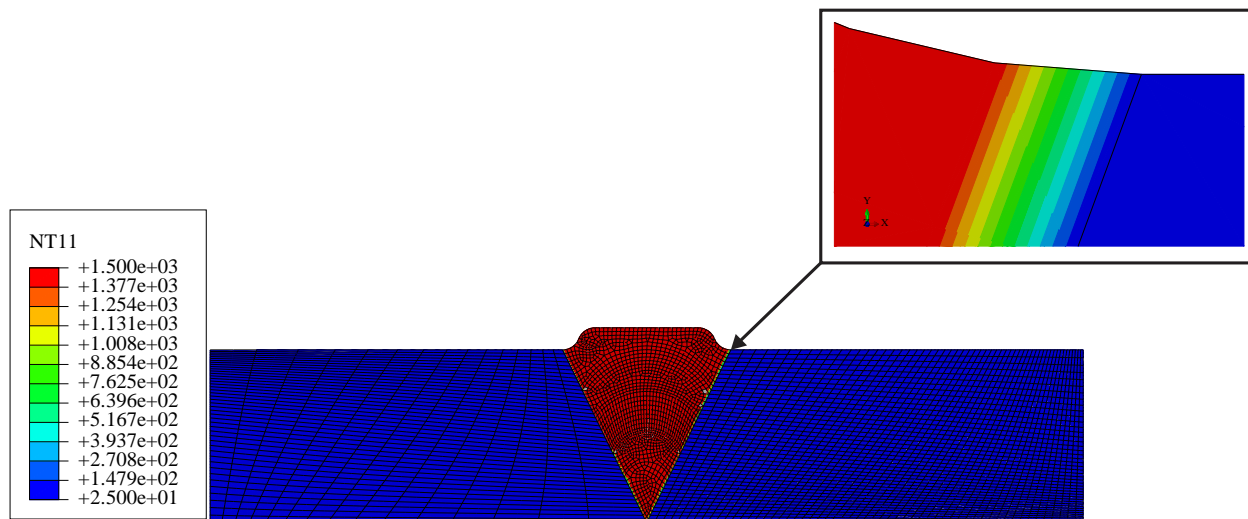


Figure 3.8 Nodal temperature distribution throughout the welded cross section

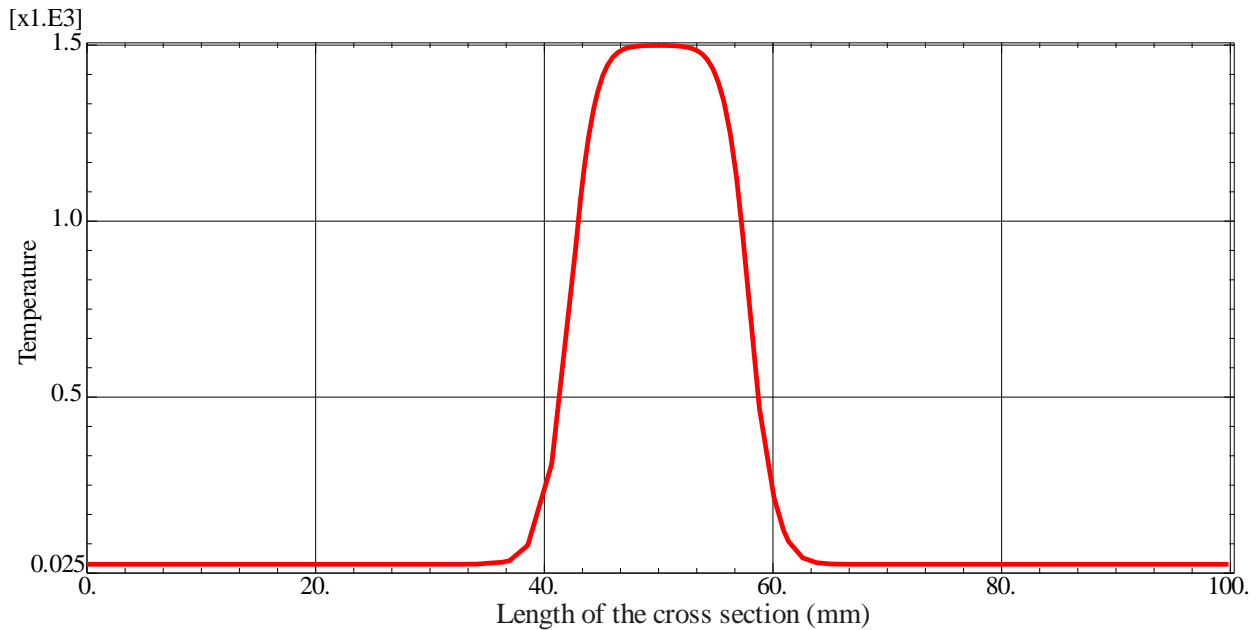


Figure 3.9 Graph of temperature distribution throughout the welded cross-section

Figure 3.9, shows the variation of the nodal temperature distribution on the welded joint at different parts, i.e. at WM, BM and HAZ. It can be seen that the maximum temperature reduces from $1500^{\circ}C$ to $25^{\circ}C$. In addition, the figure shows that cooling down rates is high from WM to B.M. and almost reaches a steady-state rate at $200^{\circ}C$. The temperature of welded metal reaches $1500^{\circ}C$; suggesting that the weld metal is melted. The heat input from the heat source to the weld metal gradually transferred to the rest part of the welded cross-sections to the HAZ and BM in all direction. The transient temperature distribution depends on the heat source movements, as the distance from heat source increases the temperature distribution is decrease; it becomes to an ambient temperature. The non-uniform distribution of temperature can result in non-uniform heat flow, which leads to the formation of the non-uniform flow of heat and the expansion and contraction during the welding sequence, which leads to the formation residual stress.

3.6.2 Welding induced residual stress results and observation

The distribution of Welding induced residual stress is shown in Figure 3.10; the figure presents the typical distribution of Welding induced residual stress due to non-uniform heat transfer during the welding process. 2D shell-type finite element model is used, the longitudinal residual stress is considered, which acts perpendicular to the weld line. The longitudinal residual stresses are tensile at the weld centerline along with the weld bead and then becoming compressive and approach to zero as the distance from the weld line on the welded cross-section increases. High tensile residual stress is balanced by compressive away from the weld bead along the transverse direction. The residual stress in weld centerline is around 300MPa, close to the yield stress of the material. Figure 3.10 shows von mises stress distribution in the welded cross-section as well as stress components parallel to the welding direction (S22), along the length of the welded cross-section (S11). The maximum longitudinal residual stress appears in the welded region.

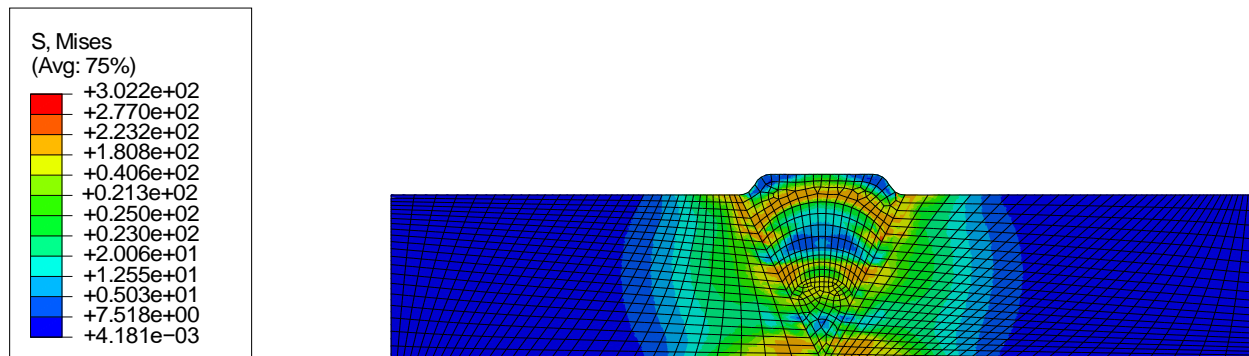


Figure 3.10 Mises stress distribution in the welded cross-section

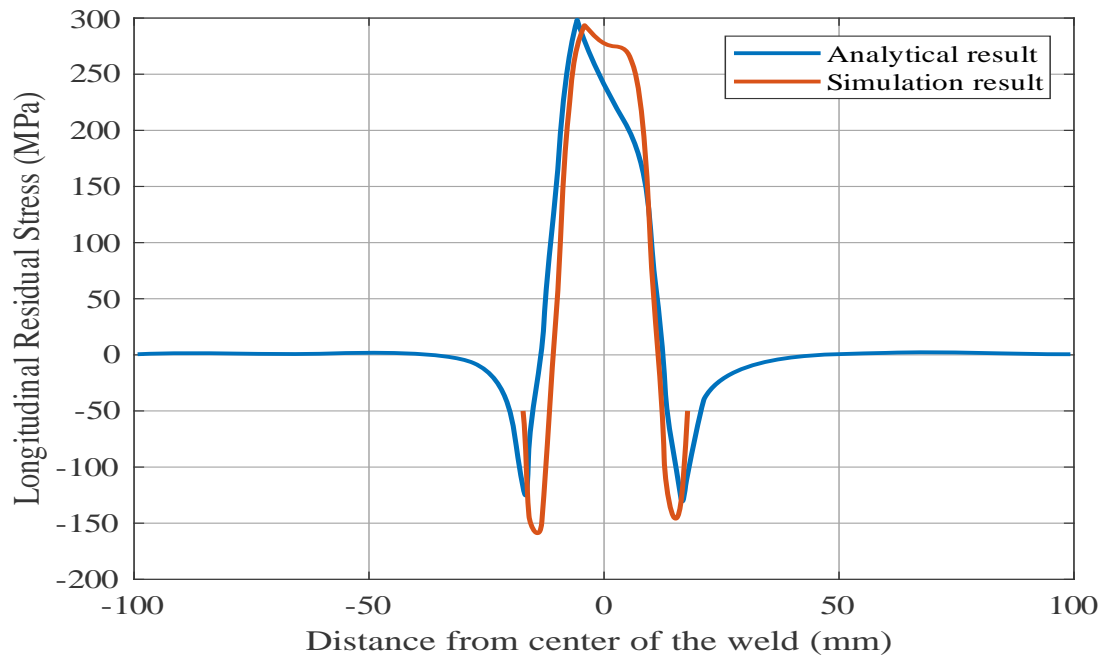


Figure 3.11 Graph of longitudinal residual stress distribution throughout the welded cross-section

The welded joint undergoing multi-pass Welding will have complex Welding induced residual stress distribution. Figure 3.11 shows the distribution of Welding induced residual stress on the concerned zone. The maximum value is around 300MPa which occur at the middle of the WM, and its minimum value around -170MPa which is compressive between WM and HAZ, this indicates that Welding induced residual stress is tensile in WM (weld bead), compressive near heat affected zone and becomes zero at the base metal region and the following points can be discussed

- The longitudinal residual stress magnitude depends on the amount of heat input during the welding process.
- The maximum Welding induced residual occurs on the weld axis along the welding direction.
- The longitudinal residual stress is tensile at weld centre and becomes compressive at the heat affected zone and in the base metal region becomes uniform and values approaches to zero

3.6.3 Comparisons and validation of results

Comparing the analytical and simulation results with experimental results, Figure 3.12 shows the results of analytical and experimental and their relationship. Experimental results by (Ren et al., 2019a) using local post-weld heat treatment (LPWHT) to measure the distribution and magnitude longitudinal residual stress the results were obtained. The relationship between the analytical results and experimental results shows linear characteristics with the correlation coefficient of $R^2 = 0.091621$. Longitudinal residual stress calculated by the analytical and experimental method is 300MPa and 268MPa, respectively. The deviation of analytical results from experimental results is due to an error during iterative computation, assumption and simplification of welding model parameters. The proposed analytical approach by Masubuchi and Martin (Arthur et al., 1980) is effective in computing the distribution of Welding induced residual stress

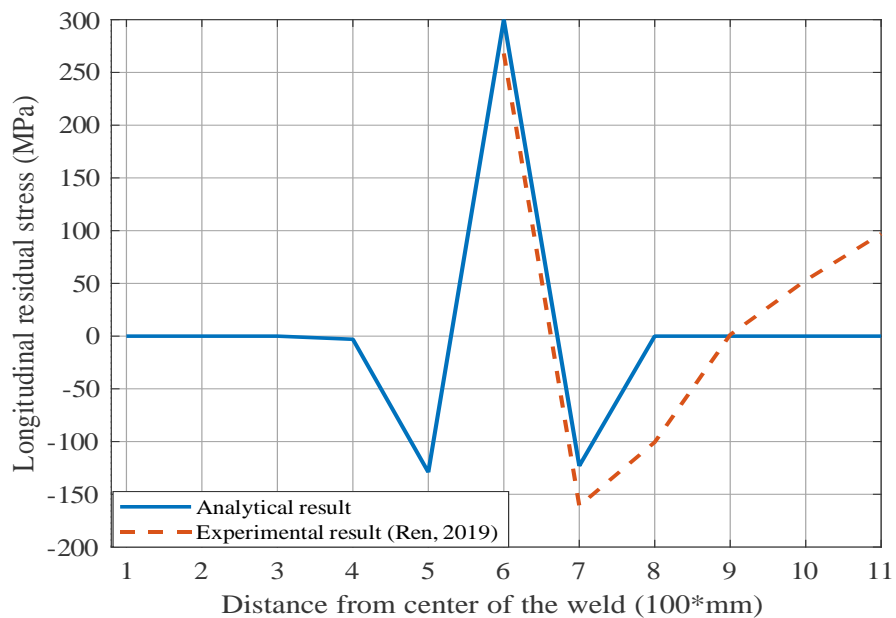


Figure 3.12 Comparison of analytical results with experimental results

Furthermore, Figure 3.13 shows the comparison of magnitude and distribution of longitudinal residual stress experimentally measured by (Ren et al., 2019a) and numerically obtained by ABAQUS 6.12 software. The numerical results reveal a slightly above than the experimental. This is due to the errors in the digitized data of thermal-dependent thermomechanical properties of 2.25Cr-1Mo, numerical accuracy during the simulation and assumed welding model parameters. Even though the deviation exists the relationship between and simulated and experimental results is linear with the correlation coefficient of $R^2 = 0.091058$

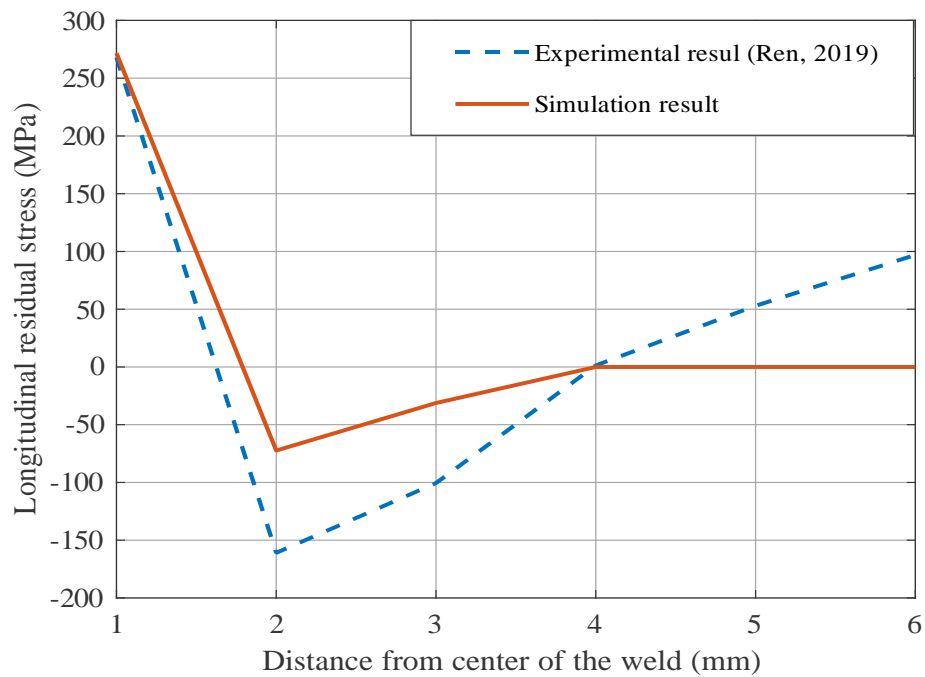


Figure 3.13 Comparison of simulation results with experimental results

CHAPTER

4

THERMOMECHANICAL STRESS ANALYSIS OF REACTOR PRESSURE VESSEL

In this chapter, the thermomechanical stress analysis of pressure vessel is performed in two approaches. 1 Analytical Approach and 2 Numerical Approach, an analytical approach, uncoupled thermomechanical stress analysis whereas in numerical approach coupled is performed. Thermo-mechanically produced stress and its distribution at different ranges of operating pressure and temperatures of a pressure vessel is analyzed. The critical stress on the welded joint of pressure vessel due to thermomechanical load is obtained.

4.1 Introduction to a pressure vessel.

A pressure vessel is a closed device used to store vapour, flammable gas, radioactive substance, or medium of reaction etc., under high temperature and pressure, which is differ from ambient temperature and pressure. Pressure vessels are mechanical structures in the shape of a cylinder, cones, spheres and their combination. There are many application areas of pressure vessels in different companies including; power plant, a petrochemical company, oil refineries, nuclear reactors and industrial plants for storing and manufacturing (Elangovan, 2019). Welding is one of the effective methods to join metal structure; most of the Pressure vessel commonly constructed using Welding. The pressure vessel manufacturing materials should have good ductility and good weldability (Baru, 2016). In nuclear power plant pressure vessels are used as a medium of a large number of chemical reactions and storing of flammable and toxic gas, must be well welded to meet very specific requirements of integrity.

The most critical part of the pressure vessel is welded joint, the welded joint with small defects under cyclic loading condition leads to failure (Adiban and Ramu, 2018). The welded joint of the pressure vessel is common to have some weld defects like porosity, residual stress, lack of penetration, etc.

A reactor pressure vessel is used as a reaction center in different companies and power plant industry and operates under different ranges of temperatures and pressure. The different temperature and pressure ranges distributed throughout the pressure vessel and causes a different impact in the weld region or weld lines, which leads to the initiation and propagation of the cracks of the pressure vessel.

The stresses produced in the pressure vessel due to internal operating pressure and temperature are radial, hoop (circumferential) and axial stresses. Axial stress acts in the thickness direction of the vessel and remains constant through-thickness, while hoop stress acts in the longitudinal direction, and the radial stress acts in the transverse direction (Hensel et al., 2017). The hoop and radial stress are can more show the effects of working internal pressure and temperature of the pressure vessel. The plane stress or plane strain assumptions were used for the analysis of thermo-mechanical stress of cylindrical pressure vessel with infinite length by many different researchers; thus the axial strain was negligible with the comparison of radial and hoop strains (Wang et al., 2015)

There are two approaches to thermomechanical stress analysis, analytical and FEM approaches. Under the analytical approach, there are coupled and uncoupled thermomechanical conduction conditions. Coupled thermo-mechanical conduction condition is the combined stresses in one system, i.e. thermal and mechanical stress considered as at the same time, which is more complex and time-consuming. Whereas uncoupled thermo-mechanical conduction condition is the combined stresses will be the summation of both mechanical and thermal stresses for radial and hoop stresses (Habib et al., 2019a). So that in this thesis, uncoupled thermo-mechanical conduction condition is considered in the analytical approach.

4.2 Benchmarking pressure vessel analysis

2.25Cr-1Mo steel is an important structural material in nuclear power plants due to high resistance to both creep and corrosion at high temperature as well as low thermal expansion coefficient (Ren et al., 2019b). The mechanical and thermal physical temperature-dependent properties is discussed in chapter three.

The thermomechanical stress analysis is performed for a reactor pressure vessel made up of 2.25Cr-1Mo low alloy ferritic steel and subjected to both thermal and mechanical loading. The design data is taken from references (Cen et al., 2019) and (Adiban and Ramu, 2018) stated in Table 4.1, which has been used in the benchmark problem for analysis. The type of Welding used in joining the shells with shell and with dish end of a reactor pressure vessel is shielded metal arc welding type. Cylindrical vertical pressure vessel with 2:1 ellipsoidal head type is considered, Schematic representation and the welded of shell section of a reactor pressure vessel is shown in Figure 4.1.

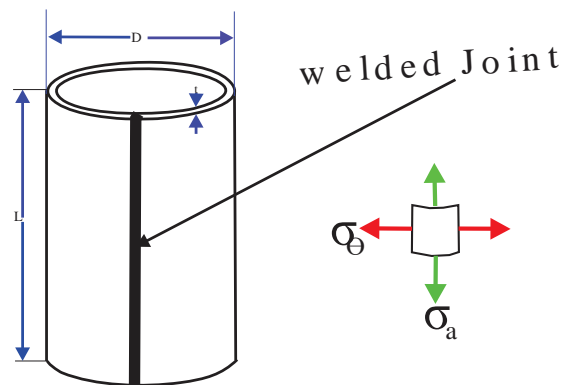


Figure 4.1 Schematic representation of vertical cylindrical pressure vessel.

Table 4.1 Dimension of the vertical cylindrical pressure vessel (Homayounfar, 2009) and (Cen et al., 2019)

Design parameter	Dimensions	Design parameters	Dimensions
Length of pressure vessel	5200mm	Maximum operating temperature	650° C
Outer diameter	2700mm	Corrosion allowance	1
Inside diameter	2640mm	Allowable stress	138MPa
Thickness of shell	30mm	Joint efficiency	0.8
Internal operating pressure	5MPa	Types of heads	2:1 Ellipsoidal head

4.3 Thermomechanical stress analysis in the analytical approach

Linear elastic fracture mechanics is considered entire this thesis. In the linear elastic behaviour of cylindrical pressure vessel uncoupled thermo-mechanical conduction condition, the combined stress will be the summation of both mechanical and thermal stresses for radial and hoop stress. Whereas the axial stress is constant throughout the wall of pressure vessel, as stated in reference (Habib et al., 2019b). So that, the coupling effect between thermal and mechanical was ignored to reduce the complexity and time during computations. In order to simplify the calculation, a cylindrical pressure vessel is taken with the weld at the center, and plane stress condition is considered.

The benchmarked pressure vessel is a thin-walled pressure vessel, based on assumption $D > 10t$; the associated stresses resulting from contained stresses are called shell membrane stress. The shell membrane stress assumed to be uniformly distributed in all direction through across the vessel and acting in radial and circumferential directions (Elamin et al., 2015). With an outer radius, r_o inner radius, r_i wall thickness t and contains internal operating pressure P_i the walls of the pressure vessel are subjected to a biaxial state stresses, i.e. the circumferential and axial directions as shown in Figure 4.1. Under the linear-elastic uncoupled thermo-mechanical stress analysis, the combined stresses will be the summation of both mechanical and thermal stresses for radial and hoop stresses which is stated in Equation (4.1).

$$\left. \begin{aligned} \sigma_r^T &= \sigma_r^m + \sigma_r^{th} \\ \sigma_\theta^T &= \sigma_\theta^m + \sigma_\theta^{th} \end{aligned} \right\} \quad (4.1)$$

Where σ_θ^T and σ_r^T the total hoop and radial stresses, respectively, σ_r^m and σ_θ^m mechanical load produced radial and hoop stresses respectively, σ_r^{th} and σ_θ^{th} thermal load produced radial and hoop stresses.

The assumption takes into account during the computations

- The thermomechanical produced stresses are uniformly distributed through the pressure vessel by neglecting holes and discontinuities.
- The axial stress is constant through the pressure vessel, which acts is in the thickness direction of the pressure vessel.

4.3.1 Mechanical stress analysis

A thin-walled reactor pressure vessel (RPV) with an internal radius r_i external radius r_o and thickness t the wall of pressure vessel subjected to stress due to internal operating of pressure. As shown in Figure 4.2, the pressure vessel under mechanical load in the form of internal pressure P_i , which results in the formation of radial and circumferential.

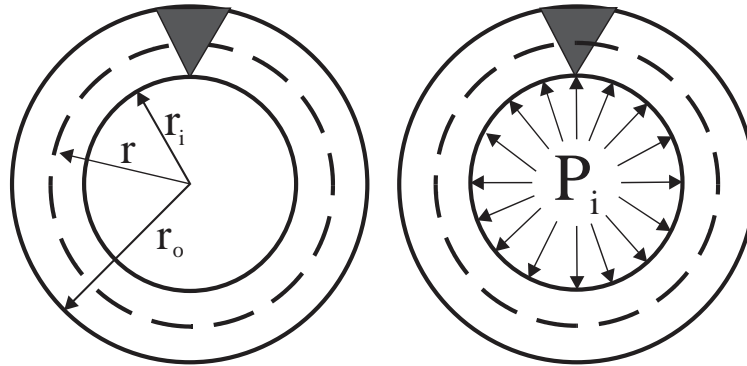


Figure 4.2 Cross-section of the shell of pressure vessel

a) Hoop (circumferential) stress

The hoop stress (σ_θ) caused by the internal operating pressure acting to expand the circumference of the pressure vessel. The hoop stress distribution is calculated by taking in to account the horizontal cut through the diametrical plane, as shown in Figure 4.3, the pressure is counteracted by hoop stress in the vessel wall. The corresponding hoop stress is expressed via lame's equation, which is stated in Equation 4.2

$$\sigma_\theta = \frac{p_i}{a^2 - 1} \left(1 + \frac{r_o^2}{r^2} \right) \quad (4.2)$$

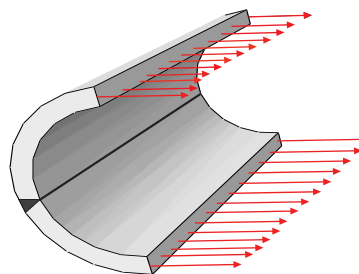


Figure 4.3 Hoop stress at the diametrical cross section

The MATLAB program is developed for above-stated Equation (4.2) to show the variation of hoop (circumferential) stress due to internal operating pressure through the thickness of the vessel and which is shown graphically in Figure 4.4. Hoop stress due to internal operating pressure is high at the innermost radius of the vessel and low at the outer radius of the vessel

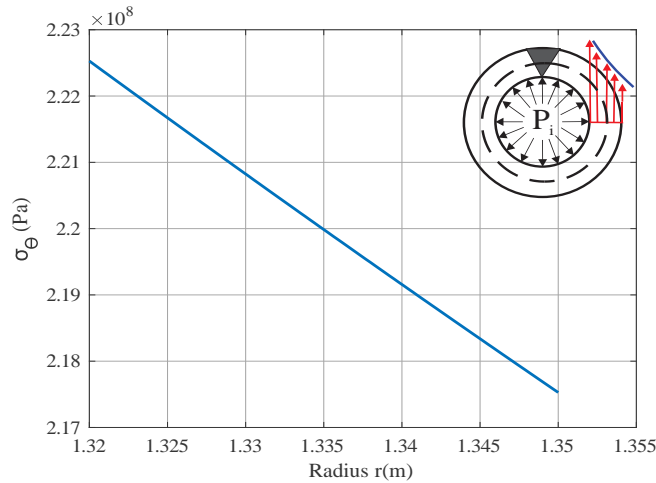


Figure 4.4 Hoop stress due to internal operating pressure through the radius of the pressure vessel

b) Radial stress

The radial stress (σ_r) caused by the internal operating pressure acting in the radial direction of the pressure vessel. The radial stress is calculated by taking in to account the radial cut through the diametrical plane, as shown in Figure 4.5. The corresponding radial stress is expressed via lame’s equation as stated in Equation (4.3)

$$\sigma_r = \frac{P_i}{a^2 - 1} \left(1 - \frac{r_o^2}{r^2} \right) \tag{4.3}$$

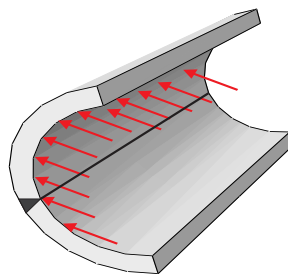


Figure 4.5 Radial stress, at the diametrical cross section

The MATLAB program is developed for the above state Equation (4.3) to show the variation of radial stress due to internal operating pressure throughout the radius of the vessel, which is shown graphically in Figure 4.4. The figure illustrates that the radial stress is compressive at the inner radius of the vessel and becomes zero at the outer radius of the vessel.

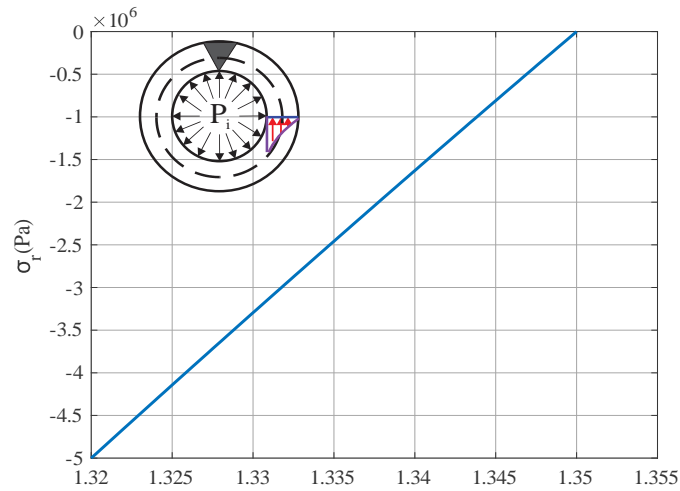


Figure 4.6 Radial stress due to internal operating pressure through the radius of the pressure vessel

4.3.2 Thermal stress analysis

The thermal loads due to the temperature variation on both sides of the wall of the vessel with T_i internal temperature and T_o external temperature, which is an ambient temperature. The wall of the cylindrical pressure vessel is subjected to a centrifugal thermal flux. In-plane stress analysis condition thermally produced stress-strain relationship can be expressed in terms of radial and circumferential stress condition. Considering a thin-walled cylindrical pressure vessel as shown in Figure 4.7, with the inner radius r_i external radius r_o and the radius r such that $r_i \leq r \leq r_o$

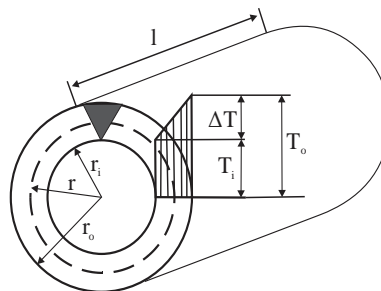


Figure 4.7 Schematic representation of the wall of pressure vessel subjected to thermal load

For one- dimensional steady state heat conduction in a cylindrical coordinate system, as shown in Figure 4.7, the temperature distribution in a cylindrical coordinate system is expressed in general solution form stated in Equation (4.5)

$$T(r) = C_1 \ln(r) + C_2 \tag{4.5}$$

With the boundary condition: - at $T(r_i) = T_i$ and $T(r_o) = T_o$

By applying boundary condition to the Equation (4.5) in terms of T_i and T_o it becomes as stated in Equation (4.6).

$$\left. \begin{aligned} T_i &= C_1 + \ln(r_i) + C_2 \\ T_o &= C_1 + \ln(r_o) + C_2 \end{aligned} \right\} \tag{4.6}$$

Solving for C_1 and C_2 , it becomes

$$\left. \begin{aligned} C_1 &= \frac{\Delta T}{\ln\left(\frac{r_o}{r_i}\right)} \\ C_2 &= T_o - \frac{\Delta T}{\ln\left(\frac{r_o}{r_i}\right)} \ln(r_o) \end{aligned} \right\} \tag{4.7}$$

Substituting the values of C_1 and C_2 of Equation (4.7) into the general Equation (4.5), gives the temperature variation of the vessel through the radius is in the function of radius r from the centre of the vessel and as stated in Equation (4.8)

$$T(r) = \frac{T_i - T_o}{\ln\left(\frac{r_i}{r_o}\right)} \ln\left(\frac{r}{r_o}\right) + T_o \tag{4.8}$$

Where $T(r)$ the radial function of the temperature that is distributed in the radius of the cylindrical pressure vessel.

The MATLAB program is developed for above stated Equation (4.8), to show the temperature variation with the radius of pressure vessel, which is shown in Figure 4.9, the maximum temperatures are at the most inner radius of the vessel and the minimum is at the outer radius of the vessel, which is equal to the ambient temperature.

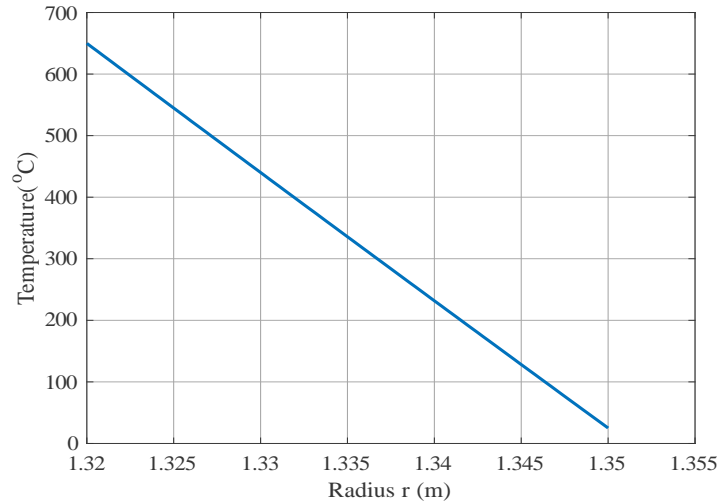


Figure 4.8 Temperature variation with the radius of pressure vessel

Thermally produced hoop and radial stresses will derive as the following

The circumference of the cylinder corresponding to radius r is given by Equation (4.4)

$$s = 2\pi r \quad (4.4)$$

The heat flux crossing the surface is given by Equation (4.5)

$$q = ks \frac{dT}{dr} \quad (4.5)$$

Where $\frac{dT}{dr}$ is temperature gradient and k is thermal conductivity coefficient, thus from

Equations (4.4 and 4.5) dT is given by Equation (4.6)

$$dT = \frac{qdr}{k2\pi r} \quad (4.6)$$

Integrating Equation 4.6, both sides it gives the temperature distribution at a given radius r , as stated in Equation (4.7)

$$T = \frac{q}{2\pi k} \ln r + C \quad (4.7)$$

Where C is an integration constant

By indicating that ΔT is the temperature difference between T_i and T_o internal and external temperature corresponding to r_i and r_o respectively thus ΔT is given by Equation (4.8)

$$\Delta T = T_i - T_o = \frac{q}{2\pi k} (\ln r_i - \ln r_o) = \frac{q}{2\pi k} \left(\ln \frac{r_o}{r_i} \right) \quad (4.8)$$

From Equation (4.6), $\frac{q}{2\pi k}$ is given by Equation (4.9)

$$\frac{q}{2\pi k} = r \frac{dT}{dr} \quad (4.9)$$

Inserting Equation (4.9) into Equation (4.8), the rate of change of temperature across the wall thickness of pressure the vessel is, given by Equation (4.10)

$$\frac{dT}{dr} = \frac{\Delta T}{r \left(\ln \left(\frac{r_o}{r_i} \right) \right)} \quad (4.10)$$

To compute the stresses on the cylinder due to the effect of ΔT according to (Donatello Annaratone, 2012), which is stated in Equation (4.11).

$$\left. \begin{aligned} \sigma_\theta - \sigma_r - r \frac{d\sigma_r}{dr} &= 0 \\ \varepsilon_r - \varepsilon_\theta - r \frac{d\varepsilon_\theta}{dr} &= 0 \end{aligned} \right\} \quad (4.11)$$

Where, σ_θ , σ_r , ε_r and ε_θ is hoop stress, radial stress, radial strain and hoop strain respectively.

From Equations (4.10, 4.11), the hoop and radial stresses produced due to temperature difference in a cylindrical pressure vessel at a distance r are given in Equation (4.12 and 4.13) respectively.

Where, in the expressions $a = \frac{r_o}{r_i}$ and $z = \frac{E\alpha\Delta T}{2(1-\nu)}$ E , α and ν is young modulus, thermal expansion coefficient and Poisson's ratio respectively

$$\sigma_{\theta}^{th} = z \left[\frac{(a)^2 - \left(\frac{r_o}{r}\right)^2}{(a)^2 - 1} - \frac{\ln\left(\frac{r}{r_i}\right)}{\ln(a)} \right] \quad (4.12)$$

$$\sigma_r^{th} = z \left[\frac{(a)^2 + \left(\frac{r_o}{r}\right)^2}{(a)^2 - 1} - \frac{1 + \ln\left(\frac{r}{r_i}\right)}{\ln(a)} \right] \quad (4.13)$$

a) Hoop (circumferential) stress

The thermal produced hoop stress (σ_{θ}^{th}) is caused by when the inner surface of the cylindrical pressure vessel is exposed to uniform heat flux, and the outer surface is exposed to airstream at T_o which causes the expansion of the circumference of the pressure vessel. The change in uniform heat distribution is responded by the formation of hoop stress in the pressure vessel wall. The corresponding thermally produced hoop stress was derived and expressed in terms of Lamé's equation which is stated in Equation (4.14).

$$\sigma_{\theta}^{th} = z \left[\frac{(a)^2 - \left(\frac{r_o}{r}\right)^2}{(a)^2 - 1} - \frac{\ln\left(\frac{r}{r_i}\right)}{\ln(a)} \right] \quad (4.14)$$

The MATLAB program is developed for above-stated Equation (4.14), to show thermally produced hoop (circumferential) stress variation throughout the radius of the pressure vessel at different temperature ranges as shown in Figure (4.10), which is increases as the temperature increase.

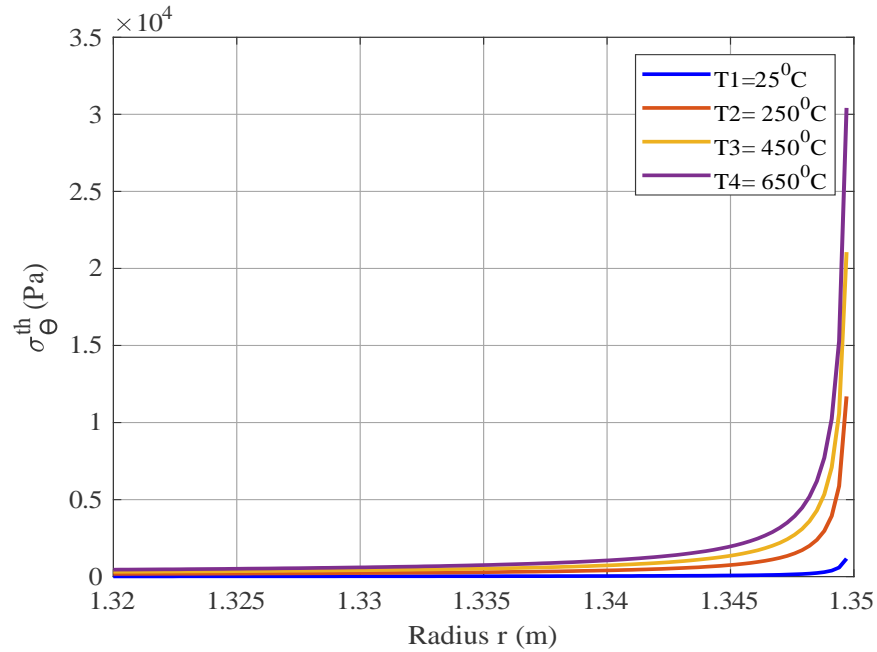


Figure 4.9 Thermal produced hoop stress variation with the radius of the pressure vessel at different temperature ranges

b) Radial stress

The thermal produced radial stress (σ_r^{th}) is caused by uniform distributed heat flux in the radial direction of the pressure vessel. The corresponding thermally produced radial stress equation was derived and expressed in terms of lame’s equation as stated in Equation (4.15)

$$\sigma_r^{th} = z \left[\frac{(a)^2 + \left(\frac{r_o}{r}\right)^2}{(a)^2 - 1} - \frac{1 + \ln\left(\frac{r}{r_i}\right)}{\ln(a)} \right] \quad (4.15)$$

The MATLAB program is developed for above-stated Equation (4.15) to show thermally produced radial stress distribution throughout the radius of the vessel as shown in Figure 4.11, which is compressive at the highest working temperature of the vessel and it becomes constant at the outermost surface of the vessel.

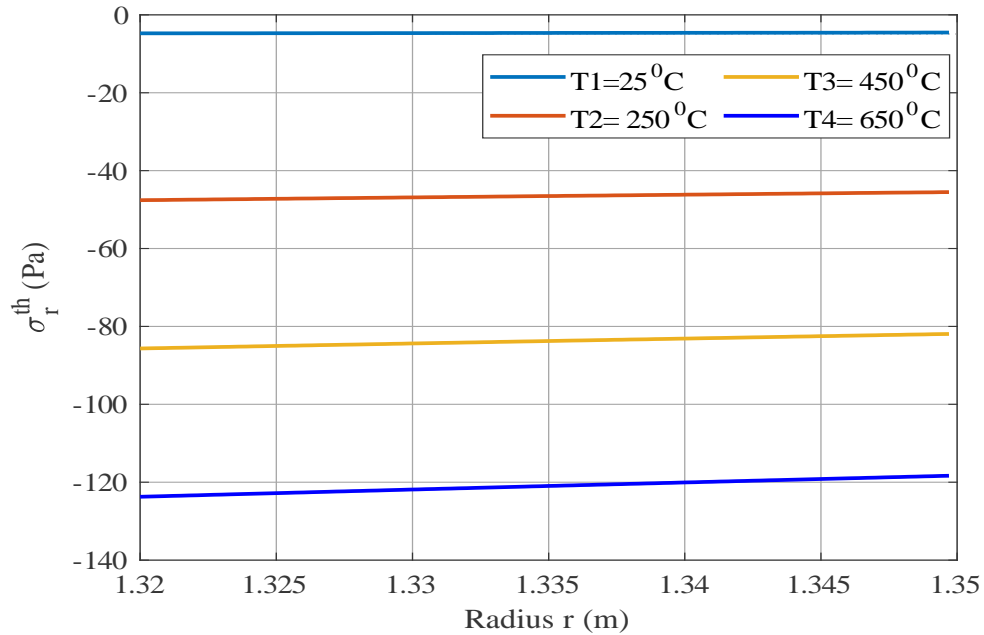


Figure 4.10 Thermal produced radial stress variation with the radius of the pressure vessel at different temperature

From the expression of uncoupled thermo-mechanical stress analysis, the combined stresses will be the summation of both mechanical and thermal stresses for radial and hoop stresses which is stated in Equation (4.16).

$$\left. \begin{aligned} \sigma_r^T &= \sigma_r^m + \sigma_r^{th} \\ \sigma_\theta^T &= \sigma_\theta^m + \sigma_\theta^{th} \end{aligned} \right\} \quad (4.16)$$

The total uncoupled thermomechanical stresses numerically after substitution all values into the assigned formulas, can be

$$\left. \begin{aligned} \text{At } (r = 1.32m) \quad \sigma_r^T &= -5MPa \\ \sigma_\theta^T &= 222.5MPa \end{aligned} \right\} \text{ and at } (r = 1.35m) \quad \left. \begin{aligned} \sigma_r^T &= -12.3Pa \\ \sigma_\theta^T &= 217.5MPa \end{aligned} \right\}$$

4.4 Finite element methods

Cylindrical reactor pressure vessel which is subjected to both mechanical and thermal loadings; the thermomechanical coupled FE model is performed to verify the analytical solutions. In finite element analysis, 2D axisymmetric element model using ABAQUS 6.12 is employed. The benchmarked problem is a reactor pressure vessel used in nuclear power plant with an internal working pressure of 5MPa , External diameter $D_o = 2700\text{mm}$, the thickness of $t = 30\text{mm}$ and 2D FE model is used to avoid the analysis of the whole vessel and to reduce the time of the simulation. The mechanical, thermal physical property temperature-dependent of 2.25Cr-1Mo low alloy ferritic steel is taken as a function varying with temperature to discretize the exponential gradient properties of the material with a more accurate manner.

Figure 4.11, shows the finite element meshing of the cross-section of the pressure vessel and the type of element is CPS4T (A 4-node plane stress thermally coupled quadrilateral, bilinear displacement and temperature.), the model meshed into 1006560 elements and 1023336 nodes. As the stresses varying through the thickness of the pressure vessel in the radial and circumferential directions to get more results that are accurate, the finer meshing is applied. The thin-walled cylindrical pressure vessel, the stress distribution due to thermo-mechanical stress through the thickness of vessel graphically presented. Finally, the finite element results compared with analytical results.

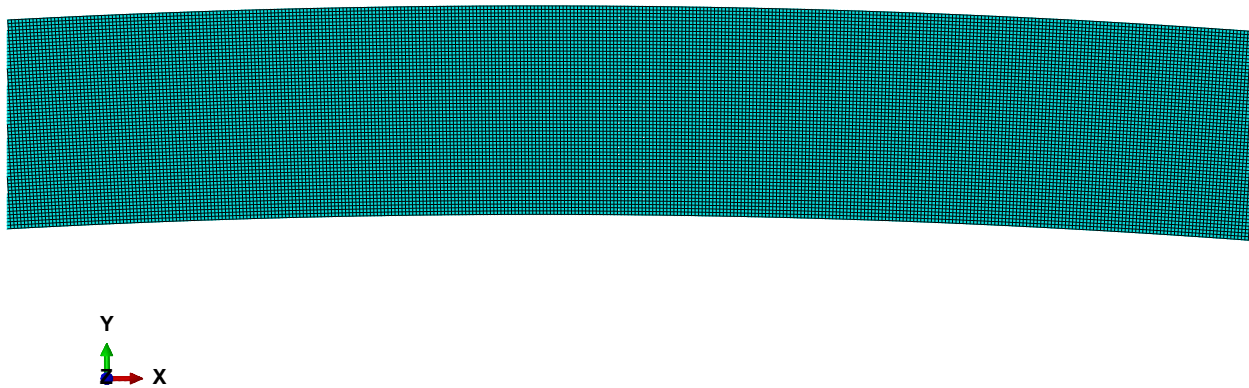


Figure 4.11 Mesh of the cross section of cylindrical pressure vessel

4.5 Result and discussion

4.5.1 Results

When the cylindrical reactor pressure vessel used in the nuclear energy power plant is subjected to the inner operating pressure of $5MPa$ and the maximum operating temperature of $650^{\circ}C$ the hoop stress ($s, s_{22}(scys-1)$) and radial stress ($s, s_{11}(csys-1)$) generated in the cylindrical pressure vessel.

a. Hoop (circumferential) stress

The internal operating pressure and temperature produces hoop stress ($s, s_{22}(scys-1)$) tensile at the most inner radius of the cylindrical pressure vessel and decreases gradually from the inner surfaces to the outer surface as shown in Figure 4.12, which $223MPa$ at the inner surface and $218MPa$ at the outer surface of the pressure vessel.

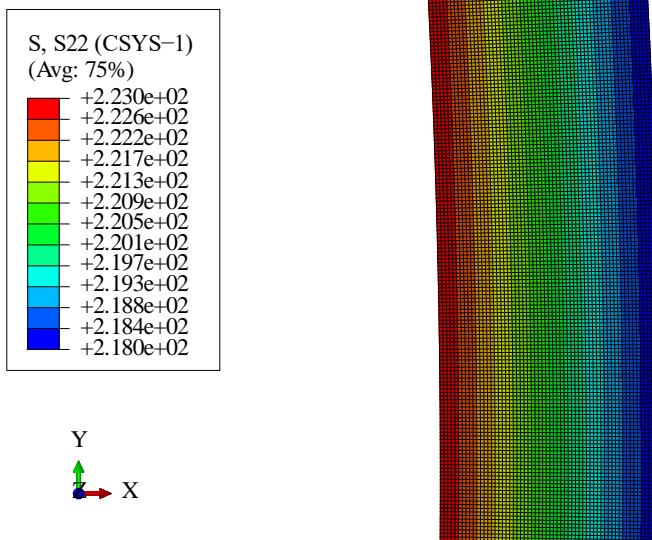


Figure 4.12 Hoop stress distribution through the radius of pressure vessel

b. Radial stress

The radial stress ($s, s_{11}(csys-1)$) is caused due to the internal operating pressure and temperature is compressive more at the inner surface of, and it becomes zero at the outer surface of the pressure vessel as shown in Figure 4.13. In the inner, surface ($-4.968MPa$) which is equal to the internal operating pressure and in the outer surface ($-0.0342MPa$), which is almost equal to zero at the outer surface, radial stress acts in the transversal direction, which is in the same direction of transverse welding induced residual stress. So that radial stress can add the stress effect on the transverse welding induced residual stress of welded joint of the shell of the cylindrical pressure vessel.

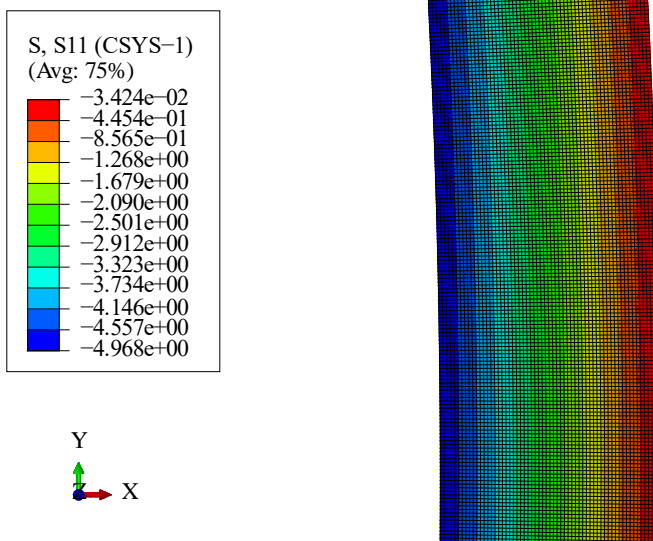


Figure 4.13 Radial stress distribution through the radius of the pressure vessel

4.5.2 Discussions

In this chapter both analytical and FEM, approaches have been developed for thermomechanical stress analysis of an internally pressurized thin-walled cylindrical pressure vessel with the inner surface is subjected to uniform heat flux and the outer surface is subjected to airstream temperature. In the case of an analytical approach, uncoupled thermomechanical stress analysis is performed because to reduce complexity and reducing the time of computation, whereas, in FEM, the coupled thermo-mechanical stress analysis is performed.

2D axisymmetric FE model has been performed, to investigate produced hoop and radial stresses due to the internal operating pressure and temperature in the wall of the vessel. In addition, the effects of these stresses on the welding induced residual stress of welded joint of the shell of the pressure vessel are analyzed. According to both the analytical and FEM simulated the following points discussed.

The hoop stress determined by the analytical solution and FEM is shown in Figure 4.14. In this figure, it can be seen that the analytical solution agrees with the FEM results. The error between two graphs of hoop stresses is less than 10% because the analysis conducted by FEM has some errors due to numerical accuracy of the software. Generally, the analytical solution is good agreement with the FEM solution.

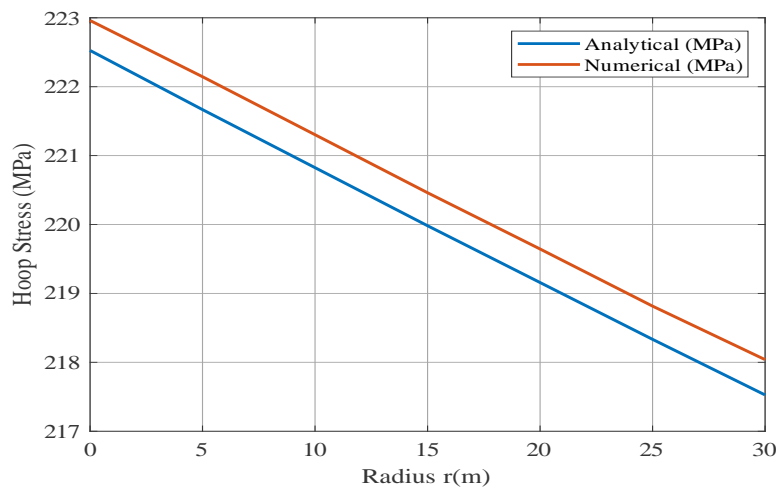


Figure 4.14 variation of hoop stress with cylindrical pressure vessel radius

The radial stress determined by the analytical solution and FEM is shown in Figure 4.15, in this figure it can be seen that the analytical solution and FEM solution almost the same with the error of less than 8% , these illustrate that the analytical solutions good agreement with FEM solutions.

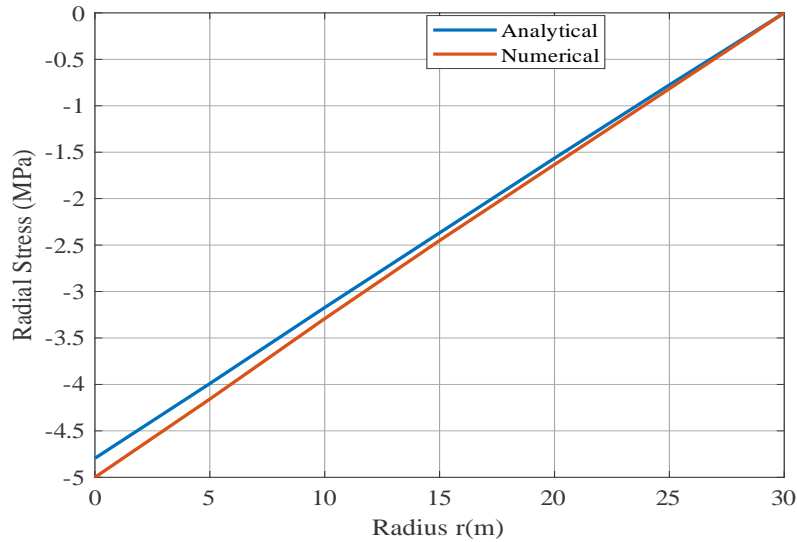


Figure 4.15 Variation of radial stresses with the cylindrical pressure vessel radius

Furthermore, the direction of the hoop (circumferential) stress acts perpendicular to the longitudinal direction of cylindrical pressure vessel, the radial stress acts in the radial direction whereas the axial stress acts in the thickness direction of the cylindrical pressure vessel and which remains constant through the thickness.

CHAPTER

5

THERMOMECHANICAL FATIGUE MODELLING

This chapter presents the approaches of modelling of thermomechanical fatigue of reactor pressure vessel. Two types of modelling approaches to modelling of thermomechanical fatigue of reactor pressure vessel was used. 1) Analytical modelling and 2) Finite element modelling was considered. Fatigue crack growth rate equation proposed by Forman is used to predict the fatigue life of reactor pressure vessel, and the rate of fatigue crack growth of welded joint of pressure vessel with different stress intensity factor was modelled. Thermomechanical overview and fatigue crack growth modelling are presented first. Then, the fatigue life prediction is presented.

5.1 Overview of Thermomechanical fatigue

Thermomechanical Fatigue (TMF) is a combined failure mechanism, which is caused by cyclic thermal and mechanical loading. Thermomechanical fatigue concept was investigated early of the 1970s, which is used to simulate loading conditions of the turbine blade (Stekovic, 2007). Under thermal loading condition, stresses are developed under thermal cycling without the effect of the external loading. While under thermomechanical fatigue conditions, stresses are developed under a simultaneous change in temperature and mechanical strains. The temperature in thermomechanical fatigue varying cyclically. According to thermomechanical testing which consists two phases, i.e. in-phase and out of phase, in-phase when the maximum temperature of the cycle coincides with peak tensile strain and out of phase when the maximum temperature of the cycle is, and maximum compressive strain coincide.

Thermomechanical fatigue loading condition during the operation of the reactor pressure vessel is a cyclic start-up and shutdown operations, and alternating stresses are being developed in the reactor pressure vessel. The condition, which used for fatigue evaluation are peak and valley as shown in Figure 5.1 and illustrating as the following

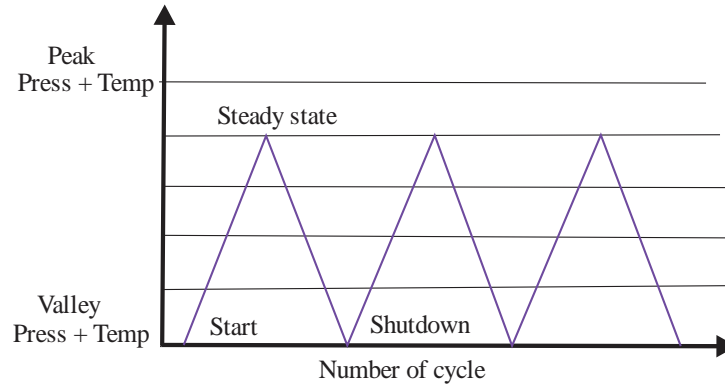


Figure 5.1 Fatigue cycle of reactor pressure vessel

- When the reactor pressure vessel has just started the temperature inside the reactor vessel is increasing ($25^{\circ}C - 250^{\circ}C$) which is starting from ambient temperature; the thermal load case 1 condition will arise, the temperature inside the reactor pressure vessel becomes increasing.
- Once the steady-state condition is attained after the reaction operation is started the temperature inside the reactor pressure vessel attains its maximum state, which is $650^{\circ}C$.

Reactor pressure vessel consists two types of load cases as stated in Table 5.1, which are mechanical and thermal loads; mechanical load includes; operating pressures, the weight of the vessel and weight of other attachments to the vessel. Besides, the thermal load include the maximum and minimum operating temperature of the reactor pressure vessel. However, in this thesis, only pressure and operating temperatures are considered, both mechanical and thermal loads are evaluated for which fatigue life to be determined.

Table 5.1 Loads cases of reactor pressure vessel

Types of loads	Values	
	Maximum	Minimum
Mechanical	5MPa	Ambient
Thermal	650°C	25°C

5.2 Fatigue crack growth modelling

Typical failures in welded joints of engineering structures are due to geometrical discontinuity, manufacturing defects and local mismatch in the strength when different materials welded together (Kumar et al., 2019). Fatigue crack growth of welded joint occurs due to cyclic loading condition with cracks growing a given increment (Δa) in a given number of cycle (ΔN), and the final failure occurs when the size of the crack reaches a critical level, and the crack growth becomes unstable. According to the linear elastic fracture mechanics (LEFM), the plastic deformation near the crack tip is controlled by the stress intensity factor range, which depends on modes of loading.

5.2.1 Modes of loading

Commonly there are three types of modes of loading on the cracked body, namely mode *I*, *II* and *III* which are shown in Figure 5.2, Mode *I* is tensile or opening mode, the applied load is pulls apart the crack faces. Mode *II* is sliding or in-plane sliding mode, i.e. faces are sheared forwards and backwards. Mode *III* is the tearing or anti-plane shear mode, i.e. faces are sheared sideways. Many engineering structures are subjected to all of these three modes of load-carrying may occur. In this thesis work of crack growth of welded joint of reactor pressure vessel, only mode *I* loading condition is considered.

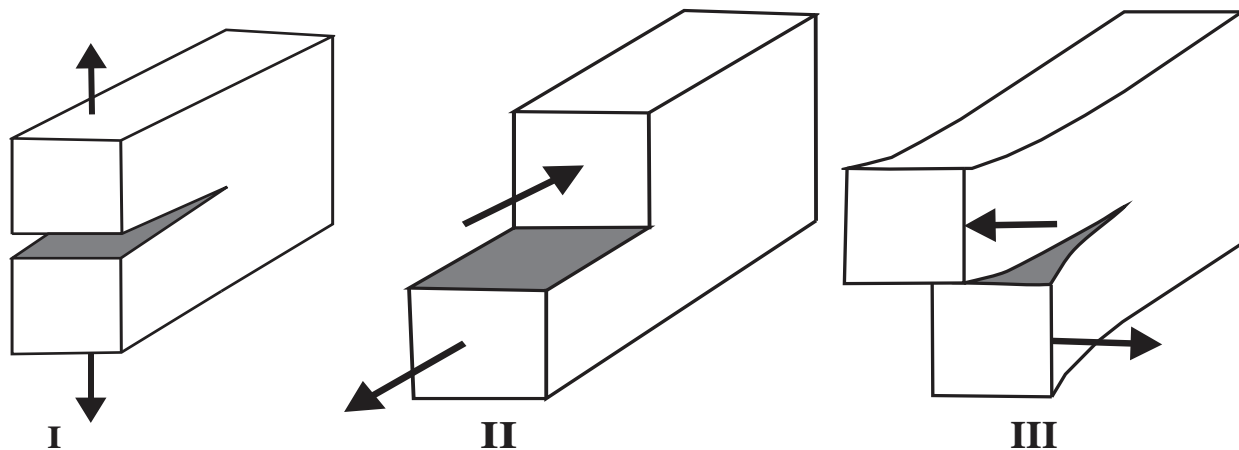


Figure 5.2 Three modes of loading that can be applied to a crack

5.2.2 Stress intensity factor of mechanical load

Based on linear elastic fracture mechanics, which is focus on the analyzing of the structures containing an initial crack due to that affects the load-carrying capacity of engineering structures. In the welded joint of reactor pressure vessels, there are two types of crack orientation are there, i.e. circumferential crack and longitudinal crack according to (Adiban and Ramu, 2018) and shown in Figure 5.3 a and b, respectively. Circumferential cracks occur along the circumference direction of pressure vessel when the welded joint is highly restrained, whereas longitudinal crack is parallel to the welding direction, and more commonly found than circumferential crack.

The initial cracks, which are shown in Figure 5.3, can be created during service life and by fatigue, or during the manufacturing process like welding. During welding, the heat input results in the formation of residual stress; cracks formed due to welding induced residual stress mainly controlled by stress intensity factor. The stress intensity factors due to mechanical load (internal operating pressure) at the crack tip that depends on the applied load, the initial crack length and geometrical configuration of the cracked shell of vessel and which is derived as the following. There is an initial crack in the welded joint at the internal side of the reactor pressure vessel with an initial crack length of (a), internal radius (r_i), the thickness of the shell of the vessel (t) and internal operating pressure (P).

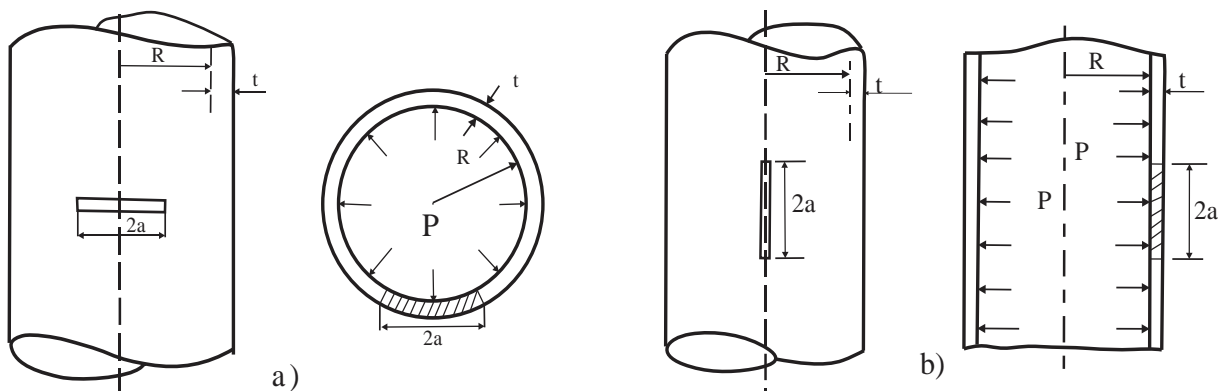


Figure 5.3 a) Circumferential crack and b) longitudinal crack configuration of welded joint

The stress due to internal operating pressure which is used to derive stress intensity factor is for the longitudinal crack type is given by Equation (5.2) and the internal operating pressure ($p = 5MPa$), internal radius ($r_i = 1320mm$), the thickness of the shell ($t = 30mm$) and the initial crack length ($a = 4mm$) are used.

$$\sigma = p \times \frac{r_i}{t} \quad (5.2)$$

$$K_I = \sigma \sqrt{\pi a} \times f(\lambda) \quad (5.3)$$

Where $\lambda = \frac{a}{\sqrt{r_i t}} = \frac{1}{\sqrt{1320mm \times 30mm}} = 2.52 \times 10^{-5}$ and $f(\lambda) = \begin{cases} (1+1.25\lambda^2)^2 & \text{for } 0 \leq \lambda \leq 1 \\ (0.6+0.9\lambda) & \text{for } 1 \leq \lambda \leq 5 \end{cases}$

In the same manner, the stress due to internal operating pressure which is used to derive the stress intensity factor circumferential crack type is given by Equation (5.4) depending on reference (Paul C. Paris and Hiroshi Tada, 2000) for both types of crack orientation.

$$\sigma = \frac{1}{2} \times p \times \frac{r_i}{t} \quad (5.4)$$

$$K_I = \sigma \sqrt{\pi a} \times f(\lambda) \quad (5.5)$$

Where $\lambda = \frac{a}{\sqrt{r_i t}} = \frac{1}{\sqrt{1320mm \times 30mm}} = 2.52 \times 10^{-5}$ and $f(\lambda) = \begin{cases} (1+0.3225\lambda^2)^2 & \text{for } 0 \leq \lambda \leq 1 \\ (0.9+0.25\lambda) & \text{for } 1 \leq \lambda \leq 5 \end{cases}$

Therefore, the stress intensity factor for two types of cracks numerically after substitution all values into the assigned formulas in Equations (5.3 and 5.5), can be

$$K_I = 225MPa\sqrt{\pi a} \text{ for longitudinal crack type}$$

$$K_I = 112.5MPa\sqrt{\pi a} \text{ for circumferential crack type}$$

5.2.3 Residual stress intensity factor

Determination of crack tip stress intensity factor (SIF) due to welding induced residual stress is the necessary part in welded joint analysis (Bao et al., 2010b). The welded joint induced residual stress intensity factor can be calculated by using a weight function method and finite element method. The stress intensity factor usually depends on many parameters, but it is more dependent on crack length (i.e. stress intensity factor increases as the crack size increases and crack length increases) (Adiban and Ramu, 2018). In this thesis work, linear elastic material behaviour is considered, according to the linear elastic fracture mechanics (LEFM) approach, the superposition principle is frequently utilized to evaluate the stress intensity factor (SIF). For a reliable prediction of fatigue crack growth rate, accurate estimation of SIF is needed (Gadallah et al., 2018b).

Residual stress is self-balanced, built-in field, which requires no special treatment when using the weight function method (WFM). The method is based on the superposition principle (i.e. The stress system due to two or more loads acting together is equal to the sum of the stresses due to each load acting separately) (Bao et al., 2010a). In Fig 5.4, two-dimensional plane stress problems of a crack length (a) in an infinite length shell of the vessel is subjected to an arbitrary symmetrical loading can be solved providing that certain results are known for one symmetrical loading

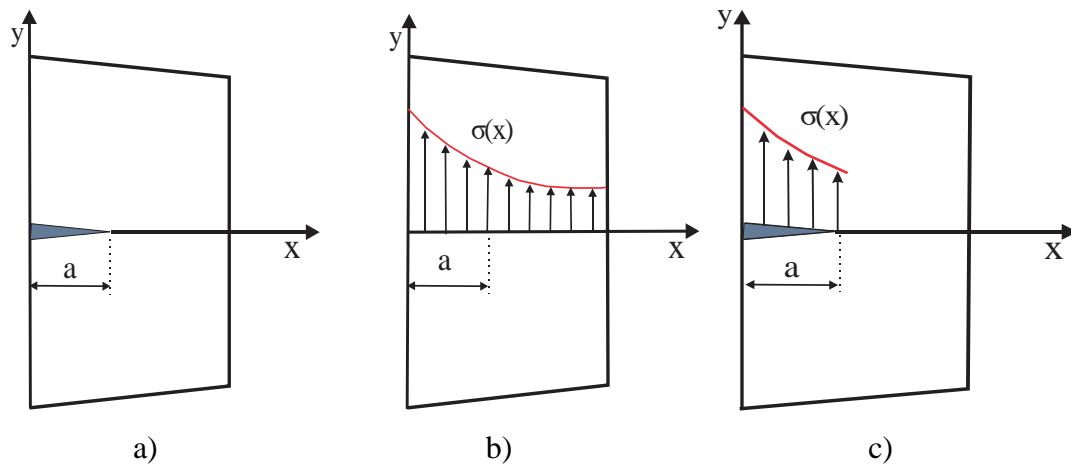


Figure 5.4 Schematic illustration of the principle of super position

Weight function method

The weight function is an analytic method which is developed for an existing crack to determine stress intensity factor (SIF) from the stress distribution over the cracked faces (Al-Mukhtar, 2013). The weight function method for the determination of stress intensity factor (SIF) is based on the principle of the superposition principle, as shown in Figure 5.5, i.e. by considering one-dimensional crack, the stress intensity for the cracked shell of the vessel in Figure 5.3a, subjected to internal loading is the same as the stress intensity factor in the geometrically identical body in Figure 5.5c

For two-dimensional plane stress problem analysis mode-I crack growth, i.e. the stress is acting normal to the crack face and acting perpendicular to the crack growth direction. The arbitrary stress distribution intensity factor (SIF) can be calculated by integrating weight function $m(x, a)$, and the stress distribution normal to the crack ($\sigma(x)$) is given by Equation (5.6)

$$k_I(a) = \int_0^a m(x, a) \sigma(x) dx \quad (5.6)$$

Where a is the initial crack length in Figure 5.5, $\sigma(x)$ the stress over the crack site in un-cracked site body $m(x, a)$ the weight function that independent of $\sigma(x)$ which is given by Equation (5.7)

$$m(x, a) = \frac{8G}{1+k} \frac{1}{K_I^{(1)}} \frac{\partial v^{(1)}}{\partial a} \quad (5.7)$$

The proposed weight function method is an analytic technique for deriving stress intensity factor from known of the stress distributions in the un-cracked body (Bao et al., 2010a). So that from integrating Equations (5.6 and 5.7), the stress intensity factor due to welding induced residual stress is given by Equation (5.8).

$$k_{res} = \sigma_o \sqrt{\pi a e}^{-0.42 \left(\frac{a}{c}\right)^2} \left[1 - \frac{1}{\pi} \left(\frac{a}{c}\right)^2 \right] \quad (5.8)$$

Where a is the initial crack length and a/c , crack aspect ratio

The MATLAB program is developed to compute the above-explained Equation (5.8), for various crack aspect ratio values to show the variation of residual stress intensity factor at different crack aspect ratio with respect to crack length is shown in Figure 5.5 and as the crack length increases the residual stress intensity factor is decrease.

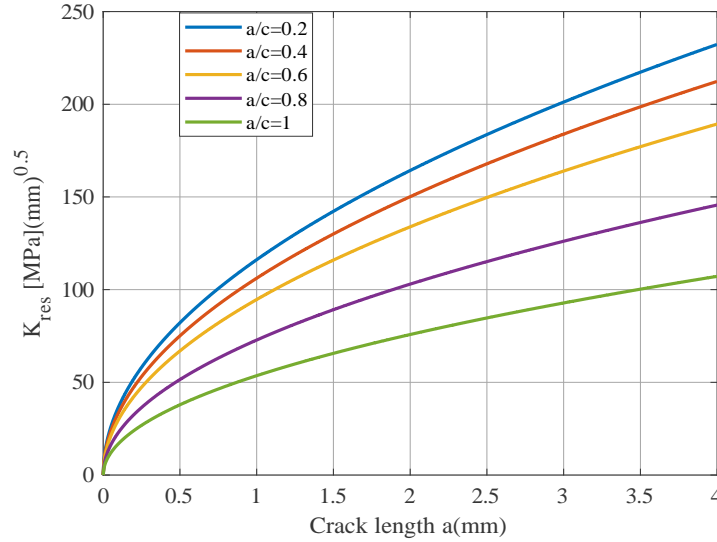


Figure 5.5 Residual stress variation at the different crack aspect ratio

5.2.4 Fatigue crack growth rate due to mechanical load

The crack growth rate, which is used to describe the fatigue, crack propagation behaviour of mechanical structures subjected to an initial crack. There are different mathematical equation exist to express the relationship between the crack and growth rate. Some of them are proposed by Paris-Erdogan, Forman and walker (Akramin et al., 2020), and their equations are given by Equations (5.9, 5.10 and 5.11) respectively.

$$\frac{da}{dN} = C(\Delta k)^m \quad (5.9)$$

$$\frac{da}{dN} = \frac{C}{(1-R)k_c - \Delta k} \times (\Delta k)^m \quad (5.10)$$

$$\frac{da}{dN} = C \left(\frac{\Delta k}{(1-R)^{1-\gamma}} \right)^m \quad (5.11)$$

Where $\frac{da}{dN}$ is the crack growth rate, Δk is stress intensity factor, R is stress ration and C , m and γ are material constant. To analyze the fatigue crack growth rate of welded joint of reactor pressure vessel the equation proposed by Forman is used to describe the effects of residual stress on the fatigue of reactor pressure vessel and crack growth behaviour in the region *III* in S-N curve.

The mutual effect applied to internal operating pressure and the welding induced residual stress on the crack tip stress field can be derived as follow, the selected mathematical equation by Forman is stated in Equation (5.12)

$$\frac{da}{dN} = \frac{C}{(1-R)k_c - \Delta k} \times (\Delta k)^m \quad (5.12)$$

Where Δk stress intensity factor range and R is stress ratio which is given by Equations (5.12 and 5.13) respectively

$$\left. \begin{aligned} \Delta k &= k_{tot\ max} - k_{tot\ min} \\ &= (k_{app\ max} + k_{res}) - (k_{app\ min} + k_{res}) \\ &= (\Delta k) \end{aligned} \right\} \quad (5.12)$$

$$R = \left. \frac{k_{app\ min} + k_{res}}{k_{app\ max} + k_{res}} \right\} \quad (5.13)$$

And K_c is fracture toughness of 2.25Cr-1Mo low alloy ferritic steel, which is $45MPa\sqrt{m}$ taken from reference (WADA, 2002). The stress intensity factor not the same at the crack tip, due to the presence of welding induced residual stress, so in the presence of residual stress the crack growth rate equation is transferred to the more convenient for numerical analysis and stated in Equation (5.14).

$$\frac{da}{dN} = \frac{C}{k_R} \times (\Delta k)^m \quad (5.14)$$

Where
$$k_R = \frac{k_c}{k_{app,minn}} - 1 = R \left(\frac{k_c - k_{app,max}}{k_{app,min}} \right)$$

The MATLAB program is developed compute the above-explained Equation (5.14), for applied mechanical load and welding induced residual stresses values to show the rate of crack growth with respect to stress intensity factors as shown in Figure 5.6 log-log scale. The figure illustrates that the crack growth rate is high in the presence of welding induced residuals tress than without considering residual stress.

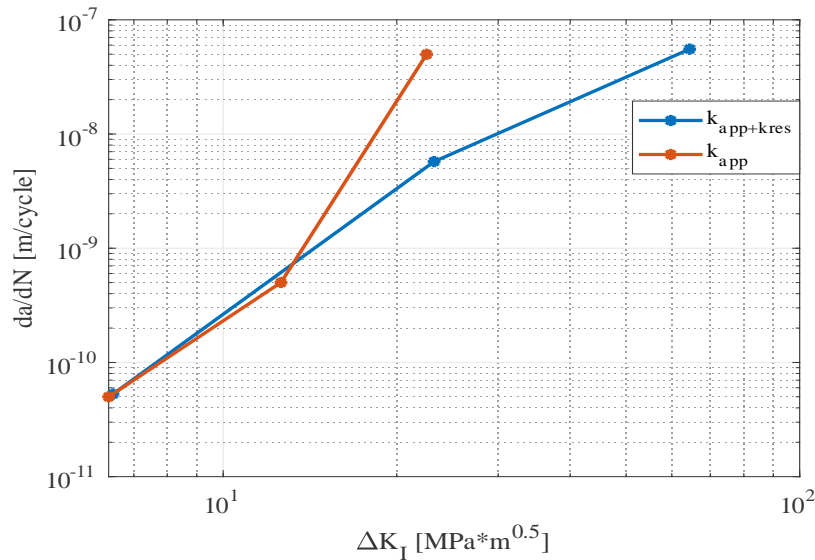


Figure 5.6 Crack growth rate versus stress intensity factor log-log scale

5.2.4 Fatigue crack growth rate for cyclic thermal load

In thermomechanical, fatigue there are mechanical and thermal cycling conditions, in thermal cycling condition, some assumption has to made on the basic crack growth equation, which is to specify the temperature dependence of Paris constant C as stated in reference (Bauerbach et al., 2010). The temperature-dependent crack growth law is given by Equations (5.16 and 5.17)

$$\frac{da}{dN} = C_{\delta} (CTOD)^m \tag{5.15}$$

$$\frac{da}{dN} = \frac{C_{\delta}}{(\Delta\sigma_y(T))^m} \cdot (J_{eff})^m \tag{5.16}$$

$$\frac{da}{dN} = C(T) \cdot (J_{eff})^m \tag{5.17}$$

In addition, the final crack growth expression due to thermal load is given by Equation (5.18)

$$\left. \begin{aligned} \frac{da}{dN} &= C(T) \left(\frac{k_I}{E} \right)^m \\ C(T) &= C(RT) \cdot \left(\frac{\Delta\sigma_y(T=TR)}{\Delta\sigma_y(T=T_0)} \right)^m \end{aligned} \right\} \tag{5.18}$$

Where $C(T)$ Paris constant temperature-dependent, Δk stress intensity factor range with the presence of residual stress, RT is room temperature, $\Delta\sigma_y$ yield strength of the 2.25Cr-1Mo as a function of temperature and T_0 is the temperature of the upper reversal point of the hysteresis loop.

The MATLAB program is developed for above-explained Equation (5.18) to show thermal load fatigue crack growth rate at different temperature ranges ($T = 250^\circ C, 450^\circ C$ and $650^\circ C$) with respect to stress intensity factor as shown in Figure 5.7 and the figure illustrate that fatigue crack growth rate is increase as the temperature increase.

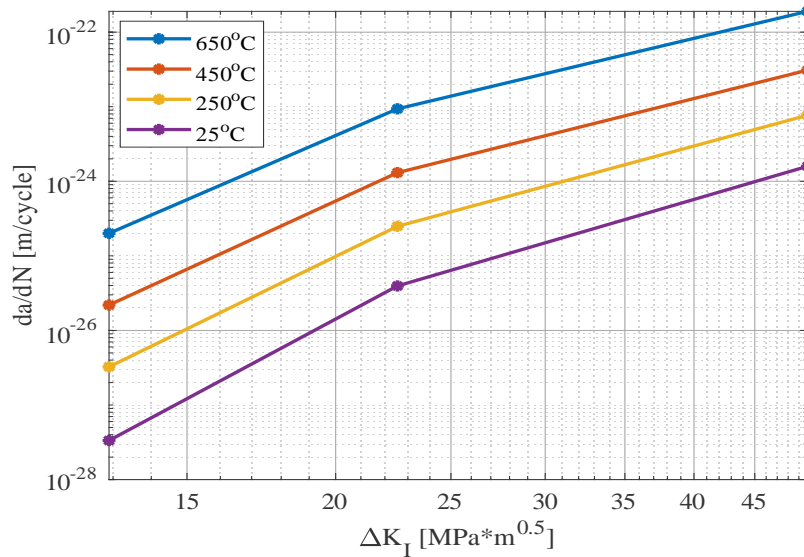


Figure 5.7 Fatigue crack growth due to thermal cyclic load rate versus stress intensity factor log-log scale

The total thermomechanical fatigue crack growth rate of reactor welded joint is the summation of fatigue crack growth of mechanical load and fatigue crack growth of thermal load cycles so that Equation (5.19) is proposed

$$\left(\frac{da}{dN}\right) = \left(\frac{da}{dN}\right)_{mechanical} + \left(\frac{da}{dN}\right)_{thermal} = \frac{C}{(1-R)k_c - \Delta k} \times (\Delta k)^m + C(T) \left(\frac{k_I}{E}\right)^m \quad (5.19)$$

5.2.5 Fatigue life calculation

The fatigue life can be calculated by integrating the Equation (5.10). The number of cycles for an initial crack grows, and the crack size a_N after N the number of cycles is calculated in fatigue life calculation. Integrating Equation (5.10) which consist of the effects of residual stress with an initial and final crack limit and the fatigue life is given by Equation (5.21). From Equation (5.10), can be reduced to the more general one which is the same as the Paris Erdogan equation which is stated by Equation (5.20)

$$\frac{da}{dN} = \frac{C}{k_R} (\Delta k)^m = C^- (\Delta k)^m \quad (5.20)$$

$$N = \int_{a_i}^{a_f} \frac{da}{C^- (\sigma\sqrt{\pi})^m} \quad (5.21)$$

$$N = \left[\frac{a_N^{\frac{2-m}{2}} - a_i^{\frac{2-m}{2}}}{C^- \left(\frac{2-m}{2}\right) (\sigma\sqrt{\pi})^m} \right] \quad (5.22)$$

Where a_i is the initial crack size and from Equation (5.22) the size of crack a_N after N cycles is calculated by using of Equation (5.23).

$$a_N = \left[NC \left(1 - \frac{m}{2}\right) (\sigma\sqrt{\pi})^m + a_i^{\frac{2-m}{2}} \right]^{\frac{2}{2-m}} \quad (5.23)$$

The MATLAB program is developed to compute the above-explained Equation (5.23), for applied and welding induced residual stresses values to show the rate of crack growth with respect to the number of cycle (N) as shown in Figure 5.8

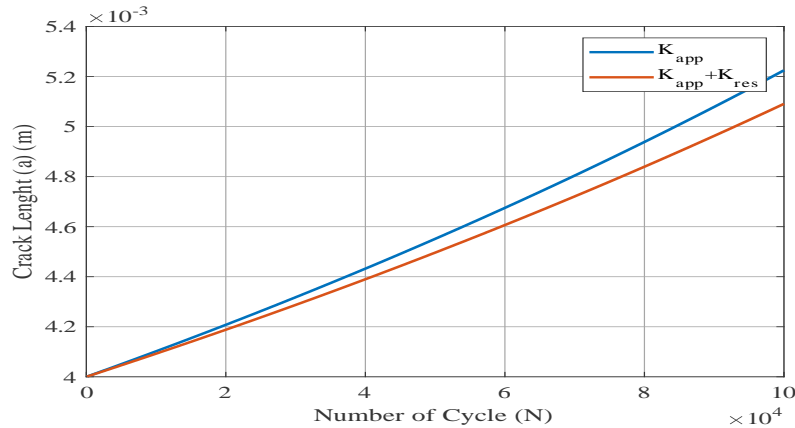


Figure 5.8 Crack length versus the number of cycles

Evaluating of low cycle fatigue tension and compression using the strain-life equation proposed by (Ličková et al., 2016) which is based on total strain approach is the most common description of thermomechanical fatigue process which is given by Equation (5.24)

$$\frac{\Delta \varepsilon_{mech}}{2} = \frac{\sigma'_f}{E} (2N_f^{fatigue})^b + \varepsilon'_f (2N_f^{fatigue})^c \quad (5.24)$$

Where σ'_f fatigue strength coefficient, b fatigue strength exponent, ε'_f fatigue ductility coefficient, C fatigue ductility coefficient and E elastic modulus

The MATLAB program is developed to compute the above-explained Equation (5.24), for mechanical strain amplitude to show the rate of crack growth with respect to the number of cycle N.

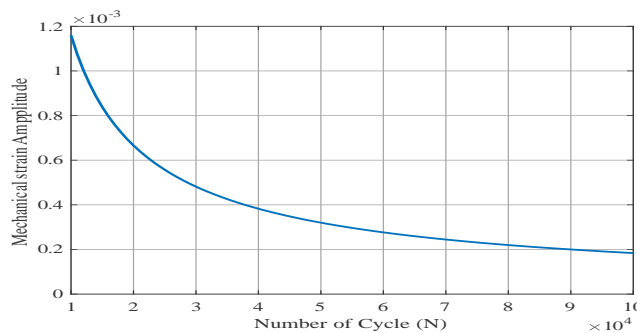


Figure 5.9 Strain-based evaluation of the crack growth versus the number of cycles

5.3 Finite element modelling

Finite element, modelling approaches the of fatigue crack growth welded joint of the reactor pressure vessel is characterized, in terms of determining of thermomechanical fatigue crack growth behaviour for welded joint edge cracked plate by using finite element software using ABAQUS 6.12. The benchmarked problem is a reactor pressure vessel with dimensions of the internal diameter of ($D_i = 2640mm$) and thickness of ($t = 30mm$) as discussed in chapter four. In finite element analysis, 2D element model is employed to avoid the analysis of the whole vessel and to reduce the time of the simulation. Modelling both longitudinal and circumferential cracks through the thickness of the vessel using finite element methods. The element types and number of elements for both types of cracks were identified.

Figure 5.10, shows the finite element meshing of the welded joint cross-section of the pressure vessel cracked circumferentially and longitudinally to the weld bead with an initial crack length of ($4mm$) and the element type is CPS4T (A 4-node plane stress thermally coupled quadrilateral, bilinear displacement and temperature) the model meshed into 1006560 elements and 1023336 nodes.

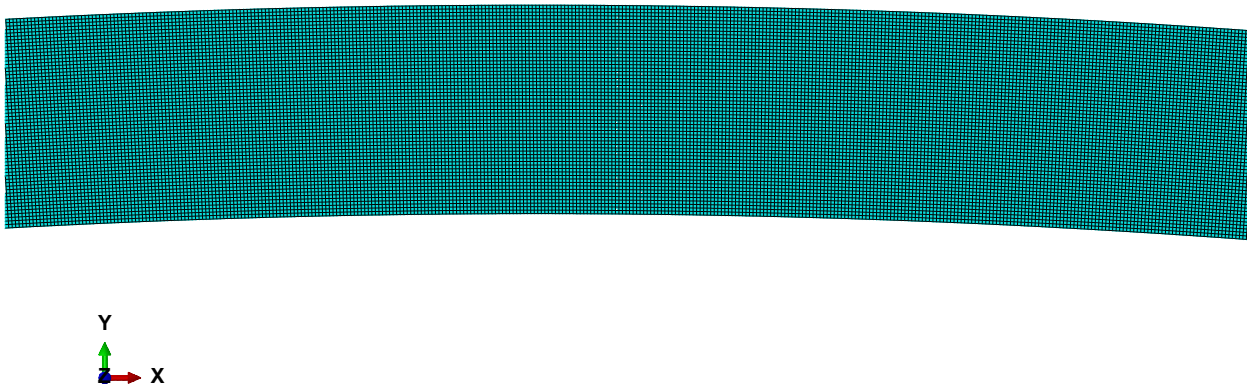


Figure 5.10 Mesh of the cross section of cylindrical pressure vessel

5.4 Result and discussion

5.4.1 Longitudinal crack along the weld line

The longitudinal crack is at the centre or corner of the weldment, the circumferential stress of the vessel is perpendicular to the crack path, during start-up and shut down cycle plastic deformation occurs near the crack tip, as shown in the Figure 5.11 the crack propagates in the weld direction.

The von Mises stress distribution in the welded joint of a reactor pressure vessel under the internal operating pressure of $5MPa$ and temperature ranges ($25^{\circ}C - 650^{\circ}C$) is shown in Figure 5.11. The maximum von Mises stress value obtained is $87.57MPa$. Figure 5.12 shows von mises stress distribution at the crack front. From this curve, the maximum von mises stress distribution has occurred at the crack tip

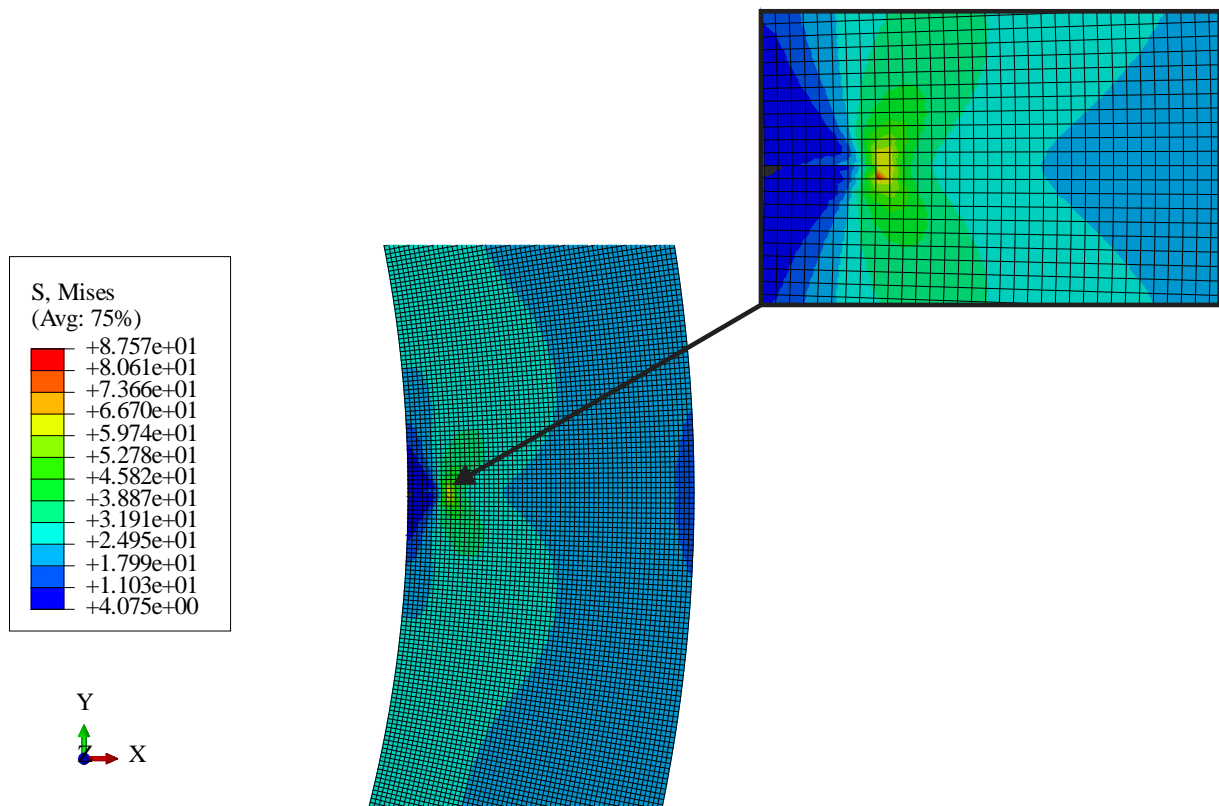


Figure 5.11 Longitudinal Von-Mises stress distribution in the welded joint

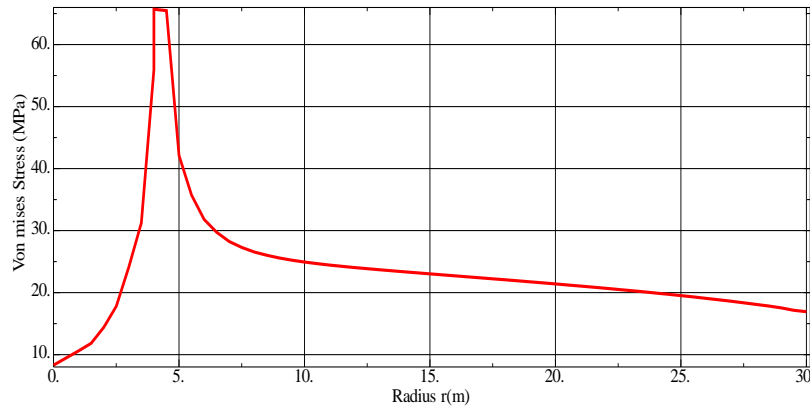


Figure 5.12 Longitudinal Von-Mises stress distribution in the welded joint at the crack tip

5.4.2 Circumferential crack growth in the welded joint of the vessel

Circumferential crack is located in the region along the circumference of the vessel. The effect of welding induced residual stress in addition to operating temperature and pressure on the crack growth of the internal surface circumferentially cracked of a reactor pressure vessel of the welded joint is analyzed. The von mises stress distribution in the welded joint circumferentially cracked is shown in Figure 5.13. The maximum von mises stress value is (28.05MPa). Figure 5.14 shows von mises stress distribution through the thickness of the vessel. From this curve, the von mises stress vary sinusoidally at the crack tip so that the circumferential crack effects on fatigue crack growth of welded joint less than longitudinal crack type.

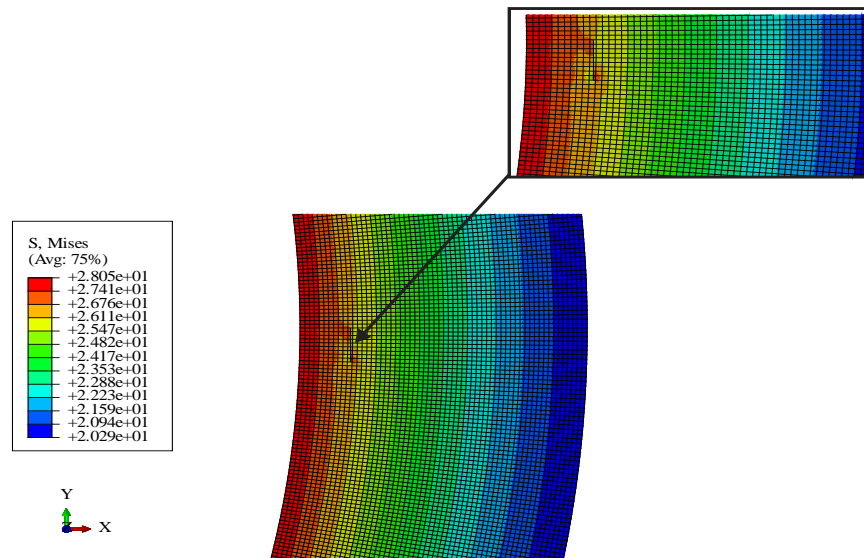


Figure 5.13 Circumferential Von-Mises stress distribution in the welded joint

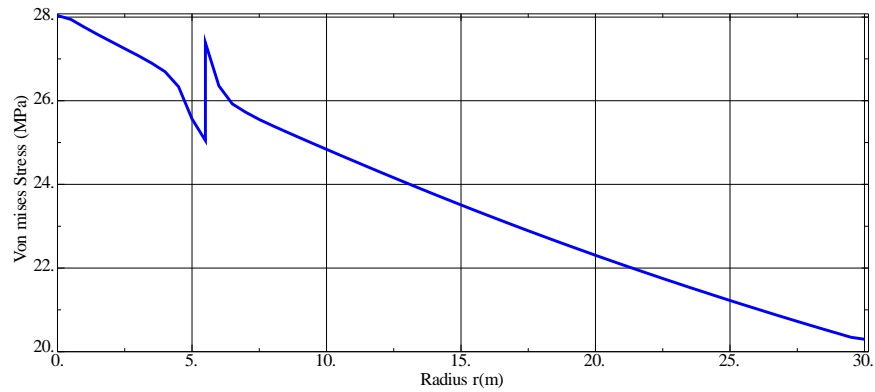


Figure 5.14 Circumferential Von-Mises stress distribution in the welded joint at the crack tip

5.4.3 XFEM Results

The STATUS XFEM output in the XFEM analysis is red for crack growth surface, and different colour spectrum for a growing crack and PHILSM and PSILM are the two set values, which represents the crack growth from the welded region of the vessel to other parts to show the crack growth behaviour. Figure 5.15 (a, b) shows the STATUSXFEM of the surface of the welded joint of the vessel for both circumferential and longitudinal crack types. Whereas as the PSILSM and PHILSM of the crack growth behaviour is illustrated in Figure 5.17, respectively.

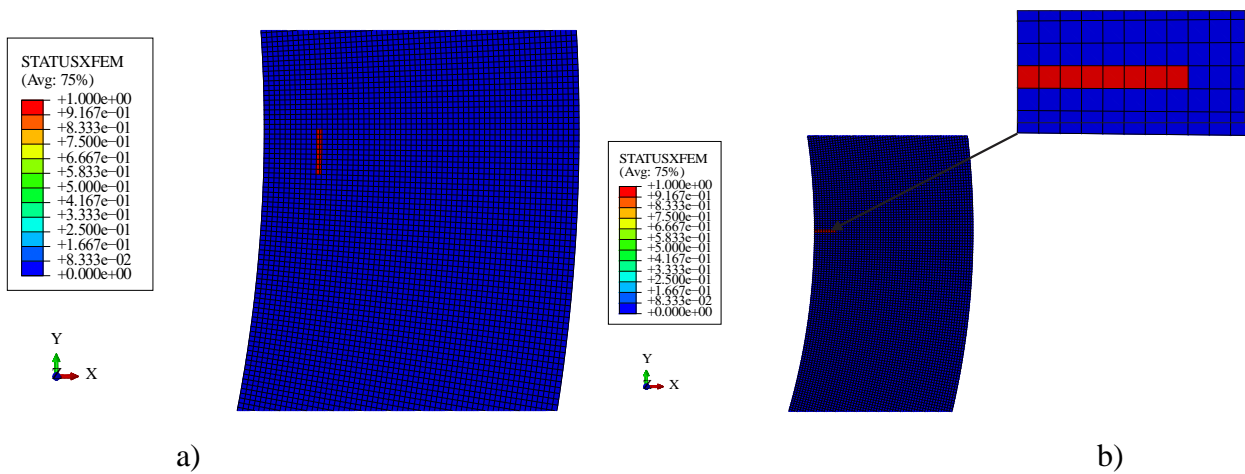


Figure 5.15 STATUSXFEM result of welded joint a) circumferential and b) longitudinal crack type

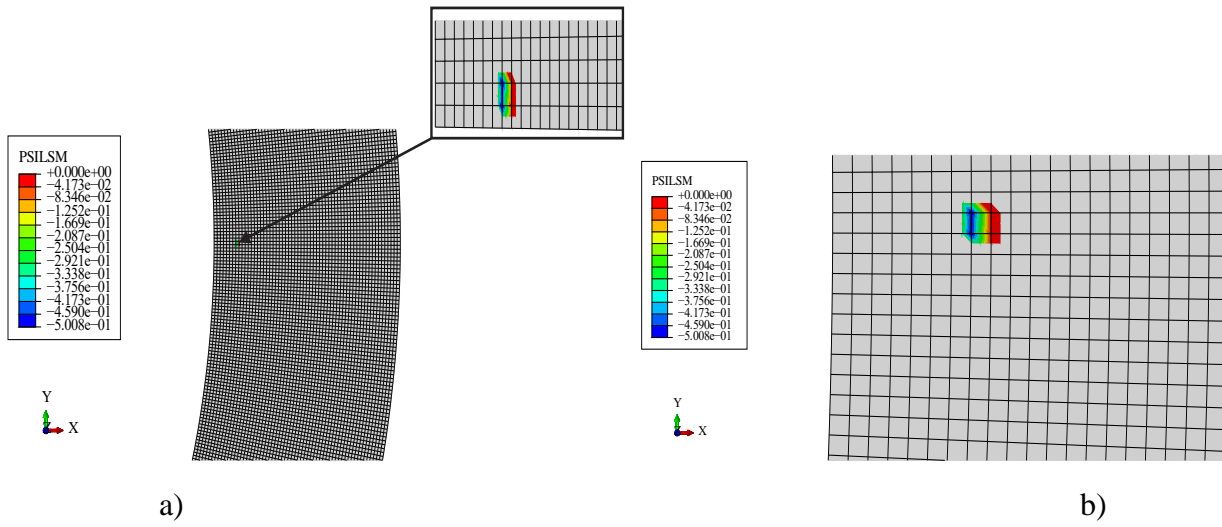


Figure 5.16 PSILSM result of the welded joint a) circumferential and b) Longitudinal crack type

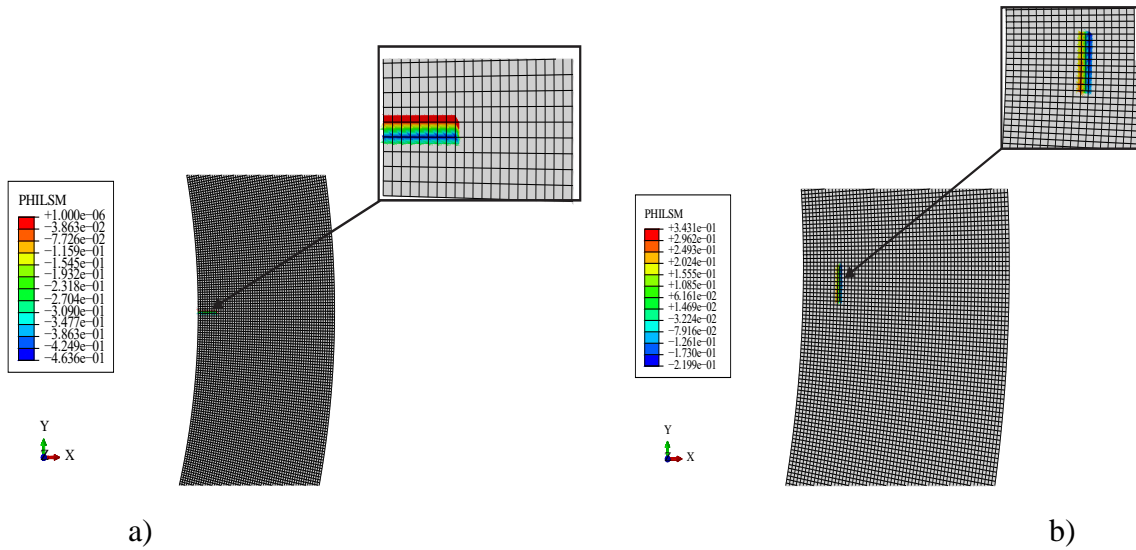


Figure 5.17 PHILSM result of welded joint a) longitudinal and b) circumferential crack type

CHAPTER

6

CONCLUSIONS AND SUGGESTED FUTURE WORK

6.1 Conclusions

This objective of this thesis is to numerically investigate the fatigue crack growth behaviour of welded joints at elevated temperature. It covers modelling welding induced residual stress, thermomechanical stress analysis and thermomechanical fatigue model in case of the reactor pressure vessel. Due to lack of sufficient high process computers, 3D FEM model analysis is not considered and also insufficient laboratory and expensive material cost, and the experiment is not conducted.

The of modelling welding induced residual stress which done by analytical approach and numerical approach using ABAQUS 6.12 welding interface to investigate the formation of welding induced residual stress. A single V groove longitudinal butt welded joint of a reactor pressure vessel made up of material 2.25Cr-1Mo low alloy ferritic steel and 2D shell-type FE model with the dimension of 100mm length from the centre of the weld and 30mm height were modelled. During the simulation, the effect of solid-state phase transformation, tempering and creep was ignored. The following conclusions can be summarized;

- It was possible to design the heat source model which coincident in the result of actual heat source using analytical approach; the designed model has based kinds of approximation or simplification of reality with some discrepancy are possible and did occur.
- The residual stress formation and distribution largely influenced by thermomechanical property of the material, amount heat input during welding and welding conditions
- The maximum longitudinal residual stresses occur at the centre of the weld. The stress decreases as the distance from the centre of the weld increase compressive, near heat affected zone and becomes zero at the base metal region.

- The comparison between the results obtained by both analytical and simulation with the experimental result has good agreement with some errors; the errors due to assumption of welding parameters, iterative computation and simulations and largely influenced by errors in the digitized data of thermal-dependent thermomechanical properties of 2.25Cr-1Mo

Thermomechanical stress analysis is performed for reactor pressure vessel using the analytical and numerical approach, with the internal diameter ($D_i = 2640mm$), thickness ($t = 30mm$), internal operating pressure ($P_i = 5MPa$) and at different temperature ranges. During the simulation, it is assumed that the distribution of stress in the vessel is uniform by neglecting holes and discontinuities. The following conclusions can be summarized.

- Thermomechanical generated hoop stress is critical stress which acts in the same direction with welding induced residual stress. It increases the plastic deformation of the welded joint of the reactor pressure vessel, which accelerates the fatigue crack growth of the welded joint of the shell of the cylindrical pressure vessel.
- Thermomechanical produced stresses depend on the operating temperature and pressure, as the temperatures inside the reactor pressure vessel varying thermomechanical produced stresses are varying.
- The uncoupled thermomechanical stress analysis in the analytical approach is good agreement with coupled thermomechanical stress analysis in a numerical approach using ABAQUS 6.12 with a small deviation.

Thermomechanical model is performed for reactor pressure vessel using the analytical and numerical approach, with the internal diameter ($D_i = 2640mm$), thickness ($t = 30mm$), internal operating pressure ($P_i = 5MPa$) and at different temperature ranges. The vessel shell-welded joint is initially cracked with the crack length of ($a = 4mm$). During the simulation, both types of crack configuration of the welded joint, i.e. longitudinal and circumferential cracks were considered. The following conclusions can be summarized.

- Linear elastic fracture mechanics analysis is performed to estimate the crack growth rate for both types cracks, i.e. the normal and interface cracks to the weld. The stress intensity factor range for both crack types is estimated, stress intensity factor for the longitudinal crack type is greater than circumferential crack type
- Crack growth behaviour of welded shell of the vessel influenced by thermomechanical stress produced by both thermal and mechanical load, as the temperature increases the stress intensity factor range is increase. And the welding induced residual stress effects on fatigue crack of welded joint of the shell of the vessel is decrease as the crack length increase
- With the initial crack length, the crack growth is modelled using ABAQUS 6.12 and mode I crack growth model orientation is considered, for computational efficiency, the 2D finite element analysis is considered. The estimated von mises stresses show that longitudinal crack type is more propagate than circumferential crack type.
- In ABAQUS 6.12 the STATUS XFEM the output analysis is a red colour for crack growth and different colour spectrum for a growing crack behaviour, PHILSM and PSILM are the two set values which represents the crack growth from the welded region of the vessel to other parts and shows the crack growth behaviour
- Finally, the life of reactor pressure vessel welded joint was determined from the equivalent stress factor range consists due to applied load and welding induced residual stress, which is calculated from the analytical results.

6.2 Recommendation

In this thesis, numerical modelling of fatigue crack growth behaviour of welded joints at elevated temperature was performed. Consists modelling of welding induced residual stress, thermomechanical stress analysis and thermomechanical fatigue model in case of the reactor pressure vessel is studied. The XFEM in ABAQUS 6.12 was used to study the crack growth from the welded region to other parts. However, this study only focuses on low cycle fatigue life.

Generally, other researchers can consider the following suggestion for future work

- High cycle fatigue modelling fatigue crack growth could be considered.
- Welding distortion effect could be considered.
- The numerical results could be verified with experimental results.
- Creep fatigue interaction effect could be considered.

REFERENCES

- Adiban, S. V, Ramu, M., 2018. ScienceDirect Study on the effect of weld defects on fatigue life of structures 5, 17114–17124.
- Akramin, M., Marizi, M., Husnain, M., Shaari, M.S., 2020. Analysis of Surface Crack using Various Crack Growth Models. Presented at the Journal of Physics: Conference Series, IOP Publishing, p. 042074.
- Al-Mukhtar, A., 2013. Residual stresses and stress intensity factor calculations in T-welded joints. *J. Fail. Anal. Prev.* 13, 619–623.
- Arai T, A.N., 2013. Residual stress and distortion in laser welding. ‘Simulation Thin Met. Deform. Laser Welding’ Proc. ICALEO 2, 676–683.
<https://doi.org/10.1533/9780857098771.2.374>
- Arthur, G., Christian, J.W., Phil, D., 1980. Analysis of Welded Structures. p. 649.
- Atreya, T.S.A., Engineering, M.E.I.S., 2017. Improve the hazop techniques to prevent the accidents caused by pressure vessels 1–14.
- Bao, R., Zhang, X., Ahmad, N., Yahaya, N.A., 2010a. Evaluating stress intensity factors due to weld residual stresses by the weight function and finite element methods. *Eng. Fract. Mech.* 77, 2550–2566. <https://doi.org/10.1016/j.engfracmech.2010.06.002>
- Bao, R., Zhang, X., Yahaya, N.A., 2010b. Evaluating stress intensity factors due to weld residual stresses by the weight function and finite element methods. *Eng. Fract. Mech.* 77, 2550–2566.
- Baru, A., 2016. Akademia Baru Common Root Causes of Pressure Vessel Failures : A Review Akademia Baru 21, 22–37.
- Bauerbach, K., Vormwald, M., Rudolph, J., 2010. Fatigue assessment of thermal cyclic loading conditions based on a short crack approach. *Procedia Eng.* 2, 1569–1578.
- Beckmann, C., Kennerknecht, T., Preußner, J., Farajian, M., Luke, M., Hohe, J., 2018. Micromechanical investigation and numerical simulation of fatigue crack formation in welded joints. *Eng. Fract. Mech.* 198, 142–157.
- Beckmann, C., Kennerknecht, T., Preußner, J., Farajian, M., Luke, M., Hohe, J., 2017. Micromechanical investigation and numerical simulation of fatigue crack formation in welded joints 1–16. <https://doi.org/10.1016/j.engfracmech.2017.08.008>
- Beltrão, M.N., Castrodeza, E., Bastian, F., 2011. Fatigue crack propagation in API 5L X-70 pipeline steel longitudinal welded joints under constant and variable amplitudes. *Fatigue Fract. Eng. Mater. Struct.* 34, 321–328.
- Benedetti, M., Berto, F., Marini, M., Raghavendra, S., Fontanari, V., 2020. Incorporating residual stresses into a Strain-Energy-Density based fatigue criterion and its application to the assessment of the medium-to-very-high-cycle fatigue strength of shot-peened parts. *Int. J. Fatigue* 105728.
- Cen, Q., Kwong, D., Tsang, L., Lu, Y., 2019. International Journal of Pressure Vessels and Piping Creep damage analysis of thin-walled pressure vessel based on continuum damage model under static loading. *Int. J. Press. Vessels Pip.* 177, 103994.
<https://doi.org/10.1016/j.ijpvp.2019.103994>
- Chang, P., Teng, T., 2004. Numerical and experimental investigations on the residual stresses of the butt-welded joints 29, 511–522. <https://doi.org/10.1016/j.commatsci.2003.12.005>
- Chaudhry, V., 2014. Thermo-Mechanical Transient Analysis of Reactor Pressure Vessel, in: Thermo-Mechanical Transient Analysis of Reactor Pressure Vessel.

- Chen, D., Sun, S., Dulieu-barton, J.M., Li, Q., Wang, W., 2018. Crack growth analysis in welded and non-welded T-joints based on lock-in digital image correlation and thermoelastic stress analysis. *Int. J. Fatigue* 110, 172–185.
<https://doi.org/10.1016/j.ijfatigue.2018.01.020>
- Chen, Q., Yang, J., Liu, X., Tang, J., Huang, B., 2019. Effect of the groove type when considering a thermometallurgical- mechanical model of the welding residual stress and deformation in an S355JR-316L dissimilar welded joint. *J. Manuf. Process.* 45, 290–303.
<https://doi.org/10.1016/j.jmapro.2019.07.011>
- Chernyatin, A., Matvienko, Y.G., Razumovsky, I., 2018. Fatigue surface crack propagation and intersecting cracks in connection with welding residual stresses. *Fatigue Fract. Eng. Mater. Struct.* 41, 2140–2152.
- Description, I., 2008. Fatigue Crack Growth. Analysis and Predictions. *Fatigue Struct. Mater.* 209–256. https://doi.org/10.1007/978-1-4020-6808-9_8
- Donatello Annaratone, 2012. *Pressure Vessel Design*. 20129 Milano, p. 448.
- Dong, Y., Guedes Soares, C., 2019. Stress distribution and fatigue crack propagation analyses in welded joints. *Fatigue Fract. Eng. Mater. Struct.* 42, 69–83.
- Elamin, W.M., Endan, J.B., Yosuf, Y.A., Shamsudin, R., Ahmedov, A., 2015. High Pressure Processing Technology and Equipment Evolution: A Review. *J. Eng. Sci. Technol. Rev.* 8.
- Elangovan, S., 2019. Analysis of Life of Pressure Vessel 4, 8–14.
- Fu, G., Gu, J., Lourenco, M.I., Duan, M., Segen, F., 2015. Parameter determination of double-ellipsoidal heat source model and its application in the multi-pass welding process. *Ships Offshore Struct.* 10, 204–217. <https://doi.org/10.1080/17445302.2014.937059>
- Fueki, R., Takahashi, K., Houjou, K., 2015. Fatigue Limit Prediction and Estimation for the Crack Size Rendered Harmless by Peening for Welded Joint Containing a Surface Crack 500–510.
- G.A. Moraitis, G.N.L., n.d. [moraitis2009.pdf](#).
- Gadallah, R., Osawa, N., Tanaka, S., Tsutsumi, S., 2018a. Critical investigation on the influence of welding heat input and welding residual stress on stress intensity factor and fatigue crack propagation 89, 200–221.
- Gadallah, R., Osawa, N., Tanaka, S., Tsutsumi, S., 2018b. Critical investigation on the influence of welding heat input and welding residual stress on stress intensity factor and fatigue crack propagation. *Eng. Fail. Anal.* 89, 200–221.
- Habib, E.-S., El-Hadek, M.A., El-Megharbel, A., 2019a. Stress analysis for cylinder made of FGM and subjected to thermo-mechanical loadings. *Metals* 9, 4.
- Habib, E.-S., El-Hadek, M.A., El-Megharbel, A., 2019b. Stress analysis for cylinder made of FGM and subjected to thermo-mechanical loadings. *Metals* 9, 4.
- Hensel, J., Nitschke-pagel, T., Ngoula, D.T., Beier, H., Tchuindjang, D., Zerbst, U., 2017. Welding residual stresses as needed for the prediction of fatigue crack propagation and fatigue strength. *Eng. Fract. Mech.* 1–19.
<https://doi.org/10.1016/j.engfracmech.2017.10.024>
- Hensel, J., Nitschke-Pagel, T., Ngoula, D.T., Beier, H.-T., Tchuindjang, D., Zerbst, U., 2018. Welding residual stresses as needed for the prediction of fatigue crack propagation and fatigue strength. *Eng. Fract. Mech.* 198, 123–141.

- Homayounfar, A., 2009. 3D finite element analysis of the residual stresses in butt-welded plates with modeling of the electrode-movement 10, 37–43.
<https://doi.org/10.1631/jzus.A0720127>
- Hong, J.K., 2016. Study on Weld Fatigue Evaluation Incorporating Welding Induced Residual Stress Effect. Presented at the International Conference on Offshore Mechanics and Arctic Engineering, American Society of Mechanical Engineers, p. V004T03A011.
- Hornsey, B.J.S., Relieving, S., 2006. Residual Stresses : Their Causes , and the Effective Means of Treatment to Reduce the Residual Stresses and to Improve the Fatigue Life in Engineering Components 6, 1–18.
- Howes, M., Inoue, T., Park, M., 2002. Handbook of Residual Stress and Deformation of Steel Edited by.
- John Wiley & Sons, 2016. Welding engineering, in: Welding Engineering. p. 229.
- Kang, G., Luo, H., 2020. Review on fatigue life prediction models of welded joint. Acta Mech. Sin. <https://doi.org/10.1007/s10409-020-00957-0>
- Kita-shinagawa-ku, T., 2015. The ABC's of Arc Welding and Inspection. kobe steel, ltd.
- Klassen, J., Friedrich, N., Fricke, W., Nitschke-Pagel, T., Dilger, K., 2017. Influence of residual stresses on fatigue strength of large-scale welded assembly joints. Weld. World 61, 361–374.
- Kumar, T.S., Nagesha, A., Kannan, R., 2019. International Journal of Pressure Vessels and Piping Thermal cycling effects on the creep-fatigue interaction in type 316LN austenitic stainless steel weld joint. Int. J. Press. Vessels Pip. 178, 104009.
<https://doi.org/10.1016/j.ijpvp.2019.104009>
- Lee, J.-H., Lee, H.-Y., Hong, S.-G., Lee, S.-B., 2017. Fatigue crack growth behavior of Mod. 9Cr-1Mo steel at elevated temperatures: Effect of temperature, loading frequency and R ratio. J. Mech. Sci. Technol. 31, 3665–3669.
- Ličková, D., Halama, R., Poruba, Z., 2016. Identification of Fatigue Constants by means of 3D Method. Strojnícky Časopis-J. Mech. Eng. 66, 107–116.
- Loadings, S.T., Habib, E., El-hadek, M.A., 2019. Stress Analysis for Cylinder Made of FGM and. <https://doi.org/10.3390/met9010004>
- Moghadam, D.G., Farhangdoost, K., 2016. Influence of welding parameters on fracture toughness and fatigue crack growth rate in friction stir welded nugget of 2024-T351 aluminum alloy joints. Trans. Nonferrous Met. Soc. China 26, 2567–2585.
[https://doi.org/10.1016/S1003-6326\(16\)64383-2](https://doi.org/10.1016/S1003-6326(16)64383-2)
- Paul C. Paris and Hiroshi Tada, 2000. Hiroshi Tada, ASME Press, George Rankin Irwin - Stress Analysis of Cracks Handbook, Third Edition (2000, American Society of Mechanical Engineers) - libgen.lc.pdf. p. 503.
- Phillips, D.H., 2016. Welding engineering: an introduction. John Wiley & Sons.
- Pu, X., Zhang, C., Li, S., Deng, D., 2017. Simulating welding residual stress and deformation in a multi-pass butt-welded joint considering balance between computing time and prediction accuracy. <https://doi.org/10.1007/s00170-017-0691-5>
- Ren, S., Li, S., Wang, Y., Deng, D., Ma, N., 2019a. Finite element analysis of residual stress in 2.25Cr-1Mo steel pipe during welding and heat treatment process. J. Manuf. Process. 47, 110–118. <https://doi.org/10.1016/j.jmapro.2019.09.019>
- Ren, S., Li, S., Wang, Y., Deng, D., Ma, N., 2019b. Finite element analysis of residual stress in 2.25 Cr-1Mo steel pipe during welding and heat treatment process. J. Manuf. Process. 47, 110–118.

- Schnubel, D., Huber, N., 2012. The influence of crack face contact on the prediction of fatigue crack propagation in residual stress fields. *Eng. Fract. Mech.* 84, 15–24.
<https://doi.org/10.1016/j.engfracmech.2011.12.008>
- Shen, M.H., Akanda, S., Liu, X., Wang, P., 2016a. Fatigue Crack Growth Threshold Determination for Welded Joint Constituents of a Steam Turbine LP Rotor. *Exp. Tech.* 40, 1215–1220.
- Shen, M.H., Akanda, S., Liu, X., Wang, P., 2016b. Fatigue Crack Growth Threshold Determination for Welded Joint Constituents of a Steam Turbine LP Rotor. *Exp. Tech.* 40, 1215–1220.
- Socie, D., Socie, B., 2007. Thermomechanical fatigue made easy.
- Stekovic, S., 2007. Low cycle fatigue and thermo-mechanical fatigue of uncoated and coated nickel-base superalloys.
- Stephen, M.S., Brookes, P., 2009. Thermo-mechanical fatigue behaviour of the near-.
- Tang, L., Qian, C., Ince, A., Zheng, J., Li, H., Han, Z., 2018a. Fatigue Crack Growth Behavior of the MIG Welded Joint of 06Cr19Ni10 Stainless Steel. *Materials* 11, 1336.
- Tang, L., Qian, C., Ince, A., Zheng, J., Li, H., Han, Z., 2018b. Fatigue Crack Growth Behavior of the MIG Welded Joint of 06Cr19Ni10 Stainless Steel. *Materials* 11, 1336.
- Velu, M., 2018a. ScienceDirect Fracture toughness and fatigue crack growth rates of butt-welded joints of copper and steel : Mode I cracks oriented parallel to the weld. *Mater. Today Proc.* 5, 12782–12791. <https://doi.org/10.1016/j.matpr.2018.02.262>
- Velu, M., 2018b. ScienceDirect A Short Review on Fracture and Fatigue Crack Growth in Welded Joints 5, 11364–11370.
- Wada, Y., 2002. hydrogen Embrittlement Susceptibility of temper embrittled 2.25Cr-1Mo steel 2002.2, 247–248.
- Wang, Z., Zhang, Q., Xia, L., Wu, J., Liu, P., 2015. Stress analysis and parameter optimization of an FGM pressure vessel subjected to thermo-mechanical loadings. *Procedia Eng.* 130, 374–389.

APPENDIX

MATLAB Code

```

%% Distribution of induced residual stress along the welded joint
%=====
% W = plate width (mm)
% sigma_o = is the maximum stress at the weld region (MPa)
% a = crack length -> Aa (mm)
% Sigma__(x) = K_I
% c = crack width
clear all; %close all;
w = 100;
c = 10;
Sigma_x = 300;
i=1;
for a=-100:w/100:100
Aa(i) = a;
Sigma_yy(i) = Sigma_x * exp(-0.5*(a/c)^2) * (1 - (a/c)^2);
i=i+1;
end;
figure;
plot(Aa, Sigma_yy); grid on;
xlabel('Distance from center of the weld [mm]'); ylabel('Longitudinal residual stress
\sigma yy [Mpa]');
%=====

%% 3D heat source model for pass 1 based on goldaks parameters
%=====
af=5;
ar=8;
b=4.8;
c=3.0;
ff=1.33;
fr=0.66;
% Welding Process Parameters
i=120;
u=25;
v=15;
q=u*i/v;
n=0.8;
z=0;
%
ml=6*sqrt(2)*n*q/(pi*sqrt(pi)*af*b*c);
x=-10:0.1:10;
y=-10:0.1:10;
for xc=1:length(x)
for yc=1:length(y)
if x(xc)>=0
q(xc,yc)=ml*(ff/af)*exp(-3*(x(xc)^2/af^2+y(yc)^2/b^2+z^2/c^2)
else
q(xc,yc)=ml*(fr/ar)*exp(-3*(x(xc)^2/ar^2+y(yc)^2/b^2+z^2/c^2)
end
end
end
surf(x,y,q);

```

```

shading interp
ylabel('weld direction');
xlabel('power density (wmm^-2)');
xlabel('Distance from center of the weld (mm)');
%%%%%%%%%%%%%%%%%%%%%%%%%%%%%%%%%%%%%%%%%%%%%%%%%%%%%%%%%%%%%%%%%%%%%%%%%
% 3D heat source model for pass 1 based on goldaks parameters %%%%%%%%%%
% =====%

%%%%%%%%%%%%%%%%%%%%%%%%%%%%%%%%%%%%%%%%%%%%%%%%%%%%%%%%%%%%%%%%%%%%%%%%%
% Hoop stress due to internal operating pressure %%%%%%%%%%
% =====%
pi=5*10^6;
po=0;
ri=1.32;
ro=1.35;
r=[ri:(ro-ri)/100:ro];
n=1;
while(n<=101)
sigma_t(n)= ((pi*ri^2 - po*ro^2)/(ro^2 - ri^2)) + (((ri^2*ro^2)/r(n)^2)*((pi-po)/(ro^2-ri^2)));
n=n+1;
end
figure;
plot(r,sigma_t)
grid on;
xlabel('r')
ylabel('sigma_t')
%%%%%%%%%%%%%%%%%%%%%%%%%%%%%%%%%%%%%%%%%%%%%%%%%%%%%%%%%%%%%%%%%%%%%%%%%
% Hoop stress due to internal operating pressure %%%%%%%%%%
% =====%
%%%%%%%%%%%%%%%%%%%%%%%%%%%%%%%%%%%%%%%%%%%%%%%%%%%%%%%%%%%%%%%%%%%%%%%%%
% Hoop stress at different operating temperatures %%%%%%%%%%
% =====%
E=207*10^9;
T=25;
T2=250;
T3=450;
T4=650;
A=7*10^-14;
v=0.3;
ri=1.32;
ro=1.35;
r=[ri:(ro-ri)/100:ro];
n=1;
while(n<=101)
sigma_r(n)= ((E*A*T)/(2*(1-v)))*(((ro^2/ri^2) + (ro^2/r(n)^2)/(ro^2/ri^2 - 1)) - (((1)
+log(r(n)/ro)/log(exp(1)))/(log(r(n)/ro)/log(exp(1))));
sigma_r2(n)= ((E*A*T2)/(2*(1-v)))*(((ro^2/ri^2) + (ro^2/r(n)^2)/(ro^2/ri^2 - 1)) - (((1)
+log(r(n)/ro)/log(exp(1)))/(log(r(n)/ro)/log(exp(1))));
sigma_r3(n)= ((E*A*T3)/(2*(1-v)))*(((ro^2/ri^2) + (ro^2/r(n)^2)/(ro^2/ri^2 - 1)) - (((1)
+log(r(n)/ro)/log(exp(1)))/(log(r(n)/ro)/log(exp(1))));
sigma_r4(n)= ((E*A*T4)/(2*(1-v)))*(((ro^2/ri^2) + (ro^2/r(n)^2)/(ro^2/ri^2 - 1)) - (((1)
+log(r(n)/ro)/log(exp(1)))/(log(r(n)/ro)/log(exp(1))));
n=n+1;
end
figure;
plot(r,sigma_r,r,sigma_r2,r,sigma_r3,r,sigma_r4)
xlabel('r')
grid on;
ylabel('sigma_r')

```

```

legend ('T1=25^{\circ}C', 'T2= 250^{\circ}C', 'T3= 450^{\circ}C', 'T4= 650^{\circ}C')
%% Hoop stress due to internal and external operating temperature
%=====
%% Temperature variation with radius of the vessel
%=====
Ti = 25;
To=625;
ri=1.32;
ro=1.35;
r=[ri:(ro-ri)/100:ro];
n=1;
while(n<=101)
Temperature_r(n)= (((To-Ti)/(log(ri/ro)/log(exp(1))))* log(r(n)/ro)/log(exp(1)))+Ti;
n=n+1;
end
figure;
plot(r,Temperature_r)
xlabel('r')
grid on;
ylabel('Temperature_r')
%% Temperature variation with radius of the vessel
%=====
%% Radial stress due to internal operating pressure
%=====
pa=5*10^6;
po=0;
ri=1.32;
ro=1.35;
r=[ri:(ro-ri)/100:ro];
n=1;
while(n<=101)
sigma_r(n)= ((pa*ri^2 - po*ro^2)/(ro^2 - ri^2)) - (((ri^2*ro^2)/r(n)^2)*((pa-po)/(ro^2-ri^2)));
n=n+1;
end
figure;
plot(r,sigma_r)
xlabel('r')
grid on;
ylabel('sigma_r')
%% Radial stress due to internal operating pressure
%=====

```

```

%% Radial stresses at different operating temperatures
%=====
E=207*10^9;
T=25;
T2=250;

T3=450;
T4=650;
A=5.67*10^-14;
v=0.3;
ri=1.32;
ro=1.35;
r=[ri:(ro-ri)/100:ro];
n=1;
while(n<=101)
sigma_r(n)= ((E*A*T)/(2*(1-v)))*(((ro^2/ri^2) - (ro^2/r(n)^2)/(ro^2/ri^2 - 1)) - ((log(r
(n)/ro)/log(exp(1)))/(log(r(n)/ro)/log(exp(1))));
sigma_r2(n)= ((E*A*T2)/(2*(1-v)))*(((ro^2/ri^2) - (ro^2/r(n)^2)/(ro^2/ri^2 - 1)) - ((log
(r(n)/ro)/log(exp(1)))/(log(r(n)/ro)/log(exp(1))));
sigma_r3(n)= ((E*A*T3)/(2*(1-v)))*(((ro^2/ri^2) - (ro^2/r(n)^2)/(ro^2/ri^2 - 1)) - ((log
(r(n)/ro)/log(exp(1)))/(log(r(n)/ro)/log(exp(1))));
sigma_r4(n)= ((E*A*T4)/(2*(1-v)))*(((ro^2/ri^2) - (ro^2/r(n)^2)/(ro^2/ri^2 - 1)) - ((log
(r(n)/ro)/log(exp(1)))/(log(r(n)/ro)/log(exp(1))));
n=n+1;
end
figure;
plot(r,sigma_r,r,sigma_r2,r,sigma_r3,r,sigma_r4)
xlabel('r')
grid on;
ylabel('sigma_r')
legend ('T1=25^oC', 'T2= 250^oC', 'T3= 450^oC', 'T4= 650^oC');
%% Radial stresses at different operating temperatures
%=====

%% Fatigue crack growth rate at different temperature ranges
%=====

da_dN4=[1.9*1e-19,9.35*1e-21,2.006*1e-22]; % unit (mm/cycle)
deltaKI4=[49.84,22.54,12.9]; % unit (MPa m^0.5)
da_dN=[3.089*1e-20,1.305*1e-21,2.19*1e-23]; % unit (mm/cycle)
deltaKI=[49.84,22.54,12.9]; % unit (MPa m^0.5)
da_dN2=[7.68*1e-21,2.49*1e-22,3.249*1e-24]; % unit (mm/cycle)
deltaKI2=[49.84,22.54,12.9]; % unit (MPa m^0.5)
da_dN3=[1.589*1e-21,3.946*1e-23,3.346*1e-25]; % unit (mm/cycle)
deltaKI3=[49.84,22.54,12.9]; % unit (MPa m^0.5)
loglog(deltaKI4,da_dN4/1000,'*-',deltaKI,da_dN/1000,'*-',deltaKI2,da_dN2/1000,'*-',
deltaKI3,da_dN3/1000,'*-',)
xlabel('\DeltaK_I [MPa*m^{0.5}]')
ylabel('da/dN [m/cycle]');
grid on;
hold on;
legend('650^oC','450^oC','250^oC','25^oC')

%% Fatigue crack growth rate at different temperature ranges
%=====

%% Residual stress variation at different crack aspect ratio

```

```

%=====
W = 100;
Gs = 67.5;
d=0.2;
i=1;
for a=0:W/100:4;
Aa(i) = a;
KI1(i) = (Gs * (sqrt(pi*a)*exp(-0.42*(0.2)^2))) * (1-1/pi * (0.2)^2);
KI2(i) =(Gs * (sqrt(pi*a)*exp(-0.42*(0.4)^2))) * (1-1/pi * (0.4)^2);
KI3(i) =(Gs * (sqrt(pi*a)*exp(-0.42*(0.6)^2))) * (1-1/pi * (0.5)^2);
KI4(i) =(Gs * (sqrt(pi*a)*exp(-0.42*(0.8)^2))) * (1-1/pi * (0.8)^2);
KI5(i) = (Gs * (sqrt(pi*a)*exp(-0.42*(1)^2))) * (1-1/pi * (1)^2);
i=i+1;
end;
figure;
plot(Aa,KI1,Aa,KI2,Aa,KI3,Aa,KI4,Aa,KI5); grid on;
xlabel('a'); ylabel('K_res [MPa]');
legend('a/c=0.2','a/c=0.4','a/c=0.6','a/c=0.8','a/c=1')

% Residual stress variation at different crack aspect ratio
%=====

% Crack length versus the number of cycles
%=====

N=100000;
delta_a0=1e-8;
K_1c=200;
delta_K_10=25.22;
delta_K_102=26.04;
a_i=0.004;
m=3;
Q=1.0;
d_sigma=225;
% [cycle] % [m/cycle]
% [MPa m^0.5] % [MPa m^0.5] % [m]
% [MPa]
n=[100:100:100000];
n0=(a_i/delta_a0)*(delta_K_10/(Q*d_sigma*(pi*a_i)^0.5))^m*(2/(m-2));
n02=(a_i/delta_a0)*(delta_K_102/(Q*d_sigma*(pi*a_i)^0.5))^m*(2/(m-2));
a=a_i./(1-(n./n0)).^(2/(m-2));
a2=a_i./(1-(n./n02)).^(2/(m-2));
K_1=d_sigma*Q*(pi*a(500)/1000)^0.5;
plot(n,a,n,a2);
disp(sprintf('a(N=50,000)= %g [mm]',a(500)));
disp(sprintf('K_I (N=50,000)= %g [MPa m^0.5]',K_1));
disp(sprintf('a(N=50,000)= %g [mm]',a(500)));
disp(sprintf('K_I2 (N=50,000)= %g [MPa m^0.5]',K_1));
legend('K_a_p_p','K_a_p_p+K_r_e_s')
grid on;
hold on;
a(N=50,000)= 0.00455129 [mm]
K_I (N=50,000)= 0.850794 [MPa m^0.5]
a(N=50,000)= 0.00455129 [mm]
K_I2 (N=50,000)= 0.850794 [MPa m^0.5]

```